Induction of astrocytes senescence by Plasmodium infection : role in cerebral malaria

Fatima Hellani

ÉCOLE DOCTORALE BIOLOGIE - SANTÉ DE LILLE

Tropical Biomes & Immunopathophysiology Team

Inserm U1019, CNRS UMR9017, Université de Lille, Université de Guyane
Institut Pasteur de Lille

THÈSE

présentée par : **HELLANI Fatima**

soutenue le : 21 Décembre 2022

pour obtenir le grade de : **Docteur de l'Université de Lille**

Induction of astrocytes senescence by *Plasmodium* infection: Role in cerebral malaria

THÈSE dirigée par :

Dr. PIED Sylviane

Composition du Jury :

Pr. EL-Moukhtar ALIOUAT : Président de Jury

Pr. Chahrazade EL AMRI : Rapporteur

Dr. Agnès AUBOUY : Rapporteur

Dr. Olivier PLUQUET : Examinateur

Dr. Valerie SOULARD : Examinatrice

Dr. Sylviane PIED : Directrice de Thèse

Abstract

Cerebral malaria (CM) is a fatal neurological disease caused by *Plasmodium (P.) falciparum* infection. A central event involved in the pathogenesis of CM is the sequestration of infected red blood cells in the cerebral capillaries, as well as the underlying activation of glial cells secreting pro-inflammatory cytokines and chemokines that contribute to local and systemic neuroinflammation. The objective of my PhD project was to decipher the mechanism involved in the activation of the pro-inflammatory response of astrocytes during CM. Using the experimental model of C57BL/6 (CM susceptible) and B6.WLA-*Berr2* (CM resistant) mice infected with *P. berghei* ANKA (*PbA*), we identified that astrocytes developed a p21-dependent senescence-like phenotype only in the brain of CM susceptible mice. This process is accompanied by an increase of CXCL-10, a chemokine of SASP (senescence-associated secretory phenotype). The involvement of senescence in CM pathogenesis was confirmed by the inhibition of inflammation and protection of mice from CM after treatment with a senolytic cocktail (Dasatinib+Quercetin), which eliminated senescent astrocytes. We then investigated the mechanisms involved in the senescence process in primary cultures of astrocytes stimulated with *PbA*-infected red blood cells (iRBCs), we observed that unconventional LC3-mediated autophagy, which is involved in the transfer of parasitic microvesicles in astrocytes, recently demonstrated in the laboratory, activates the senescence process and the production of CXCL-10. Furthermore, we found a significant increase in the expression of senescence markers in the brain and in peripheral blood cells of *P. falciparum* infected patients with CM compared to Mild Malaria patients. The second part of the project consists in studying the impact of astrocyte senescence during aging on CM susceptibility. Different behavioral tests and IRM analysis were performed on young and old mice. Data obtained suggest that the cognitive deficits observed during CM and in the long-term of the infection may be caused by astrocyte senescence. Finally, we showed that senescent astrocytes that accumulate with normal aging, can protect mice from CM. More analysis is ongoing to confirm the relationship between astrocytes senescence and cognitive deficits.

Taken together, our work demonstrated a novel mechanism by which astrocytes can participate in neuropathophysiology and the development of cognitive deficits during CM and long-term infection. We anticipate that senescence marker (p21) expression in human blood associated with high plasmatic level of CXCL-10 could be a useful CM biomarker, and that senolytics

drugs could open new therapeutic avenues in the treatment of human CM and the prevention of cognitive deficits in CM survivors.

Key words: Cerebral Malaria, senescence, astrocyte, inflammation, cognitive deficits.

Résumé

Le neuropaludisme est une immunopathologie mortelle causée par l'infection par *Plasmodium falciparum* chez l'homme. La neurophysiopathologie résulte de la séquestration des globules rouges infectées dans les capillaires cérébraux, ainsi qu'une activation des cellules gliales qui sécrètent des cytokines et des chimiokines pro-inflammatoires, contribuant à la neuroinflammation locale et systémique. L'objectif de mon projet de thèse était de décrypter le mécanisme impliqué dans l'activation de la réponse pro-inflammatoire des astrocytes au cours du neuropaludisme. En utilisant le modèle expérimental de neuropaludisme, la lignée de souris C57BL/6 (sensible) et les souris congéniques C57BL/6.WLA (résistante) infectées par *Plasmodium berghei* ANKA (*Pb*A) nous avons mis en évidence une sénescence précoce des astrocytes. Ce processus est accompagné d'une augmentation de CXCL-10, une chimiokine du SASP (phénotype sécrétoire associé à la sénescence). L'implication de la sénescence dans le neuropaludisme est confirmée par l'inhibition de l'inflammation et la protection des souris contre le neuropaludisme par le traitement des souris avec un cocktail de drogues sénolytiques (Dasatinib + Quercétine) qui inhibe la sénescence des astrocytes. Nous avons ensuite étudié les mécanismes impliqués dans le développement de la sénescence. En utilisant des cultures primaires d'astrocytes stimulées par le parasite *Pb*A, nous avons observé que l'autophagie non-conventionnelle LC3-dépendante impliqué dans le transfert de microvésicules parasitaire dans l'astrocyte récemment mise en évidence dans la laboratoire active le processus de sénescence et la production du CXCL-10. Nous avons aussi montré une augmentation significative d'expression des marqueurs de sénescence dans le cerveau et dans les cellules sanguines périphériques de patients infectés par *P. falciparum* atteints de neuropaludisme comparés au paludisme non sévère. La deuxième partie du travail consistait à étudier l'impact de la sénescence des astrocytes sur la sensibilité au neuropaludisme. Différents tests comportementaux et des analyses d'IRM ont été effectués sur des jeunes et des souris agées. Les résultats obtenus suggèrent que les troubles cognitifs observés au cours du neuropaludisme et à long terme de l'infection peuvent résulter de la sénescence des astrocytes. Enfin, la sénescence des astrocytes au cours du vieillissement protégerait les souris du neuropaludisme. D'autres analyses sont en cours pour confirmer la relation entre la sénescence des astrocytes, le SASP et le développement des déficits cognitifs.

Ainsi, ces études montrent un nouveau mécanisme par lequel les astrocytes peuvent participer au neuropaludisme. Nous proposons que l'expression du marqueur de sénescence p21 dans les

cellules du sang périphérique associée à un taux plasmatique élevé de CXCL-10 puissent être un biomarqueur du neuropaludisme chez l'homme. Ainsi, les médicaments sénolytiques pourraient ouvrir de nouvelles voies thérapeutiques dans le traitement du neuropaludisme et la prévention des déficits cognitifs observés chez les survivants du neuropaludisme.

Mots clés : Neuropaludisme, sénescence, astrocyte, inflammation, déficits cognitifs.

To the soul of my brother HADI,
To my father, my mother, my brother, my sisters and my husband

Acknowledgments

I would like to express my sincere gratitude to the jury members, Pr. Chahrazade AL AMRI, Dr. Agnès AUBOUY, Dr. Valerie SOULARD, Dr. Olivier PLUQUET and Pr. El-Moukhtar ALIOUAT, who agreed to evaluate this work.

I am extremely thankful to all the persons without whom my project would not be achieved.

I would like to thank to my supervisor Dr. Sylviane PIED most sincerely for all her support and commitment to me from the very first moment and for giving me the opportunity to spend these very pleasant years in her team where I had the chance to work in a very nice project. Thank you for your patience and helpful advice.

I'd like to thank Pr. Pierre-André CAZENAVE, especially for these very enriching immunology courses, that take place every Friday. I would like to express my appreciation to Jacques ROLAND and Corinne GLINNEUR, for giving me good advice each time we talked. Inès and Nasr, I would like to thank you for all your help and your investment on this project. A huge thanks also to my TBIP friends, Jeremy and Kevin. I appreciate all the TBIP team members in Guyana for their attentive listening and wise counsel during each presentation.

For her contribution to statistical analysis, Cecile LECOEUR has my deepest gratitude. I'm grateful to Pr. Corinne ABBADIE, Dr. Charlotte LALOUX, Dr. Florent AUGER, and Nicolas DURIEUX for their collaboration in this project.

I would like to express my deep gratitude and appreciation to my PhD thesis committee Pr.Corinne ABBADIE, Dr. Valerie SOULARD and Dr. Emmanuel HERMANN for their guidance and advice throughout my PhD journey.

Most importantly, to my caring, loving, and supportive family: my deepest gratitude. I thank my dear parents, Hassan and Hanan, who have always been there for me. You have sacrificed everything for your children, sparing neither health nor effort. You have given me a magnificent model of hard work and perseverance. I would like also to thank my brother Jawad, my sisters Waed, Zeinab and Nour for their immense support they have given me. Your support and your countless attentions allowed me to find the energy to progress in my work.

I would like to thank with all my heart and soul to my best friend and love of my life Aly. None of the things I have achieved could have been possible without you. You are my biggest support and I love you for that, always and forever.

Thank you to my lovely friends Alaa, Batoul, Zeinab, Lama, Israa, Doha, Jana, Kawthar and Zainab, for being my second family and sharing the wonderful times and memories together in France. My sincere thanks to Aya, Doha, Rim, Zeinab, Hindia, Mirna, Fatima and Nour, who, despite the distance, was always by my side.

Hadi, I know you will be always proud of me.

I am grateful to everyone in my life who helped shape who I am today and who will help shape who I will be tomorrow.

نحن أحياءٌ وباقون، وللحلمِ بقية..
وآخر دعوانا أن الحمدلله رب العالمين ❤️

Table of contents

List of Figures

List of Tables

List of abbreviations

^{1}HMRS	Proton magnetic resonance spectroscopy
AD	Alzheimer's disease
ADC	Apparent diffusion coefficient
AKT	AKR mouse Thymoma
APAF-1	Apoptotic peptidase activating factor 1
ARDS	Acute respiratory distress syndrome
ASF1	Anti-silencing function 1
ATG	Autophagy related Genes
ATM	Ataxia Telengectasia Mutated
ATR	ATM and RAD3-related
Aβ	Amyloid-β
B6	C57BL/6
BAF A1	Bafilomycin A
BAX	BCL-2 Associated X apoptosis regulator
BBB	Blood-brain barrier
BBB	Blood–Brain Barrier
Bcl	B cell lymphoma
BDNF	Brain-derived neurotrophic factor
Brdu/EdU	Bromodeoxyuridine/ 5-Ethynyl-2′-deoxyuridine
Bub1b	Budding Uninhibited by Benzimidazoles 1 Beta
C/EBPβ	CCAAT/Enhancer Binding Protein Beta
Calr	Calreticulin
CCF	Cytoplasmic chromatin fragments
CCL	Chemokine ligand
CD	Cluster differentiation
CDC6	Cell Division Cycle 6
CDKi	Cyclin-dependent kinase inhibitor
CDKN	Cyclin Dependent Kinase Inhibitor
CDKs	Cyclin-dependent kinase
cDNA	Complementary DNA
Cgas	Cyclic GMP-AMP synthase

CHK	Checkpoint kinase
CM	Cerebral Malaria
CM^{+}	*Pb*A-infected B6 mice developing CM
CMA	Chaperone Mediated Autophagy
CM^{R}	CM-resistant
CM^{S}	CM-susceptible
CNS	Central nervous system
COPD	Chronic obstructive pulmonary disease
CSF	Cerebrospinal fluid
CT	Computational Topography
CXCL	C-X-C motif chemokine ligand
CXCR3	C-X-C Motif Chemokine Receptor 3
D	Dasatinib
DAPI	4',6-diamidino-2-phenylindole
DDR	DNA Damage Response
DI	Discrimination index
DMEM	Dulbecco's Modified Eagle Medium BA
DPI	Days post infection
DSBs	DNA Double-Strand Breaks
DWI	Diffusion-weighted images
ECM	Experimental Cerebral Malaria
ECs	Endothelial cells
EPCR	Cytokine-activated endothelial protein C receptor
EPM	Elevated plus maze
FAK	Focal adhesion Kinase
FBS	Fetal bovine serum
FOXO4	Forkhead box protein O4
GADD45	Growth Arrest and DNA Damage-inducible
GCS	Glasgow Coma Scale
GFAP	Glial Fibrillary Acidic Protein
GO	Gene Ontology
GRO	Growth-related oncogene
H2O2	Hydrogen peroxide
H3K9me3	Histone 3 trimethylated at lysine 9

HCMV	Human cytomegalovirus
HIRA	Histone cell cycle regulation defective A
HIV	Human immunodeficiency virus
HMGB	High-mobility group B
HP1	Heterochromatin protein 1
HP-1	Histone protein 1
HRSV	Human respiratory syncytial virus
HSC70	Heat Shock Cognate Protein
ICAM-1	Intercellular adhesion molecule-1
IFN	Interferon-induced protein
IGFBP	Insulin-like Growth Factor Binding Protein 5
IL	Interleukin
INK4	Inhibitor of CDK4
INK-ATTAC	INK-linked apoptosis through targeted activation of caspase
IPF	Idiopathic pulmonary fibrosis
iRBCs	Infected red blood cells
IRF3	Interferon Regulatory Factor 3
JAK	Janus Kinase
Kap-1	KRAB-associated protein 1
Kb	kilobases
L28	B6.WLA-*Berr2*
LAD	Lamin-Associated domains
LAMP2A	Lysosomal-associated membrane protein 2a
LC3	Microtubule-associated protein 1 light chain 3
LPS	Bacterial lipopolysaccharide
LTα	Lymphotoxin α
Mdm2	Murine double minute 2
MEK	MAK/ERK Kinase
MIP-3	Macrophage Inflammatory Proteins
MM	Mild Malaria
MMP	Matrix metalloproteinases
MOD	Multiple Organ Dysfunction
MOS	Moloney murine Sarcoma viral oncogene homolog
MRI	Magnetic Resonance Imaging

MRS	Spectroscopy
mTOR	Mammalian Target of Rapamycin
MVs	Microvesicles
NF1	Neurofibromatosis type 1
NF-κb	Nuclear Factor-Kappa B
NK	Natural Killer
NOR	Novel object recognition
NOXA	Phorbol-12-myristate-13-acetate-induced protein 1
OIS	Oncogene-induced senescence
P.	*Plasmodium*
p38MAPK	p38 mitogen-activated protein kinases
***Pb*A**	*P. berghei* ANKA
PBMCs	Peripheral blood mononuclear cells
PBS	Phosphate-buffered saline
PD	Parkinson's disease
PDGF-A	Platelet-derived growth factor AA
PECAM-1	Platelet endothelial cell adhesion molecule-1
***Pf*EMP-1**	Erythrocyte membrane protein-1
PI3K	Phosphoinositide 3-Kinase
PI3K	Phosphoinositide-3-kinase
PML	Inducer of acute promyelocytic leukemia
PML	Promyelocytic leukemia
POT1	Protection of Telomeres 1
pRB	Retinoblastoma protein
PTEN	Phosphatase and Tensin homolog
PTOP	POT1 and TIN2 Organizing Protein
PUMA	p53 upregulated modulator of apoptosis
Q	Quercetin
RAF	Rat Fibrosarcoma
RAG2	Recombination activating gene 2 protein
RAP1	Transcription Repressor/Activator Protein 1
RAS	Rat Sarcoma
RBCs	Red Blood cells
ROS	Reactive oxygen species

RS	Replicative senescence
RT	Room temperature
SAHF	Senescence-Associated Heterochromatin-Foci
SASP	Senescence Associated Secretory Phenotype
SA-β-Gal	Senescence- associated β- Galactosidase
SCID	Severe combined immune deficiency mice
SIPS	Stress-Induced Premature Senescence
SM	Severe Malaria
SMS	Senescence-messaging secretome
ST-2	Interleukin-1 receptor family member
STAT3	Signal transducer and activator of transcription 3
STING	Stimulator of Interferon Genes
T2W	T-2-weighted
TASCC	TOR-autophagy spatial coupling compartment
TGF	Transforming Growth Factor
TIN2	TRF1 Interacting Nuclear factor 2
TLR	Toll like receptors
TNF	Tumor necrosis factor
TRAF3IP2	TRAF3 Interacting Protein 2
TRF	TTAGGG Repeats Factor
VCAM-1	Vascular cell adhesion molecule-1
VEGF	Vascular Endothelial Growth Factor
VIS	Virus-induced senescence
WHO	World Health Organization
WT	Wild type
X-gal	5-bromo-4-chloro-3-indolyl β-galactopyranoside

Introduction

Cerebral malaria (CM) is the deadliest complication of *Plasmodium* (*P.*) *falciparum* infection transmitted to human by an infected anopheles female mosquito bite. Malaria affects approximately 241 million people and resulted the death of 627 000 individuals in 2020 according to WHO by CM [1]. The pathophysiology of this disease is complex and multifactorial, and several aspects of CM are still unknown. In experimental model of CM (ECM) induced by *P. berghei* ANKA (*PbA*) in C57BL/6 mice, the sequestration of infected red blood cells (iRBCs) in brain microvessels causes mechanical obstruction and reduction in blood flow, hypoxia, coma and death [2]. This process induces an exacerbated inflammatory response of glial cells characterized by the release of pro- inflammatory cytokines and chemokines such as tumor necrosis factor-alpha (TNF-α) and C-X-C motif chemokine ligand 10 (CXCL-10) involved in CM pathogenesis [3, 4]. This neuroinflammatory pathway promotes the breakdown of the blood–brain barrier (BBB) and the infiltration by pathogenic $CD8^+$ T lymphocytes expressing CXCL-10 receptors in the central nervous system (CNS) [5-7]. However, the exact mechanisms underlying the induction of inflammatory response of astrocytes are yet incompletely understood.

It has been demonstrated that despite anti-malaria treatment, about 25 % of CM survivors develop brain damage, as well as neurological sequelae manifested by cognitive deficits and long-term mental health disorders [8-10]. Similarly, cognitive deficits were also observed during ECM. Desruisseaux *et al*, proved an impairment in visual memory correlated with significant histological alterations, hemorrhage, inflammation, and microglial activation [11]. Reis *et al,* found also that cognitive impairment persisted 30 days after the initial infection in mice treated with chloroquine [12]. However, the precise mechanisms implicated in cognitive impairment during CM remain incompletely understood.

A potential contributor of pro-inflammatory phenotype of astrocyte and microglia during ageing and neurodegenerative disease could be cellular senescence. Senescence is a cell cycle arrest process characterized by different morphological and functional changes, including activating of the senescence-associated secretory phenotype (SASP)[13]. Moreover, accumulation of senescent cells in tissues and organs and accelerated telomere attrition are implicated in many human pathologies related to ageing, neurodegeneration, and dementia [14]. It is known that senescence astrocyte generates several detrimental effects, such as glutamate excitotoxicity, impaired synaptic plasticity, neural stem cell loss and BBB dysfunction [15]. It has been reported that the senescence of astrocytes is correlated with irreversible cognitive

decline in aging and neurodegenerative diseases [16]. Notably, the clearance of senescent astrocytes preserves cognitive dysfunction [17].

This thesis work is divided into 3 axes that aim to:

1-Investigate whether astrocyte cellular senescence could contribute to the neuroinflammatory process involved in CM pathogenesis.

2- Determine if this senescence process participated in cognitive deficits observed during acute CM and long-term in chloroquine-rescued animals.

3- Evaluate the impact of senescent astrocytes, which accumulates with normal aging on CM development.

The first section of this work will be submitted soon in Nature communication journal. This part was conducted is in collaboration with two PhD student in our laboratory: Inès Leleu and Nasreddine Saidi. Additional experiments are being planned to achieve the remaining two sections, which will be the subject of a second publication.

State of the art

Chapter 1: Malaria

1. Definition

Malaria is one of the most widespread infectious diseases in the world. It is caused by infection with protozoan parasites of the genus *Plasmodium* (*P.*) and transmitted to human by an infected anopheles female mosquito bite. Patients' clinical manifestations range from asymptomatic to severe Cerebral Malaria (CM).

2. Epidemiology

According to the World Health Organization (WHO), a third of the world's population is currently exposed to malaria risk. In 2020, Malaria prevalence was estimated to be 241 million cases, with 627,000 deaths caused by *P. falciparum*. Africa is the most exposed region of the world to this disease, accounting for more than 95% of all malaria cases and 96% of deaths. South-East Asia, Latin America and the Middle East are also threatened. The South-East Asia Region accounted for approximately 2% of the global malaria cases. India represented about 82% of all malaria deaths in this region [1].

Globally, Malaria mortality rate decreased steadily over the period 2000–2019, from 896 000 in 2000 to 558 000 in 2019. In contrast, there was a 12% increase in 2020 compared to 2019, with 14 million more cases and 69,000 more deaths compared to 2019 due to service disruptions during the COVID-19 pandemic[1].

Malaria is highly prevalent among children under 5 years old. They accounted for about 77% of deaths from *P. falciparum* in 2020 [1]. They were followed by pregnant women, especially during their first pregnancy. The accumulation of infected red blood cells in the placenta leads to maternal mortality, maternal anemia, miscarriage, abortion, low birth weight or preterm birth [18]. In 2020, the WHO estimated 11.6 million pregnancies (34%) were infected by *P.falciparum* in Africa [1].

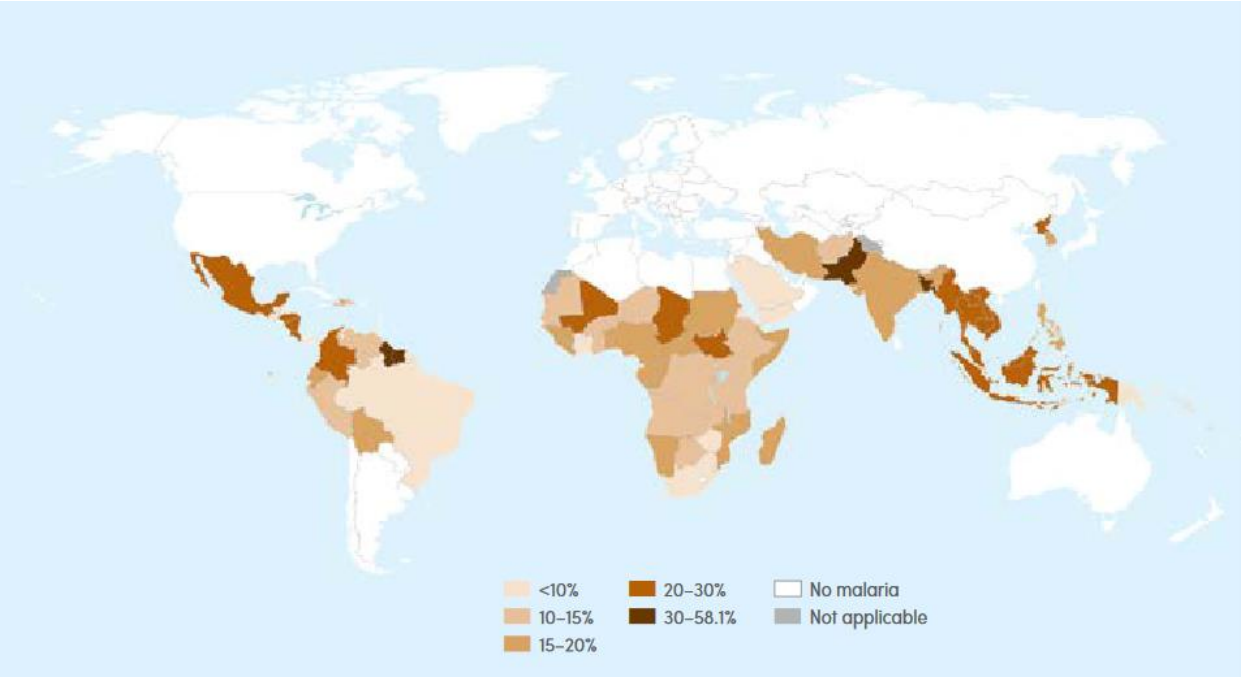

Figure 1 : Global distribution of Malaria. Reprinted from (WHO 2021) [1].

3. Parasite

Phylum: *Apicomplexa*
Class: *Sporozoea* (Sub-class: *Coccidia*)
Order: *Eucoccidia* (Sub-order: *Haemosporina*)
Family: *Plasmodidae*
Genus: *Plasmodium*

Plasmodium is an obligate intracellular protozoan parasite capable of invading different cell types. It has an apical complex composed of rhoptries, dense granules and micronemes, which participate in the invasion of red blood cells (RBCs) by creating parasitophorous vacuole, separating the parasite from the cytoplasm [19, 20] (Figure 2).

Five species of *Plasmodium* can infect humans: *P. vivax*, *P. ovale*, *P. knowlesi*, *P. malariae* and *P. falciparum*. These species differ in their pathogenicity and geographic distributions. Mixed species infection, which means the possibility of getting infected by multiple species at the same time, could occur.

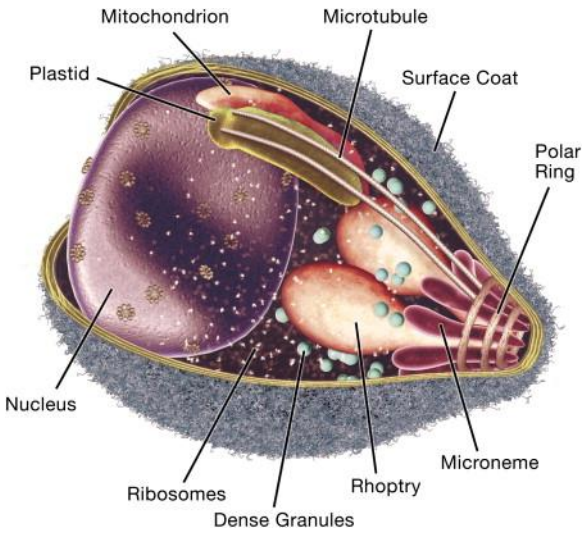

Figure 2 : A Plasmodium merozoite's structure. **Reprinted from (Cowman et al., 2016) *[20].***

P. falciparum and *P. vivax* are the most widespread species. They are involved in the development of severe forms of malaria. *P. falciparum* is found in tropical and subtropical areas (primarily in Africa), infect humans only, and causes most of severe malaria cases, particularly CM. *P. vivax* exists in all tropical areas, especially in Asia and Latin America, while it is rarely seen in Africa. *P. malariae* and *P. ovale* cause only minor malaria incidence but sometimes can evolve into severe malaria. *P. ovale* sprouts in African West Coast while *P. knowlesi*is mainly found in Southeast Asia. Initially, it only affects macaques, but occasionally can also infect humans.

4. Vector

Malaria is transmitted to humans via a vector: the female *Anopheles* mosquito (Figure 3). Among more than 465 species of Anopheles described in the literature, not all are capable of transmitting malaria. There are, however, about fifty of which the main ones are *Anopheles gambiae* in Africa, *Anopheles darlingi* in South America and *Anopheles stephensi* in Asia. Anopheles grow in hot and humid areas, which explains the high prevalence of malaria in these places [21]. The male Anopheles mosquito only once fertilizes the female. Their reproduction takes place in the water, where the female will lay eggs. The eggs will then transform into aquatic larvae, Pupa and adult *Anopheles*. The lifespan of an adult is only a few weeks and is highly dependent on environmental conditions, including temperature. Its longevity will thus have consequences on the efficiency of the transmission of the parasite and, therefore, the disease[22].

Figure 3 : Anopheles female mosquito, Reprinted from Biogents Malaria mosquitoes.

5. Parasite life cycle

Plasmodium parasites have an extraordinarily complex life cycle, involving two hosts (Figure 4):

1) An invertebrate host (Female *Anopheles* mosquitoes, definitive host), where it conducts its sexual (or sporogony) stage.
2) A vertebrate host (Human, Intermediate host). Where she performs two asexual (or schizogonic) phases: first phase is hepatic (pre-erythrocytic), and the second is blood (erythrocytic).

5.1. Sexual cycle in the mosquito

During a blood meal, a female *Anopheles* mosquito can be contaminated by gametocytes. These will, in the midgut of the mosquito, be transformed into gametes. Fusion of male and female gametes generates the zygote, which develops into ookinete, a mobile form capable of crossing the midgut epithelium, over approximately 18h. The ookinete penetrates the midgut epithelium and forms oocysts on the outer surface. After multiplication, the oocyst will evolve into sporocyst containing about 10,000 sporozoites (infectious forms) which will migrate to the mosquito salivary glands and will be release during a future blood meal (Figure 4) [23, 24] .

5.2. Pre- erythrocytic stage

It begins after the mosquito's inoculation of the parasite (in the form of sporozoites) during a blood meal. Sporozoites travel via lymphatics or the circulatory system to the liver, where they enter hepatocytes. Once inside hepatocytes, the parasites develop into mature liver schizonts,

each containing thousands of merozoites. The rupture of mature schizonts release merozoites which will infect red blood cells (RBCs) and initiate the intraerythrocytic phase (Figure 4) [25].

5.3. Erythrocytic stage

The cycle begins after the penetration of merozoites into RBCs. The parasite undergoes asexual replication, processing through a set of stages (Ring, trophozoite and schizont), and produces an average of 16 new daughter merozoites per schizont.

During each erythrocyte cycle, merozoites differentiate first into trophozoites and then into erythrocyte schizonts. This phase is accompanied by the infection of thousands of RBCs, causing clinical signs [25].

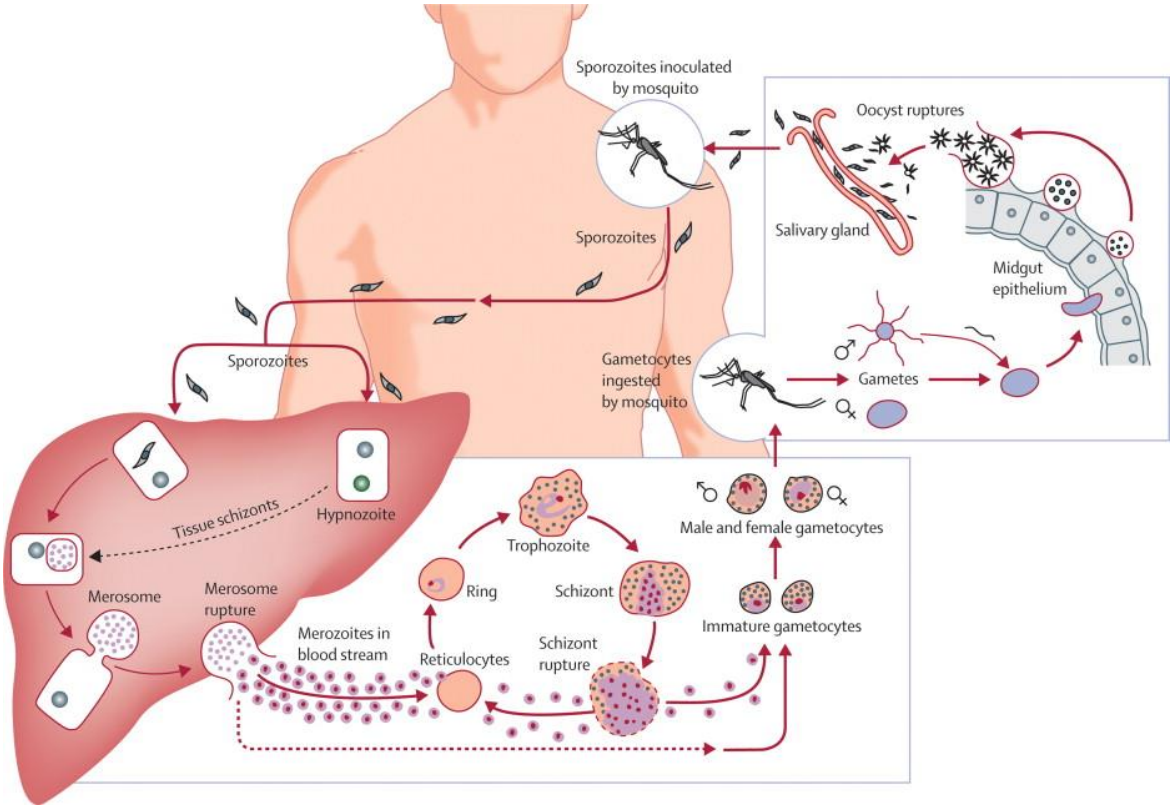

Figure 4 : Plasmodium life cycle, Reprinted from (Mueller et al., 2009) [23].

5. Clinical Features

The clinical signs of malaria are primarily due to the rupture of schizont and the destruction of erythrocytes. It's very dependent on the immune response of the host [26].

5.1. Uncomplicated Malaria

This is the most common clinical manifestation. It is defined by a positive diagnosis and the presence of clinical manifestations of malaria without complications. The clinical manifestations of uncomplicated malaria are non-specific and look like those of common viral infections, such as a fever that can exceed 40°C (more than 92% of cases), chills (79% of cases), headache (70% of cases), and diaphoresis (64% of cases). Other common symptoms, including nausea, vomiting, diarrhea, abdominal pain, myalgia, dizziness, discomfort, and dry cough are detected. Other physical signs, such as tachycardia, orthostatic hypotension, pallor, jaundice, hepatomegaly and splenomegaly can be seen [27]. If not diagnosed early and treated correctly, *P. falciparum* infection progresses to a fatal complication.

5.2. Severe Malaria

According to the WHO, the diagnosis of severe malaria can be confirmed when asexual forms of *Plasmodium* are observed on a blood smear and at least one of the clinical signs, including impaired consciousness or unrousable coma, prostration, failure to feed, multiple convulsions (more than two episodes in 24h), deep breathing, respiratory distress (acidotic breathing), circulatory collapse or shock, systolic blood pressure < 70mmHg in adults, jaundice, Hemoglobinuria and pulmonary oedema [26].

P.falciparum is the primary cause of severe malaria. The severe malaria complications include CM, acute renal failure, pulmonary edema, and severe anemia. The metabolic complications are acidosis and hypoglycemia. Any of these complications can develop rapidly and progress to death within hours or days[27].

The clinical manifestations differ between children and adults. In children, the major complications of the disease are severe anemia, CM and metabolic acidosis. Whereas in adults, it is frequently accompanied by metabolic acidosis, acute respiratory distress syndrome (ARDS), jaundice and acute kidney failure [28]. Thus, in endemic regions where transmission is annual, it is mainly children under 5-year-old who develop severe malaria. In contrast, in regions where the transmission is seasonal, severe forms affect both children and adults [27]. For example, the severe manifestations of malaria reported in India affect a very heterogeneous population and are also characterized by disparate clinical features.

5.2.1. Severe Malaria Anemia

Following the WHO definition, anemia is defined by the presence of a hemoglobin level <5g/dL (and/ or hematocrit < 15%) in children and a hemoglobin level < 7g/dL (and/or a hematocrit < 20%) in adults, regardless of the level of parasitemia. Not all cases of severe malarial anemia are associated with high parasitemia, and a high parasitemia level is not predictive of severe anemia. In endemic areas, severe malaria anemia is a significant problem in children and can be fatal. However, in epidemic areas, it can develop in the adult population and particularly in pregnant women [26].

5.2.2. Cerebral Malaria (CM)

Detailed in chapter 2.

6. Mouse models of malaria

Rodent malaria parasites, isolated from Thamnomys thicket rats in the African Congo, have provided an invaluable resource for studying the role of the pathology of malaria. The characteristics of both infection and disease differ in the four species of *Plasmodium* that infect mice (*P. berghei*, *P. yoelii*, *P. chabaudi*, and *P. vincke*i). The life history of human malaria parasites and pathological symptoms of human malaria can be mimicked with infections of each of these different species of mouse malaria in combination with different strains of mice, allowing for a range of models in which the different syndromes can be studied (Table 1) [29].

Species	Mouse Strain and manifestations	References
P. berghei ANKA	C57BL/6J: death between 6 to10 dpi from ECM C57BL/6J.WLA-Berr1 and C57BL/6J.WLA-Berr2: Death between 22 to 25 dpi from hyperparasitemia. BALB/c: Death from hyperparasitemia. No cerebral complications. DBA/2J: Death from hyperparasitemia and anemia. No cerebral complications.	[3, 30, 31].
P. berghei NK65	C57BL/6: death in ~20 dpi from respiratory distress.	[32].
P.Yoeli XNL	C57BL/6: Resolving non-lethal infection accompanied by anemia. BALB/c: Resolving non-lethal infection.	[33, 34].
P. vinckei vinckei	CBA: death at 6 dpi from hyperparasitemia	[35].

Table 1 : Mouse models of malaria.

Chapter 2: Cerebral Malaria

1. Clinical features

CM is a severe neurological complication, and it is most of the time induced by *P. falciparum* infection. CM primarily affects children in sub-Saharan Africa and adults in Asia. Complications of CM include clouding of consciousness, cerebral seizures, and coma, which can result in death of infected individuals. WHO proposed a definition of CM as a clinical syndrome characterized by a Glasgow Coma Score of < 11/15 for adults or a Blantyre Coma Scale of < 2 for children, a coma at least 1 h after termination of a seizure and/or detection of asexual forms of malaria parasites on peripheral blood smears, with exclusion of other causes of encephalopathy. As shown in table 1, there are notable clinical differences between CM in African children and Asian adults and it is not entirely clear if these differences are associated with immunity or age [36].

Despite anti-malaria treatment, about 25 % of CM survivors develop neurological sequelae manifested by cognitive deficits, long-term mental health disorders and behavioral difficulties [37].

	African children	Adults
Clinical features		
Coma	Develops rapidly often after a seizure[9]	Develops gradually following drowsiness, disorientation, delirium, and agitation over 2–3 days or follows a generalised seizure[10]
Seizures	Over 80% present with a history of seizures and 60% have seizures during hospital admission; recurrent seizures are focal motor in >50%, generalised tonic-clonic in 34%, partial with secondary generalisation in 14%, and subtle or electrographic in 15%; status epilepticus is common[9,11]	Occurs in up to 20%, mostly generalised tonic-clonic seizures; status epilepticus is rare[10,12]
Other signs	Pallor, respiratory distress, dehydration and rarely jaundice	Jaundice (40–70%), Kussmaul's breathing, shock, and spontaneous bleeding[8,13,14]
Neurological signs	Brainstem signs are present in >30% and are associated with raised ICP;[15,16] retinal abnormalities are present in >60%;[17] brain swelling on CT scan is seen in 40%[18]	Patients typically have symmetrical upper-motor-neuron signs; brainstem signs and retinal abnormalities are less common[10,19]
Major complications and involvement of other organs	Severe anaemia in 20–50%, of whom 30% require a blood transfusion;[8] severe metabolic acidosis (presents as respiratory distress), often associated with hyperlacteamia; hyponatraemia (>50%), hypoglycaemia (30%) and changes in potassium; renal failure and pulmonary oedema are rare[8,9,20–25]	Multisystem and organ (circulatory, hepatic, coagulation, renal, and pulmonary) dysfunction; pulmonary oedema, renal failure, lactic acidosis, haemoglobinuria have been reported;[26–28] hypoglycaemia is present in only 8%[29]
Outcome		
Recovery of consciousness	Rapid, within 24–48 h[8,30]	Slower, occurs within 48 h.[31]
Mortality	18·6%[5,8] up to 75% of deaths occur within 24 h of admission	20%[8] about 50% occur within 24 h[13]
Neurological sequelae	Occurs in 11%;[5] common sequelae are ataxia (2·5%), hemiparesis (4·4%), quadriparesis (3·5%), hearing (1·9%), visual (2·3%) and speech (2·1%) impairments, behavioural difficulties (1·3%), and epilepsy[8,32,33]	Few, occurs in <5%; isolated cranial nerve palsies, mononeuritis multiplex, polyneuropathy, extrapyramidal tremor, and other cerebellar signs[10]

Table 1: **Clinical features and outcomes of cerebral malaria in African children and southeast Asian adults**

Table 2: Clinical features of CM in African children and southeast Asian adults. Reprinted from (Idro et al., 2005)[36].

Studies of the pathophysiology of malaria in humans are minimal for ethical reasons and have several limitations, such as inter individual variability and infectious and immunological history of patients. In addition, histopathological examination of human CM brains is limited to post-

mortem analysis of fatal cases. Despite the use of *in vivo* imaging techniques, such as Magnetic Resonance Imaging (MRI), Spectroscopy (MRS), and Computational Topography (CT), these studies are limited by the availability of this expensive equipment in malaria-endemic areas. In addition, peripheral blood examination (which is possible in both nonfatal and fatal cases) can provide limited information about the brain's parasitological environment. Again, patients usually come to the hospital only after the syndrome is well established. Therefore, other approaches, in combination with human studies, are needed to fully understand the pathogenesis of CM. The use of a mouse model known as ECM has contributed significantly to elucidating the pathophysiology of CM [38, 39].

2. Experimental Cerebral Malaria (ECM)

Infection of various mouse strains including C57BL/6 mice by *P. berghei* ANKA (*Pb*A), has been widely employed. *Pb*A-infected mice develop severe neurological symptoms including locomotor disorders, head deviation, paralysis, convulsions, coma and ultimately, death at 6 to 10 days post-infection (dpi) [3].

3. Mechanisms implicated in the pathogenesis of CM

The physiopathology of CM is complex and multi-factorial. One of the first mechanisms implicated in the CM is the sequestration of iRBCs in brain microvessels. That leads to further activation of Endothelial cells (ECs). The latter will then secrete cytokines and chemokines, leading to the recruitment of platelets and immune cells (monocytes/macrophages, lymphocytes, etc.) in the brain parenchyma. In parallel, the sequestration of infected red blood cells provokes the activation of glial cells, including astrocytes and microglia which secrete pro inflammatory cytokines and chemokines such as TNF-α and CXCL-10. This neuroinflammation pathway promotes the breakdown of the BBB and the recruitment of pathogenic CD8 T cells expressing CXCR3 receptors to the brain [4]. Despite the tremendous effort to better understand CM's pathophysiology, many aspects remind to be understood, and further studies are needed to embrace its complexity.

3.1. Breakdown of the BBB

The BBB is a semipermeable barrier that separates the CNS from the circulatory system. The BBB comprises a monolayer of ECs joined together by tight junctions and the underlying basal lamina. The integrity of the BBB is supported by pericytes, astrocytes endfeet, microglia and neurons (Figure 5) [40, 41]. The BBB plays an important role in CNS homeostasis by facilitating the transport of nutrients such as glucose and amino acids from the blood to the CNS and removing metabolic waste products from the CNS into the blood via specific transport channels [41].

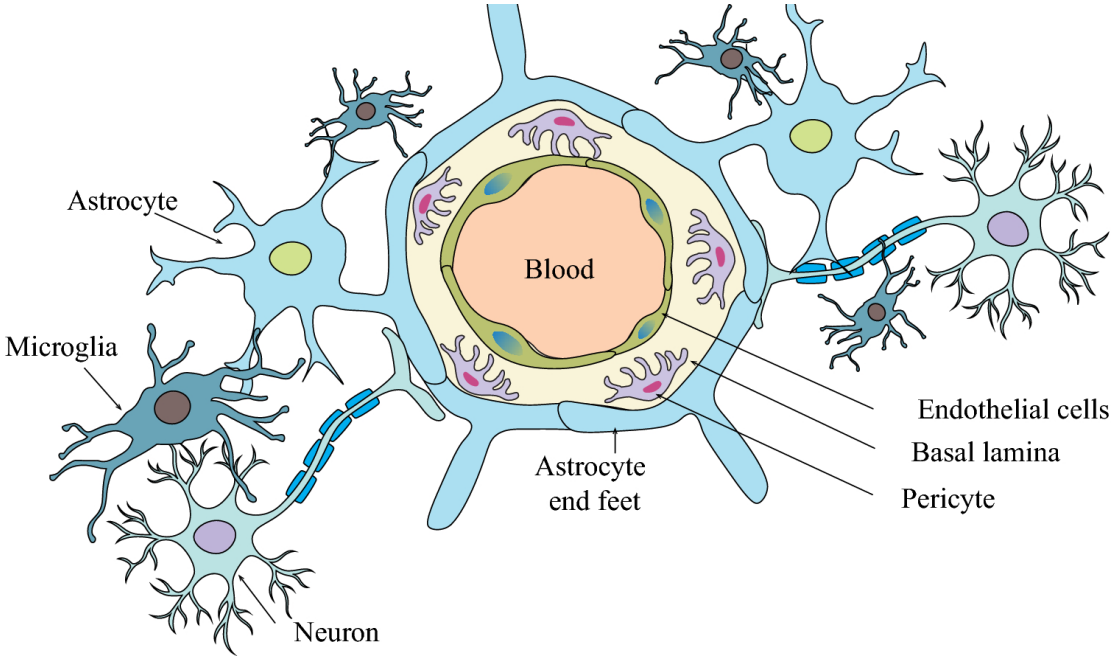

Figure 5: The composition of the BBB. Adapted from (Panda et al., 2022) [42].

BBB breakdown has been associated with the development of CM in mice and humans [43]. Until now, the precise underlying mechanisms disrupting of BBB integrity during CM have remained unknown [44]. Several events have been associated with the breakdown of the BBB in human and murine studies, including the sequestration of iRBCs within cerebral microvessels, an excessive proinflammatory response, the dissemination of intravascular coagulation and endothelial dysfunction (Figure 6) [44].

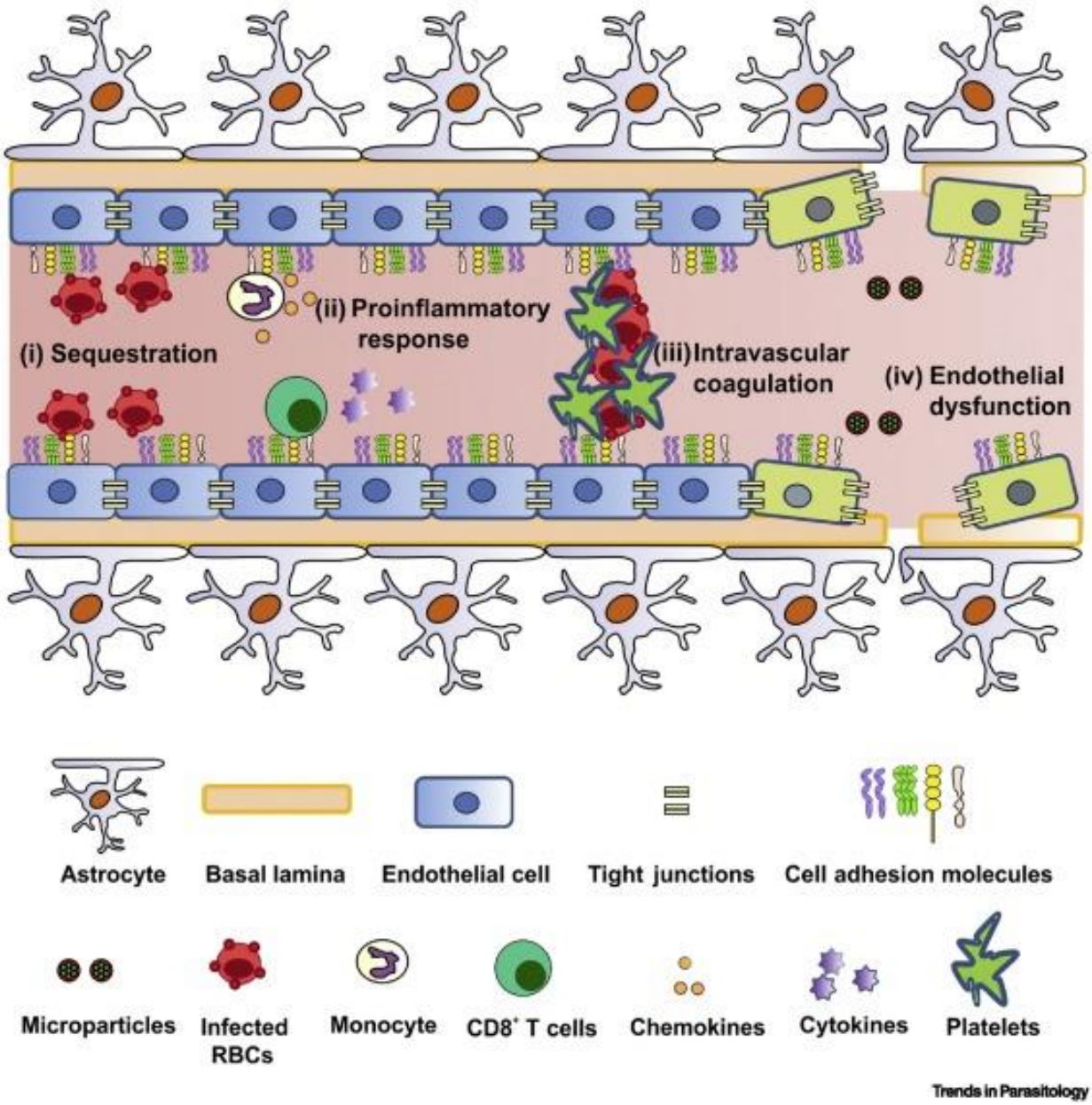

Figure 6 : Mechanisms associated with the destruction of the BBB integrity. Reprinted from (Nishanth et al., 2019) [44].

3.2. Sequestration of iRBCs in brain microvessels

The sequestration of iRBCs in brain microvessels is a hallmark of CM in humans, observed in children and adults who died from CM. The iRBCs containing mature forms of the parasite disappear from the peripheral blood and are found localized in brain microvessels (Figure 7) and other organs, including the heart, lungs and submucosa of the small intestine [45, 46]. The expression of the *P. falciparum* erythrocyte membrane protein-1(*Pf*EMP-1) on the surface of infected erythrocytes allows their binding to different adhesion molecules expressed by ECs

such as VCAM-1, ICAM-1, PECAM-1, E-selectin and EPCR, thereby immobilizing the iRBCs on the vascular endothelium [44]. CM Patients show an expansion of parasites expressing *Pf*EMP1 that bind to both ICAM-1 and EPCR [47, 48] . Sequestered iRBCs partially obstruct the capillaries, thereby severely reducing blood flow. Capillary obstruction may be worsened by decreased erythrocyte deformability and by the rosetting phenomenon, in which iRBCs aggregate with non-parasitized erythrocytes [49].Furthermore, Platelets induce the adhesion of iRBCs to one another, forming large autoagglutinates [50].

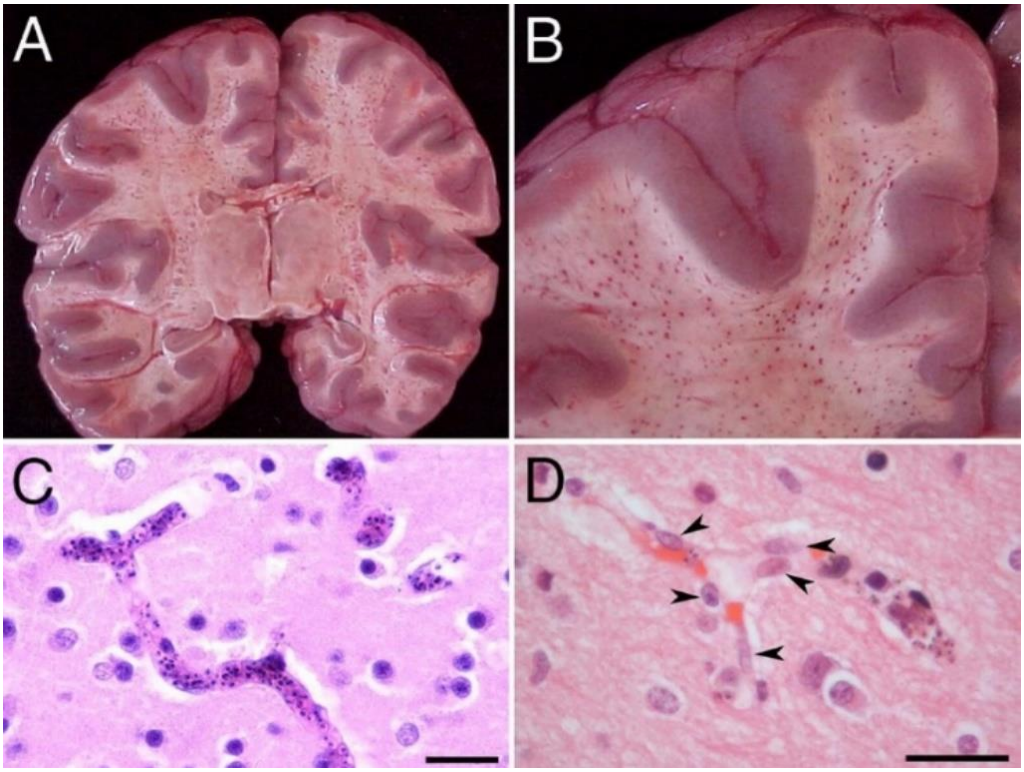

Figure 7: Sections from brain of CM patients showing the distribution of petechial hemorrhages and the sequestration of iRBCs in brain microvessels. Reprinted from (Dorovini-Zis et al., 2011) [51].

In the same way, Baptista *et al*, show that the accumulation of iRBCs in the brain microvasculature is crucial for CM development in mice [2], and that this accumulation was not observed in the brain during *P.berghei* NK65 infection (a line of parasites that does not cause ECM) [52]. In agreement, in ICAM-1$^{-/-}$ mice, the mortality was delayed after *Pb*A infection, which correlated with a decrease of iRBCs sequestration, indicating the importance of this receptor in the pathophysiology of ECM [53]. Notably, the sequestration of iRBCs during ECM can be prevented by using of drugs such as rapamycin and ethanolic extracts of

the fungus *Trichoderma stromaticum*. These treatments prevent the cytoadherence of iRBCs by reducing the expression of ICAM-1 and VCAM-1 [54, 55].

Binding of *Pf*EMP1 to the receptors on the ECs may trigger multiple signaling pathways in ECs, resulting in the reorganization of tight-junction complexes, ultimately leading to the BBB disruption [44]. *In vitro* studies using human and mouse ECs have shown that ICAM-1 is responsible for rearrangements of the cytoskeleton of ECs by Rho-dependent phosphorylation of cytoskeleton-associated proteins, including FAK, paxillin, p130 Cas, and cortactin resulting in loosening of tight junctions. Moreover, studies on human ECs showed that the interaction of *Pf*EMP1 with the EPCR receptor results in the activation of tissue factors VIII a and V a, leading to the generation of thrombin and fibrin, which in turn promotes the activation of NF-κB pathway, inducing a proinflammatory response that disrupts the BBB (Figure 8) [44, 56].

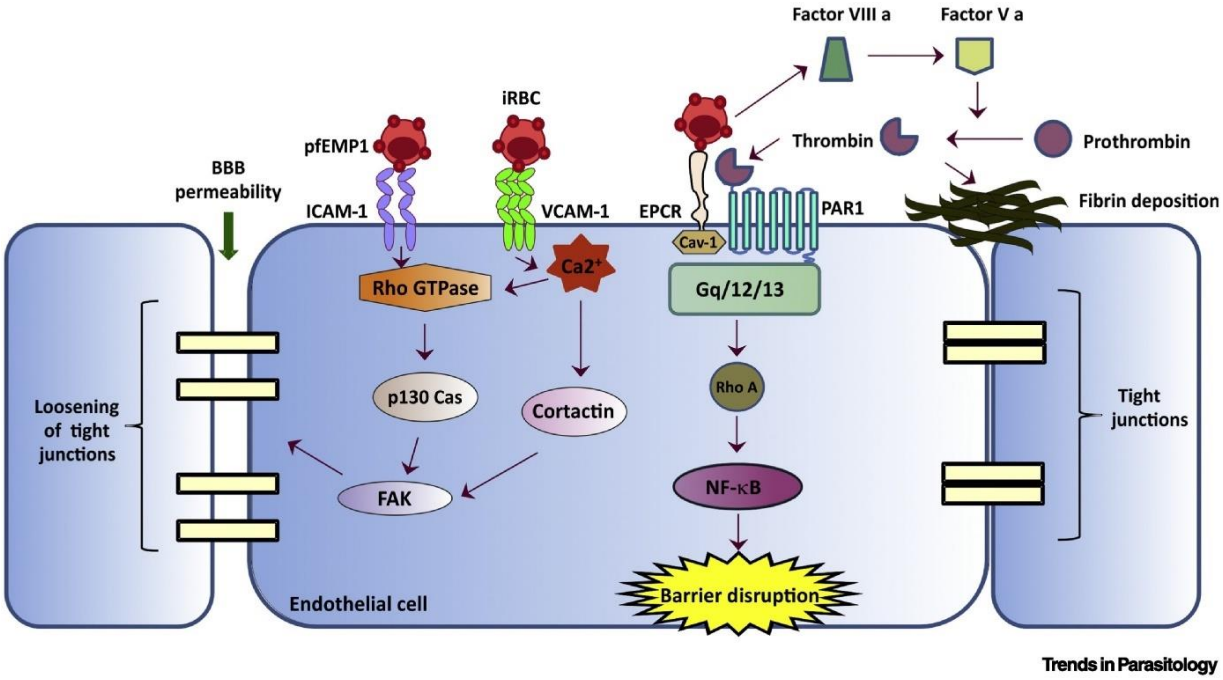

Figure 8: Mechanism of sequestration of iRBCs in the brain. Reprinted from (Nishanth et al., 2019) [44].

3.3. Inflammation and endothelial activation

Another feature associated with CM is the intracerebral inflammation caused by a heightened proinflammatory immune response. Several studies show that proinflammatory cytokines such as TNF, lymphotoxin α (LTα), interferon-γ (IFN-γ), interleukin-1α (IL-1α), and interleukin-1β (IL-1β) are upregulated during CM and play a pathogenic role in the disease [57]. TNF levels are high in the plasma of CM patients. Of note, despite an association of TNF with disease

severity, the treatment with anti-TNF does not protect from CM [58]. Furthermore, LTα knockout mice are completely protected from ECM. LTα can upregulate the expression of ICAM, thereby fostering the intracerebral recruitment of leukocytes [59]. Monocytes and macrophages in the brain produce proinflammatory cytokines such as IL-1α and IL-1β [44, 57, 60]. These cytokines can activate the ECs, which release chemokines such as CCL-2, CCL-4, CXCL-4, CXCL-8, and CXCL-10 and contribute to the recruitment of leukocytes in the brain [57]. Accordingly, the deletion CCL-2, CCL-4, CXCL-4, CXCL-8, and CXCL-10 reduces ECM pathology [57]. Recruited leukocytes may secrete cytokines and chemokines, exacerbating local inflammation, endothelial activation, and disruption of the BBB (Figure 9). For example, potential endothelial cell-induced recruitment of CXCL10-expressing neutrophils and monocytes may promote further recruitment of CXCR3 cells, such as Natural killer (NK) and T cells, to the brain [57].

Several studies have shown the sequestration of leukocytes and platelets in the brain of patients who died from CM [51, 61]. However these observations are not universal [62, 63]. The accumulation of leukocytes or platelets was not observed in Thailand adult patients [63]. However, during ECM, transmigration of leukocytes into the brain appears simultaneously as the neurological signs [64]. It has been documented that Neuregulin-1 treatment protected mice from CM by reducing the expression of the proinflammatory cytokines such as TNF, IL-6, IL-1α and the chemokine CXCL-10, thus decreasing leukocyte accumulation in the brain [65].

3.4. T Lymphocytes

Our lab and other groups have shown an accumulation of CD4 and CD8 T cells in the brain of mice during CM [64, 66-70]. Supporting evidence has been obtained by depleting of CD4 or CD8 T cells or using CD8-deficient mice. In these models, infected mice were protected from ECM [66, 71]. CD8 T cells isolated from the brains of mice developing CM exhibited an activated phenotype, as demonstrated by the expression of the CD69 and CD25 surface markers. Nevertheless, these cells may constitute a source of proinflammatory cytokines such as IFN-γ and TNF-α, which play an important role in CM pathogenesis [70]. In addition, our lab has shown that *Pb*A infection induces an expansion of the CD4 + CD25 ^{high} T cell subpopulation expressing Foxp3 in the spleens of C57BL/6 mice. Surprisingly, these cells do not migrate to the brain at the time of neurological symptoms and did not able to prevent the pathogenic T cell response associated with CM [72]. It has been documented that CD8 T cells participate in the pathogenesis of CM by fostering leukocyte accumulation and their production

of perforin/granzyme B [44]. During ECM, most of CD8 T cells that migrate into the brain express perforin [73]. Adoptive transfer of CD8 T cells isolated from C57BL/6 infected mice induces CM in RAG2-KO mice (mice resistant to ECM due to a lack of T and B lymphocytes) [68]. CM's development also depends on perforin because the adoptive transfer of CD8 T cells isolated from perforin-deficient mice into RAG2-KO did not cause ECM [68]. Other studies show that Granzyme B is essential for the development of CM [74]. The mice deficient in Granzyme B are resistant to CM [74]. Together, these results suggest that the cytotoxic activity of CD8 T cells is implicated in the pathogenesis of ECM. This cytotoxic activity induces endothelial apoptosis (Figure 9) [44]. Baptista *et al*, have shown that the depletion of CD8 T cells protected mice from ECM and decreased the accumulation of iRBCs in the brain. Additionally, they demonstrated that the treatment of mice with antimalarial did not change the number of CD8 T cells in the brain [2], suggesting that the concomitant presence of both CD8 T cells and iRBCs in the brain plays a crucial role in the development of ECM [75]. The chemokine receptor CXCR3 has been shown to play an integral role in the trafficking of pathogenic T cells to the brain. The inhibition of protein tyrosine phosphatase activity prevented ECM by reducing CXCR3 expression on T cells, thereby impairing their recruitment to the brain [75].

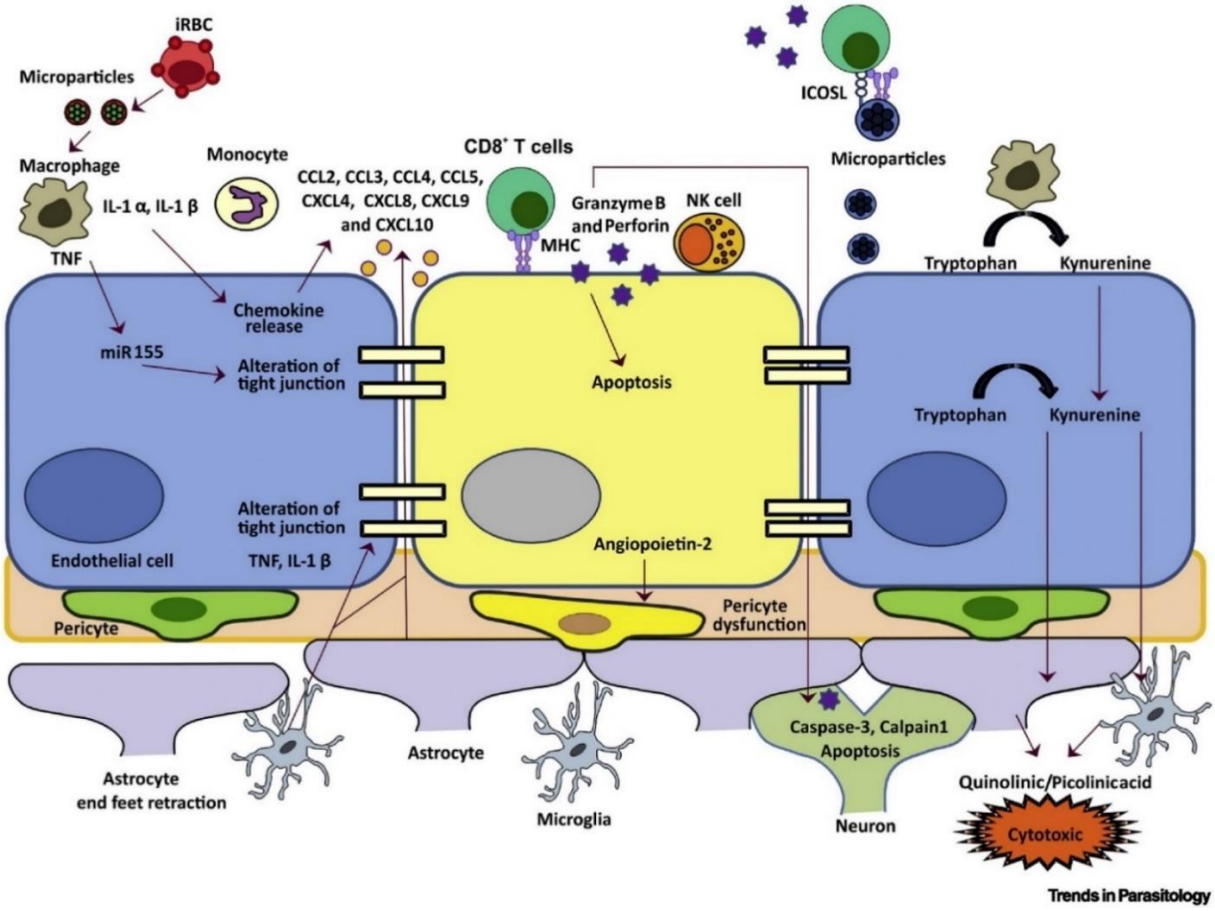

Figure 9: Molecular mechanisms implicated in the breakdown of the BBB. Reprinted from from (Nishanth et al., 2019) [44].

3.5. Activation of glial cells and neuroinflammation

Astrocytes are one of the most abundant glial cells, representing 20-40% of total brain cells. They are a heterogeneous population that varies according to species and brain areas [76]. Astrocytes have been divided into two subtypes: *Protoplasmic* and *fibrous*, based on their morphological characteristics and localization. *Protoplasmic astrocytes* are mainly located in grey matter and exhibit a morphology of several stem branches that give rise to many finely branching processes in a uniform globoid distribution (Figure 10). However, *Fibrous astrocytes* are found in the white matter and exhibit a morphology of many long fiber-like processes (Figure 10) [77, 78]. A recent single-cell RNA sequencing study showed five different astrocyte populations in the adult mice brain [79].

Astrocytes are involved in a myriad of functions in the CNS to maintain homeostasis and support neuronal function, as well as the maintenance of BBB integrity [78, 80]. Astrocytes are also primary immune effector cells of the CNS. They are involved in many CNS pathology [80, 81]. Astrocytes can be activated in in response to brain injury, and undergo a morphologic and

functional change known as astrogliosis. This process is characterized increased of Glial Fibrillary Acidic Protein (GFAP) [82]. Reactive astrocytes have recently been classified as A1 and A2. According to Liddelow *et al*., A1 astrocytes released a neurotoxin that caused apoptosis of neurons and oligodendrocytes [83]. However, during ischemia, A2 astrocytes promote neuronal survival and tissue repair [83]. These findings suggest that astrocytes can play a neuroprotective or detrimental function in the brain during various neurological disorders [84].

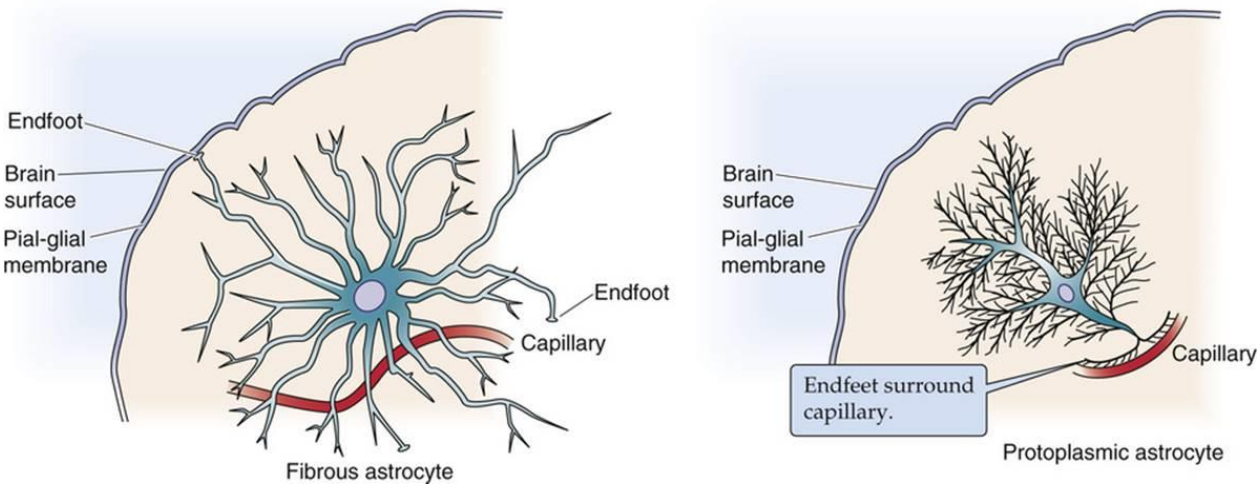

Figure 10: Schema of fibrous (left) and protoplasmic (right) astrocyte (Reprinted from Medical Physiology, 3rd Edition Glial Cells).

Microglial cells represent 5-20% of the total glial cells in the brain[85]. Like astrocytes, multiple microglia types exist and vary between the different CNS regions [86]. Microglia were seen in grey rather than white matter [84]. In white matter, microglia show elongated somatic and process-oriented along fibers. Microglia exhibit a compact morphology in the periventricular organs with few short processes. In the grey matter, microglia are radially ramified. Microglia can be activated upon acute brain injury. They undergo morphological changes, reduce the number of processes and release pro- and anti-inflammatory cytokines [87].

The activation of astrocytes and microglia has been observed in both human and murine CM. An increase in activated astrocytes has been observed in Vietnamese patients who died from severe malaria [88] and in the brains of Malawian children who died from CM [51]. An accumulation of activated microglia in microvessels containing sequestered parasites was reported, too [89]. Microglia adopt an amoeboid form and express the MHC class II and CD68, in CM patients. These changes induce their activation and stimulation of their phagocytic activity[90]. These studies did not address the effects of activating these cells on the brain. This

may be large because post-mortem brain tissues from CM patients are not easily accessible. Due to these limitations, most of the research on the function of glial cells in the pathogenesis of CM has been conducted using ECM.

During ECM, astrocytes and microglia are activated before the onset of neurological symptoms (at 2-3 dpi) [91, 92]. As ECM progressed, morphologic changes in microglia were observed, including retraction of ramified processes, soma enlargement, an amoeboid appearance, and vacuolation [92]. Additionally, at 5dpi, mouse brain sections showed increased in TNF-α expression by activated astrocytes and microglia [85]. The production of TNF and IL-1β by microglia impair BBB integrity by altering the expression of tight-junction proteins such as zona occludens-1, claudin-5, occluding, and P-glycoprotein 1 (Figure 9) [44]. Furthermore, a genome-wide transcriptomic analysis of the microglia of *Pb*A-infected mice revealed upregulation of CXCL-9, CXCL-10, CCL-8, and CCL-12 [93]. In our laboratory, we are particularly interested in the role of astrocytes and microglia during CM. Results previously obtained showed that the stimulation of astrocytes and microglia by *Pb*A-iRBCs induces a dynamic transfer of vesicles from the parasite to astrocytes and phagocytosis of *Pb*A-iRBCs by microglia. This was accompanied by a morphological change in the microglia. These mechanisms are associated with a significant increase in the production of TNF-α and CXCL-10 [4]. Interestingly, microvesicles were transferred from the parasite to the astrocytes via a non-conventional autophagy pathway involving LC3 (microtubule-associated protein 1 light chain 3). This process involved parasite degradation within astrocytes and was associated with the production of CCL-2 and CXCL-10. The inhibition of autophagy by treatment of stimulated astrocytes with 3-methyladenine, inhibits the transfer of parasitic microvesicles (*Pb*A-MVs) and the production of CCL-2 and CXCL-10. Moreover, inhibiting autophagy by treating infected mice with Bafilomycin A1, protected the mice from ECM [94]. The upregulation of CXCL-10 by activated glial cells could induce the recruitment of CD8 T cells to the brain by binding to CXCR3 highly expressed on the surface of CD8 T cells leading to ECM [84]. Infected CXCL10-deficiency mice are resistant to ECM. Furthermore, this protection from ECM was associated with decreased in leukocyte sequestration in the brain [95]. CXCL-10 levels have significantly increased in the serum and CSF of CM Children from Ghana [96], as well as in the serum of CM patients from India [97]

Knowledge of the role of astrocytes in the pathogenesis of ECM is limited, and further studies are needed to pinpoint the exact mechanisms underlying the inflammatory response of astrocytes. That can be an attractive strategy for the design of novel therapeutics.

Herein, we investigated whether cellular senescence of astrocytes participated in the brain inflammation involved in CM pathogenesis.

3.6. Pericytes dysfunction

Pericytes are perivascular cells surrounding the ECs and communicate with various parenchymal brain cells such as astrocytes, microglia and neurons (Figure 5). They play a role in the regulation of blood flow and the maintenance of CNS homeostasis. They maintain BBB integrity by inducing the expression of tight junction proteins in brain ECs [98] and regulating the expression of angiopoietin and plasmalemma vesicle associated protein-1, which are involved in vascular permeability [99]. Angiopoietin-1 stabilizes the BBB, whereas angiopoietin-2 weakens the interaction between pericytes and ECs, resulting in BBB dysfunction. During CM, angiopoietin-1 levels are reduced, while angiopoietin-2 levels are elevated, which indicating pericyte dysfunction [100-103]. The exact role of pericytes in the context of Malaria is unknown. TGF-β has been shown to induce the expression of proinflammatory cytokines by pericytes, which may lead to BBB disruption [104]. On the other hand, pericytes downregulate the expression of adhesion molecules on ECs, which may prevent leukocyte recruitment and preserve the integrity of the BBB [104]. More research is needed to understand better the role of pericytes in the pathogenesis of CM.

3.7. Disruption of Axonal flux, demyelination of axons

Myelin is primarily composed of sphingomyelin and participates in maintaining neuronal fibers by covering axons and promoting the faster transmission of nerve impulses. Destroying myelin disrupts the axonal flow, leading to neurodegenerative diseases [105]. Axonal injury and demyelination of neurons are standard features of the pathophysiology of human and murine CM. Axonal damage, demyelination, and ring hemorrhages were found in the postmortem brain tissue of Vietnamese adults who died from CM [88]. The dosage of tau, a protein involved in the maintenance of axonal microtubules, revealed axonal injury during human CM. Tau concentrations in the CSF of P. *falciparum* patients increase with severity and coma duration [106, 107]. Axonal injury and demyelination of neurons have also been reported during ECM [52].

3.8. Neuronal Death

Neurons are vitally important to brain cells which process and transmit information to other cells. They directly regulate the BBB permeability via ECs innervations[108]. Furthermore, neurons control CNS blood flow and the transport of oxygen and glucose to different brain regions. Neuronal dysfunction and cell death may be responsible for the neurological complications of CM. During ECM, granzyme-B, produced by pathogenic CD8 T cells, kills neurons directly via its cytotoxic function and activates neuronal caspase-3 and calpain1 (Figure 9)[109]. As a result, inhibiting granzyme-B would be an option for preventing neuronal cell death. Administration of ethanolic extracts of the plant *Azadirachta indica* reduced neuroinflammation and brain edema and protected neurons from apoptosis during ECM [44, 110].

4. Post CM neuro-sequelae

Post-CM, up to 25% of paediatric survivors experience persistent neurologic sequelae such as cognitive impairment, motor skills, visual coordination, seizures, and attention deficit hyperactivity disorder [8, 111-114]. Children under five were at the most significant risk of deficits in motor, language, and social development [115]. Cognitive deficits specific to working memory can worsen between 3 and 6 months after infection, with language development being the most consistently affected in paediatric survivors[9, 116-118]. Cognitive impairments, including memory and attention, can last up to nine years after a CM episode [8, 113]. In one study, 10% of paediatric CM survivors had at least one mental health sequela, with onset ranging from six to twelve months after infection and a median follow-up of 21 months. Attention deficit hyperactivity disorder, conduct disorder, and oppositional defiant disorder were the three most common mental health disorders in this group[118]. Patients with increased externalizing behaviors (poor attention and aggression) after CM have also been reported [10, 115]. Seizures are common in children with CM, and as a result, long-term seizure disorders, often resistant to at least one antiepileptic drug, can develop months after a CM episode [8, 112, 113, 119]. Seizures may contribute to developing of other neurological sequelae following CM, such as developmental delays [9, 112].

*Pb*A-infected C57BL/6 mice display behavioral impairments, such as ataxia, hemiparaplegias, and seizures, comparable to those observed in humans infected with *P. falciparum* [9, 36, 120]. According to a study by Desruisseaux *et al*., infected mice exhibit cognitive deficits (decrease in working memory) at 5dpi, that are associated with inflammation, hemorrhage, microglial activation and neuronal death. [11]. As the syndrome worsens, C57BL/6 mice with CM

experience a wide range of behavioral and functional changes and significant impairment in all functional categories when tested 36 hours before death [120]. However, the brain areas damaged during CM known to be important for memory are the fornix, cortex, and hippocampus[121]. Before neurological changes occur, astrocytes and microglia are activated, particularly in these areas [122, 123]. Additionally, it has been demonstrated that treating the parasitic infection does not prevent the development of late cognitive sequelae once ECM is established. Furthermore, C57BL/6 mice infected by Pch (a *Plasmodium* strain that does not induce CM), BALB/c mice infected by *Pb*A or non-lethal *Plasmodium yoelii NXL*, who do not develop CM, showed no persistent cognitive impairment, indicating that cognitive impairment was associated with the development of CM [12]. Several studies have shown increased in anxiety-like behavior after *Pb*A infection resolution [124]. Increased brain-cortical TNF levels, together with increases in IL-6, IL-1β levels, and changes in growth factor levels, can all contribute to the development of anxiety behavioral sequelae in ECM model [124-126]. Miranda *et al*. showed that *Pb*A-infected mice also had significant impairment in short-term aversive memory, which was accompanied by increased mRNA expression of inflammatory cytokines in the frontal cortex and hippocampus [127]. Increased levels of inflammatory cytokines (IL-6, TNF-a, IFN-γ, and CCL11) in the frontal cortex and hippocampus are linked to altered neurotrophin expression (such as BDNF), decreased hippocampal neurogenesis, and increased hippocampal cell death, which impairs memory during CM [127]. Even after complete parasitemia clearance with chloroquine therapy, BDNF levels remained low in the hippocampus of CM mice, which were associated with long-term cognitive deficits [128]. A recent study shows that the IL-33/ST2 pathway through glial cells is involved in neurocognitive impairments during ECM. IL-33 promotes the release of inflammatory cytokine by microglia (such as IL-1β, TNF-α and IFN-γ), which affects neurogenesis and cognitive processes. Furthermore, IL-1β produced by microglia stimulates oligodendrocytes to produce IL-33, resulting in an amplification loop that may affect myelination and cognition[129]. However, the mechanisms underlying neurocognitive impairments during the development of CM remain unknown.

The role of glial cells in the development of neurological sequelae need more dedication in research. Understanding of how the *Plasmodium* parasite can interact with glial cells to cause neurological damage during CM is essential. It could lead to the development of adjunct therapies that can help alleviate the burden of neurological sequelae in patients who survive from CM.

Chapter 3: Cellular Senescence

1. Definition of senescence

Senescence is derived from the Latin word "senex", which means "old man" or "old age." [130]. This process was first discovered by Hayflick and Moorhead in 1961; they demonstrated that after a certain number of serial passages (40 to 60), normal human fibroblasts stop dividing in vitro, reaching a limit called (Hayflick limit) [131], which results in replicative senescence. The concept of cellular senescence was later expanded to include premature-cellular senescence (or stress-induced senescence), which occurs in a variety of cells when they are exposed to stressors including oxidative stress, DNA damage, oncogenic activation, radiation, inflammation etc. (Figure 11) [13].

Although Hayflick's original definition of senescence was limited to a stable cessation of proliferation, more recent research has revealed that senescent cells share other characteristics, including cell hypertrophy, apoptosis resistance, Senescence-associated heterochromatin foci (SAHF) formation, increased activity of senescence-associated β-galactosidase (SA-β-Gal), DNA damage, metabolic change and nuclear alterations (Figure 11) [13]. These cells secrete a bioactive SASP (senescence-associated secretory senescence), which comprises of an extensive repertoire of pro -inflammatory factors and can act in an autocrine and paracrine manner to reinforce senescence and to spread this phenotype to neighboring cells and alter the microenvironment [132].

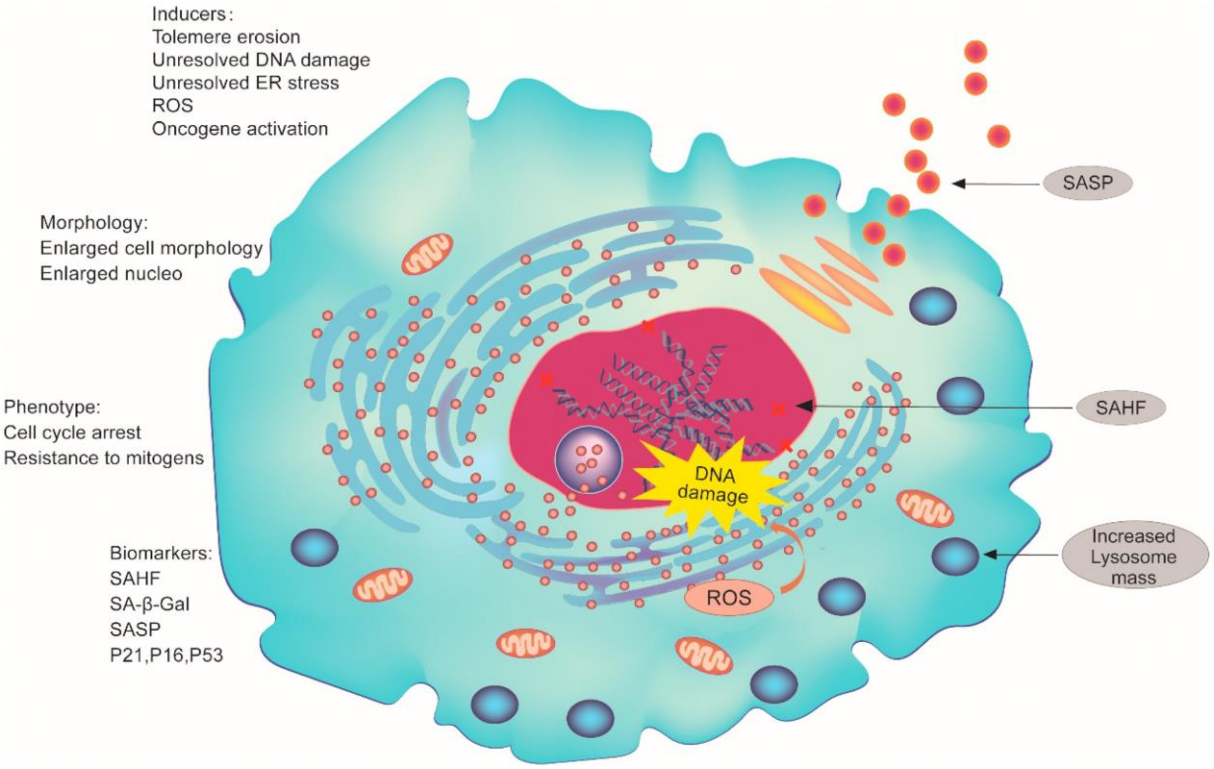

Figure 11: Characteristics of senescent cells. Reprinted from (Zhanget al., 2021) [133].

2. Characteristics of Senescence

2.1. Morphological change

Senescent cells have distinct morphological changes, including increased size and flattened morphology, enlarged and multinucleated nuclei [13]. The activation of the mTOR pathway (Mammalian Target of Rapamycin), a serine/threonine kinase, is necessary for the enlargement of the endothelial senescent cell body [134]. Senescent cells' altered shapes are linked to cytoskeleton rearrangement, which includes increased vimentin expression [13]. In addition, the upregulation of caveolin-1, a component of the plasma membrane, influences the morphology of senescent cells. Caveolin-1 appears to be upregulated by p38 mitogen-activated protein kinases (p38MAPK) [135]. Changes in size and morphology are easily measured with either routine or fluorescent microscopy but are challenging to detect and quantify *in vivo* or *in situ* [13]. According to a recent study, increased cell size may play a causal role in senescence-associated growth arrest[136].

2.2. Senescence- associated β- Galactosidase activity

Senescent cells are characterized by an increase of SA-β-Gal activity (a lysosomal enzyme), encoded by the GLB1 gene. This marker is commonly used *in vitro* and *in vivo* [137, 138]. SA-β-Gal activity is observed at pH 4 in normal cells. It is significantly amplified in senescent cells due to increased lysosomal content and is detectable at pH 6. This activity can also be detected in quiescence or confluence under certain conditions [139].

Using chromogenic substrate 5-bromo-4-chloro-3-indolyl β-galactopyranoside (X-gal), cleaved by β-galactosidase and results in the generation of a blue label perinuclear in senescent cells (Figure 12). However, this marker cannot be used on paraffin-embedded tissue sections or live cells, severely limiting its application [13].

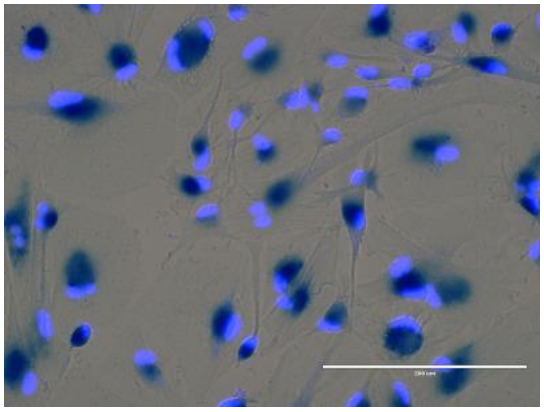

Figure 12 : SA-β-Gal staining in human senescent astrocytes. Reprinted from (Wissler Gerdes et al., 2021) [140].

2.3. DNA damage response (DDR)

Double-strand DNA breaks (DSBs) are potent activators of DDR and can lead to cellular senescence when unresolved. DSBs promote the recruitment and binding of Ataxia Telengectasia Mutated (ATM) kinase to the DNA damage site [141, 142]. This recruitment drives the phosphorylation of the histone H2AX, which facilitates the assembly of specific DNA repair complexes [143]. A complex of kap-1, heterochromatin protein 1 (HP1), and the H3K9 methyltransferase suv39h1 is loaded directly onto the chromatin at DSBs, resulting in the methylation of H3K9. Histone methylation can also aid in the assembly of damage response components. H3K9me3 acts as a binding site for the acetyltransferase Tip60, which then acetylates and activates ATM [144]. As a result, H3K9 methylation is required for ATM-

mediated DNA damage signaling during the early stages of the DDR, but it must be later reversed to promote the repair process. DDR causes G9a/GLP methyltransferase degradation, which results in a global reduction in H3K9 dimethylation, including IL-6 and IL-8 promoters, two components of the SASP [145]. ATM phosphorylates many substrates, including the two essential kinases CHK1 and CHK2, which propagate the signal by further phosphorylating their substrates [146, 147]. The persistence of DDR induces the phosphorylation of p53 at multiple serine residues, which enhances the ability of p53 to induce the transcription of many genes[148].

The level of phosphorylated p53, a key signaling player for the DDR, can be used as a senescence marker [149] or the presence of γ-H2AX foci measured by immunostaining [150]is used as a senescence marker.

However, the DDR is activated by various DNA-damaging stimuli that do not lead cells into a senescent state. Moreover, not all senescence programs are a consequence of DDR [13].

2.4. Cell cycle arrest

Cell cycle arrest is one of the most defining hallmarks of cellular senescence identified *in vivo* and *in vitro*. Senescent cells are typically arrested in the G1 phase of the cell cycle, but some cells enter senescence at the G2 or S phases. The two major pathways in cell cycle arrest are $p16^{INK4a}$/pRb and p53/ $p21^{WAF1/CIP1}$.

➢ P53/p21 pathway

In response to DNA damage induced by telomere attrition and oxidative or carcinogenic stress, the p53/$p21^{WAF1/CIP1}$ pathway is activated. Constitutive DDR signaling drives cellular senescence by chronically activating p53. However, the inactivation of p53- mediated signaling by a variety of approaches can disrupt the onset of cellular senescence [151, 152]. Activation of p53 depends on various post- translational modifications, including phosphorylation, acetylation, methylation ect..[153]. It has been reported that ATM kinase induces the phosphorylation of p53 on serine 15; this modification prevents the interaction of p53 with the E3 ubiquitin ligase Mdm2 responsible for its degradation. This allows the accumulation of p53 and increases its ability to activate the transcription of its target genes [153]. Indeed, the tumor suppressor p53 [154] can regulate the transcription of genes involved in blocking cell division, including the Cdkn1a gene, which encodes for the $p21^{CIP1}$ protein [155].

The p21 protein is a Cyclin-dependent kinase inhibitor (CDKI) of the Cip/Kip family ($p21^{CIP1}$, $p27^{KIP1}$ and $p57^{KIP2}$), leads to cell cycle arrest in the G1 phase [156]. This protein can inhibit cyclin-dependent kinases (CDKs) CDK4/CDK6 and CDK2, which are involved in cell cycle progression through inhibition of retinoblastoma protein (pRB) (Figure 13). pRB is essential to control the cell cycle since it is a strong repressor of the expression of E2F, a transcription factor involved in the synthesis of DNA and the progression in the cell cycle, by the transition from the G1 phase to the S phase [157]. The measurement of the activation of this cellular pathway constitutes a signature of senescence [158].

Growth Arrest and DNA Damage-inducible (GADD45) is another p53 target. GADD45 gene family encodes three proteins: GADD45α, GADD45β and GADD45γ. GADD45 is involved in regulating of two checkpoints, G1/S and G2/M. Overexpression of the three GADD45 isoforms in cancer cell lines results in an accumulation of cells arrested in the G1 phase [159]. Microinjection of the GADD45α expression vector into human fibroblasts causes cell cycle arrest in the G2/M phase [160]. GADD45 can interact with several proteins, including protein kinase cell division cycle 2 (Cdc2) and p21. The interaction of GADD45 with the Cdc2/cyclin B1 kinase complex is responsible for the G2/M cell cycle arrest through dissociating of the kinase complex and inhibiting of Cdc2 kinase activity. The interaction of GADD45 with p21 may induce the G1 arrest [161].

➢ P16 pathway

Cell cycle arrest during senescence may also be the consequence of the activation of p53/p21-independent cellular pathways, such as the expression of INK4 family CDKi [162]. INK4/ARF locus encodes three tumor suppressors, $p16^{INK4A}$ and $p14^{ARF}$ encoded by CDKN2A gene and $p15^{INK4B}$ by CDKN2B gene. Their expression varies depending on the cell type and the inducing signal [163]. Similar to p21, $p16^{INK4a}$ and $p15^{INK4B}$ can inhibit CDK4/CDK6 and promote cell cycle arrest by hypophosphorylation of pRb (Figure 13) [164] . $p14^{ARF}$, on the other hand, regulates the stability of p53 by binding to and suppressing Mdm2, which is responsible for its proteasome-mediated destruction [163]. In contrast to DNA damage-induced senescence, which is mostly mediated by $p21^{WAF1/CIP1}$, epigenetically induced senescence is primarily mediated by $p16^{INK4A}$ expression [165]. $p16^{Ink4a}$/pRb pathway is usually activated in replicative senescence, ROS-induced senescence and Oncogene-induced senescence (OIS), but not during DDR-induced senescence[151, 166, 167].

Two types of assays are typically utilized to demonstrate that cells have exited the cell cycle. The first comprises direct measurements of cell proliferation potential via colony- formation assays or DNA synthesis rate by BrdU/EdU incorporation assays. The second involves assessing the CDKIs p16 and p21's expression levels [150, 168].

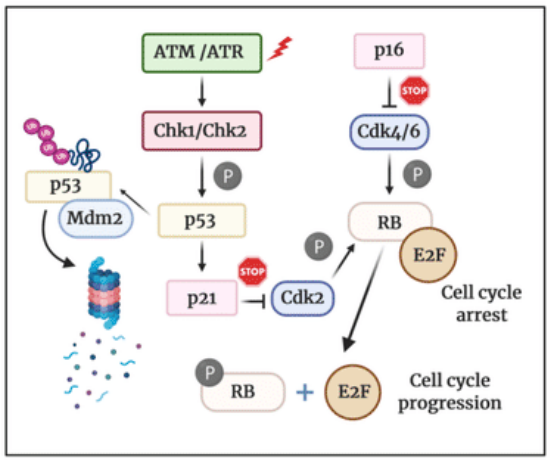

Figure 13 : Cell cycle arrest pathway. Adapted from (Demirci et al., 2021) [169].

2.5. Apoptosis resistance

Senescent cells activate several prosurvival pathways and become resistant to apoptosis [170]. Following a proapoptotic signal, BAX and BAK form a channel that permeabilizes the outer membrane of mitochondria allowing the release of cytochrome C. This then associates with APAF-1 to form the apoptosome, which activates procaspase 9 to caspase 9, which activates the caspases effectors of apoptosis, namely caspases 3 and 7. In senescent cells, overexpression of antiapoptotic proteins of the BCL-2 family, which by heterodimerization, inhibit BAX and BAK (Figure 14) [171].

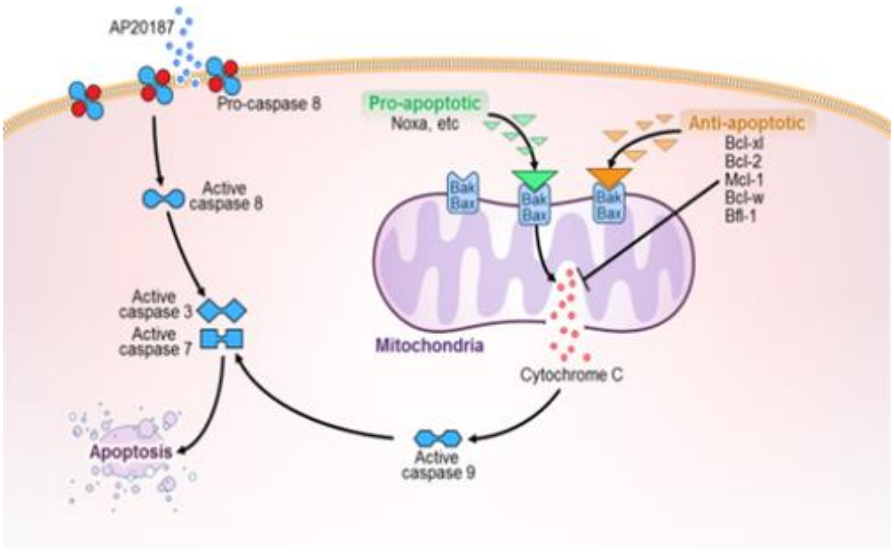

Figure 14: Apoptotic pathway. Reprinted from (Yi Zhu et al., 2016) [171].

Antiapoptotic BCL-X and BCL-W (BCL-2 family members) are necessary for senescent cell survival, located on the membranes of mitochondria and the endoplasmic reticulum. They are transcriptionally upregulated during cellular senescence [172, 173].

It has been described that p53/p21^{CIP1} pathway plays a major role in the choice between survival/apoptosis cells. Apoptosis is a mechanism that depends on the activation of genes encoding pro-apoptotic (BAX, PUMA, NOXA), which can be directly regulated by p53 [174, 175]. Furthermore, p53 also regulates p21, which is implicated in cell survival [176]. The regulatory pattern of p53 is oriented toward an apoptotic profile (BAX, PUMA, NOXA) or survival (p21), depending on the triggering signal [170, 177]. Finally, p53's cellular location plays a role in apoptotic resistance. Indeed, a recent study revealed the importance of p53 sequestration at the nuclear level via its association with FOXO4 in mechanisms of resistance to apoptosis [178]. This ability to resist apoptosis is also the Achilles heel of senescent cells since very recent work aimed at developing processes for the specific elimination of these cells uses this feature [179].

Induction of expression of members of the BCL-2 anti-apoptotic family may thus be used to identify senescent cells [13].

2.6. Senescence-Associated Heterochromatin-Foci (SAHF)

Another feature of senescent cells is the downregulation of the protein lamin B1, a significant nuclear lamina component. Lamin B1 is essential for the nucleus' structural integrity. However, in senescent cells, this integrity is disrupted, allowing the release of cytoplasmic chromatin fragments outside the nucleus, which is supposed to fuel the SASP via the cGAS/STING pathway [180]. The downregulation of Lamin B1 is known to cause global and local chromatin alterations that affect gene expression and promote SAHF formation [152, 181]. The term heterochromatin defines the areas of chromatin condensed and considered to be transcriptionally inactive. The SAHF contains proteins characteristic of heterochromatin: HP1, histone variant macroH2A and methylated histone 3 on the lysine 9 (H3K9m) [182]. The formation of SAHFs is controlled by the chromatin regulators HIRA (Histone cell cycle regulation defective A) and ASF1a (Anti-silencing function 1). It requires the presence of nuclear bodies PML (inducer of acute promyelocytic leukemia) for the onset of senescence [183, 184]. SAHFs are particularly involved in the sequestration of cell cycle genes, such as E2F, which can alter their expression [185]. Narita *et al*. showed that the pRb protein plays a vital role in forming SAHF [185].

SAHFs are observed after DAPI (4’,6-diamidino-2-phenylindole) staining as darker regions in the nucleus of senescent cells and are enriched in heterochromatin markers, such as H3K9 and HP1, H3K9 and HP1 can be detected by immunostaining [186]. In addition, the downregulation of Lamin B1 can be identified by immunoassays, immunofluorescence or immunoblotting and is often used as a senescence marker associated with SAHF [166, 187]. However, SAHF is not universal marker of senescence and is mainly observed during OIS and is generally not apparent in mouse senescent cells [150].

2.7. Senescence-associated secretory phenotype (SASP)

Senescent cells are metabolically active and produce a secretory phenotype called SASP. This latter consists of a range of factors, including proinflammatory cytokines, chemokines, proteases, and growth factors. The secreted molecules differ according to the cell type and the senescence-inducing stimulus. Indeed, we do not fully know the mechanisms implicated in the regulation of SASP. Still, several key features have been identified in the literature [152].

SASP is triggered by a variety of nuclear and cytoplasmic factors, including DNA damage, cytoplasmic chromatin fragments (CCFs), transposable elements, and toll-like receptors (TLR).

Various pathways including p38MAPK [188], JAK2/STAT3[189], mTOR [190, 191], phosphoinositide-3-kinase (PI3K) pathway [134], HSP90 [192], GATA4/p62-mediated autophagy [132], macroH2A1 and ATM[193] are all involved in the development and regulation of SASP. The different mechanisms involved in SASP regulation are shown in Figure 15 [152]. The two major factors regulating SASP are NF-κB and C/EBPβ (CCAAT/Enhancer Binding Protein Beta)[194]. The depletion of C/EBPβ substantially reduces the expression of two of the most strongly upregulated SASP cytokines, IL-6 and IL-8 [195] and the inhibition of NF-κB significantly diminishes the levels of ENA-78, NAP-2, CCL-1 and CCL-4, ect.. [196].

A new signaling pathway was recently discovered: "cGAS-STING pathway". It allows the secretion of inflammatory factors during senescence. Indeed, DNA damage associated with the destabilization of the nuclear lamina leads to molecular transfers between the nucleus and the cytoplasm. There are fragments of double-stranded DNA among the molecules that migrate from the nucleus to the cytoplasm. These pieces of DNA are recognized by cGAS, which induces the production of inflammatory cytokines by activating the cGAS-STING pathway. Linking a song of double-stranded DNA to cGAS will induce the production of GMP and cyclic AMP. These molecules will bind and activate the STING. The STING protein can control the production of type I interferon and inflammatory cytokines by regulating IRF3 (Interferon Regulatory Factor 3) and NF-κB, respectively (Figure 15). Using cGAS-/- murine fibroblasts, Yang *et al*, revealed a decrease in the expression of different factors composing the SASP, after chemical treatment or irradiation [197].

Despite the prominent role of DNA damage, NF-κB and C/EBP-β, SASP is also regulated by many other proteins, including mTOR, via two mechanisms: by inducing the translation of IL-1α, which activates NF-κB and C/EBPβ or indirectly, by inhibition of ZFP36L1 protein, which prevents the degradation of SASP mRNA [13, 191].

Indeed, the activation of p38MAPK was shown to be necessary and sufficient to cause growth arrest and SASP, even without DNA damage [198]. The inhibition of p38MAPK during oncogenic or irradiation-induced senescence significantly limits the secretion of the main components of SASP[199]. Like p38MAPK, ATM and ATR, the DNA damage pathway actors can also regulate the secretory phenotype by averting the degradation of GATA4 by p62. The accumulation of GATA4 promotes the development of SASP by inducing the expression of IL-1α and TRAF3IP2 (Figure 15) [132, 191].

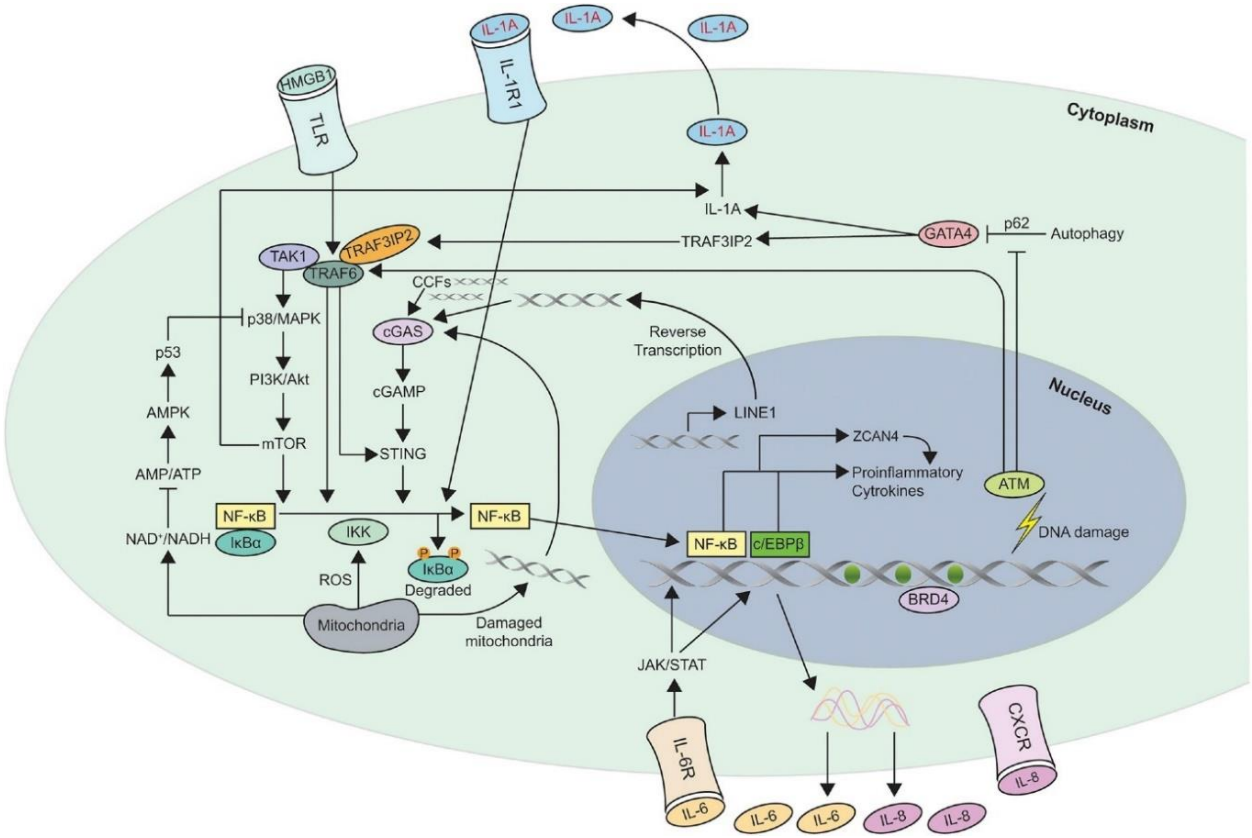

Figure 15: Mechanisms implicated in SASP regulation. Reprinted from (Kumari et al., 2021) [152].

The biological effects of senescent cells are due to the SASP. These effects can be beneficial or deleterious, thus being the key regulator of normal physiology and pathology associated with cellular senescence. As heterogenous SASP's can be in their composition, so are their functions. The functions depend on the genetic context of the cells exposed to SASP and the surrounding environment. In a specific context, the pleiotropic effect of autocrine and paracrine signaling of different SASP factors explains the paradoxical roles of cellular senescence [152].

One of the SASP's primary functions is to recruit innate and adaptive immune cells to eliminate senescent cells (immune clearance)[200]. Among the cells recruited are NK, monocytes/macrophages, B and T lymphocytes, dendritic cells and neutrophils [201]. SASP-mediated recruitment of immune cells will act as an extrinsic tumor suppressor mechanism during the initiation of tumor [200]. On the other hand, SASP-mediated recruitment of immature myeloid cells has immune suppressive effects on prostate and liver cancer [202, 203]. Furthermore, the SASP can promote tumorigenesis through angiogenesis (e.g., via VEGF and CCL5) [204, 205] or tumor growth (e.g., via osteopontin) [206]. Specific SASP components

contribute to fibrotic tissue remodeling and degrade fibrotic scar in the extracellular matrix, which may be beneficial in the context of liver fibrosis and wound healing [207, 208].

On the other hand, prolonged exposure of cells to this cocktail of SASP molecules will make it possible to reinforce senescence in cells, thanks to IL-6 and IL-8 in a phenomenon called autocrine senescence [196, 209]. Beyond the senescent cells, through a phenomenon called paracrine senescence, an increase in SASP secretion will prompt senescence in the surrounding cells [210]. The autocrine or paracrine senescence could explain some adverse effects of aberrant cell accumulation senescent during aging. As such, SASP would be partly responsible for persistent chronic inflammation, also referred to as inflammaging. It also contributes to the multiple phenotypes related to age. In addition to exercising these paracrine and autocrine phenomena that can lead to strengthening the senescence, the composition of SASP differs depending on the type of senescence. It may have either a deleterious or a beneficial role. For example, in the case of osteosarcoma, caused by radiation-induced DNA damage in mice, the secretion of interleukin IL-6 by senescent cells had an anti-tumorigenic effect since it allowed their elimination by recruiting immune cells [211]. Conversely, in thyroid cancer, senescent epithelial cells have a pro-tumorigenic role by the secretion of CXCL-2 since they support tissue invasion and resistance to cell death [212]. Faced with this great heterogeneity of the factors present in the SASP and their difference of expression depending on the cell type and the type of induction of senescence, these do not render unique specific markers of cellular senescence.

3. Inducers of senescence

Senescence is a process linked to organism aging but can be provoked prematurely in different contexts. Three types of senescence have been characterized: Replicative Senescence, stress-induced premature senescence (most often oxidant) and OIS. These stresses induce senescence mainly through their genotoxic effect, a generator of DNA damage. In addition to multiple senescence triggers and senescence-activating pathways, the mechanisms that ultimately lead to senescence vary depending on cell type and conditions [149].

3.1. Replicative senescence (RS)

We owe the discovery of senescence to Leonard Hayflick. He determined *in vitro* that primary diploid fibroblasts have a limited number of doublings after serial passaging in culture. This limited number of doublings is due to telomere shortening. Telomeres are nucleoprotein

structures located at the ends of chromosomes. In adult humans, the length of telomeres is between 3 and 15 kilobases (kb) and is composed of a sequence of six nucleotide repeats 5'-TTAGGG-3'. They form a three-dimensional structure called the T loop (Telomeric): the DNA molecule folds back on itself, and the single-stranded 3' telomeric end inserts into a double-stranded region. The free single-strand ends are then masked. The protein responsible for this conformation is a protein complex called shelterin or telosome. The telosome is composed of six subunits: TRF1 (TTAGGG Repeats Factor 1), TRF2 (TTAGGG Repeats Factor 2), TIN2 (TRF1 Interacting Nuclear factor 2), PTOP (POT1 and TIN2 Organizing Protein), POT1 (Protection Of Telomeres 1) and RAP1 (transcription Repressor/Activator Protein 1) [213]. The main role of telomeres is to protect the integrity of chromosomes. This protection is linked to the formation of the T loop, which prevents chromosomal fusions on the one hand and recognition by the DDR on the other hand. After each division, the telomeres are shortened by a few base pairs [214]. During replication, DNA polymerase needs an RNA primer to exert its activity. At the end of replication, the most distal primer is eliminated, leaving a gap that cannot be filled. This phenomenon is called the end-replication problem. When the telomeres are too short, the telosome cannot form. Since the single-strand end is no longer masked, it is recognized by the DDR. The cell perceives this signal as a double-strand break. This event is the first step triggering the replicative senescence[215]. It only takes one telomere too short to activate the onset of senescence. The size of the telomere of senescent cells is about 1.5 kb.
The DNA damage kinases, including ATM, ATR, CHK1 and CHK2 are the primary DDR mediators, which phosphorylate and activate several cell cycle proteins, including p53. Phosphorylated p53 protein, in turn, promotes the expression of p21, which binds to and inhibits some CDK-cyclin complexes, particularly those involving CDK2[149].

This phenomenon can, however, be circumvented via the expression of telomerase. The telomerase is an enzyme that allows, during replication, to preserve the length of telomeres. This enzyme is made up of two subunits: the RNA or Terc subunit, composed of an RNA of 451 nucleotides which contains the sequence 3'-CAAUCCCAAUC-5' used for the synthesis of telomere repeat; the protein subunit or TerT, with reverse transcriptase activity, ensures the synthesis of the telomeric sequence using RNA subunit as a matrix.

3.2. Stress-induced premature senescence

Replicative senescence is the process by which cells enter senescence after a certain number of divisions. However, it has been also demonstrated that senescence can be induced in response

to stress signals, such as oxidative stress, independently of successive cellular replications. In this context, it is referred to as stress-induced premature senescence (SIPS).
Oxidative stress may be endogenous and associated with aging. In this case, it is moderate and chronic. Also, it can be exogenous, intense and acute, induced by different agents such as ionizing radiation or UV radiation, which in addition to inducing oxidative stress, provokes direct DNA damage such as DSBs or cross-linking points blocking replication forks.

When the cells are exposed to a low dose of H_2O_2, it induces growth arrest and premature senescence. Thus, the treatment with antioxidants delays the entry into senescence. At the molecular level, p53, p21 and the hypophosphorylated form of pRB accumulate during senescence induced by oxidative stress [216]. Mechanistically, high intracellular levels of ROS induced by the RAS–RAF–MEK ERK cascade activate the p38 MAPK, which leads to the increased transcriptional activity of p53 and upregulation of p21 [217].

3.3. Oncogene-induced senescence (OIS)

OIS is a tumor suppressor mechanism blocking cell proliferation via constitutive activation of oncogenes or loss of tumor suppressor function. OIS was first observed on human fibroblasts expressing the oncogenic form of RAS [218]. This phenotype can be brought about by the gain of function of other oncogenes such as $BRAF^{V600E}$, AKT, E2F1/3, cyclin E, MOS (Moloney murine Sarcoma viral oncogene homolog) and CDC6 (Cell Division Cycle 6), but also by the loss of tumor suppressors function, such as PTEN (Phosphatase and Tensin homolog) or NF1 (Neurofibromatosis type 1). She intervenes in the early phases of tumor development by preventing the formation of pre-malignant lesions [219].

3.4. SMS (senescence-messaging secretome)

SASP plays both roles of a senescence phenotype and an inducer. This effect is called the SMS (senescence-messaging secretome) effect. Among the factors that makeup SASP, interleukins 6, 8 and 1α, and IFN-γ can reinforce the senescent phenotype by autocrine effect or induce senescence by the effect of paracrine [209]. Regarding IL-8, it has been shown that it acts via the CXCR2 receptor which induces senescence in a p53-dependent manner [196]. IL-6, meanwhile, would activate, via its IL-6Rα receptor, the JAK/STAT3 pathway leading to the activation of IGFBP5 (Insulin-like Growth Factor Binding Protein 5) [220]. The latter can produce oxidative stress independently of its action on the IGF. This oxidative stress will induce senescence [221].Generally, the IGFBP family proteins, including IGFBP -3, -4, -5, and -7, appear to play a major role in SASP-induced senescence [221-223]. TGF-β also appears to be

able to activate p15 and p21 to induce senescence. This activation is correlated with an increase in oxidative stress. The treatment with antioxidants prevents the activation of p21 and p15 and, therefore, senescence [224]. These different examples of SASP-induced senescence point to a major role of ROS in this induction of senescence [209].

SASP components can also trigger senescence in neighboring cells in a paracrine manner through a mechanism that generates ROS and DNA damage [210, 225, 226].

3.5. Autophagy

Autophagy is derived from the Greek words "auto", meaning self and "phage", meaning eating. It describes the phenomenon by which the cell degrades its components by a mechanism involving lysosomes. This process is designed to maintain organellar and energy turnover during injurious events [227, 228]. Autophagy is frequently activated as part of homeostatic processes in response to cellular stresses, such as hypoxia or nutrient deprivation [229, 230]. There are three types of autophagy: microautophagy, macroautophagy and chaperone-mediated autophagy. Microautophagy is the direct uptake of components to be degraded via lysosomal membrane invagination. Macroautophagy encompasses the damaged organelles, protein aggregates or invading pathogens by a double membrane resulting in the formation of an autophagosome. This autophagosome fuses then with a lysosome to degrade the sequestered components. Autophagy mediated by chaperones (or CMA, Chaperone Mediated Autophagy) requires a KFERQ sequence in the proteins to be degraded. This sequence is recognized by the HSC70 chaperone and directly internalized by the lysosome, where it will be degraded through the LAMP2A receptor (Figure 16).

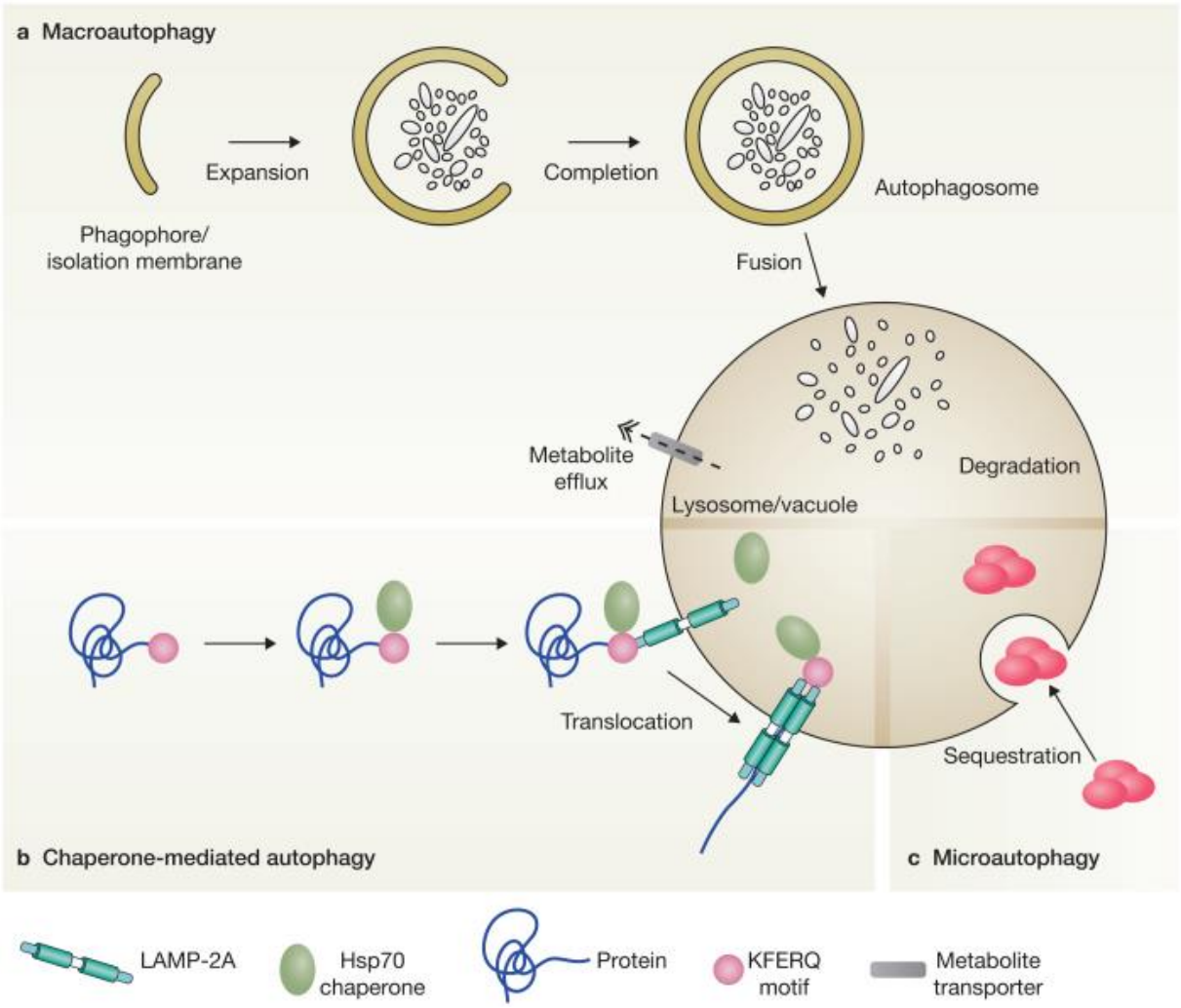

Figure 16: Different types of Autophagy. Reprinted from (Boya et al., 2013) [231].

The role of autophagy in regulating cellular senescence remains uncharted territory even though it has been found to increase senescent cells. However, as with cellular senescence, it has been demonstrated that autophagy can be activated by a variety of stresses, including those that cause cellular senescence. Several groups show that autophagy promotes cellular senescence under several conditions [232]. Narita *et al.*, show that the inhibition of autophagy delays the onset of OIS, particularly the SASP [233]. The same group of authors identified a specialized type of autophagy known as the TOR-autophagy spatial coupling compartment (TASCC), which is responsible for synthesizing of some SASP factors such as IL6 and IL8 proteins [234]. Autophagy can also support senescence by degradation of Δ133p53α, an isoform of p53 that has the property of inhibiting the functions of p53 [235]. In addition, it has been demonstrated that during OIS, Lamin B and a chromatin component known as Lamin-Associated domains (LAD) are transported and degraded in the lysosome by autophagy, reinforcing senescence

[236]. ATG5 (genes involved in autophagy) knockdown reverses OIS, indicating that autophagy positively regulates senescence [232]. Huang *et al*.'s research also demonstrated that suppressing autophagy prevents radiation-induced senescence in cancer cells [237]. Massive SASP factor synthesis can result in unfolded protein response and endoplasmic reticulum stress, leading to proteotoxic stress in senescent cells that can be managed by autophagy [232].

Conversely, some studies suggest that autophagy is an antisenescence phenomenon. Indeed, by ensuring cellular homeostasis through the degradation of molecules and organelles defective such as mitochondria having suffered a drop in membrane potential, autophagy would reduce the oxidative stress which participates in the induction of the senescent phenotype. This has been demonstrated by the inhibition of ATG7 and ATG5 in primary fibroblasts, and this inhibition induces senescence [238].

4. Role of senescence

No particular and unique marker of senescence has yet been discovered. Still, using the multiple phenotypic characteristics described above enabled the *in vivo* study of senescence. These studies have permitted the discovery of physiological and physiopathological implications of this process. With the demonstration of the deleterious role of senescence in recent years, several works have been endeavored to develop treatments that specifically target senescent cells called “senolytics”.

4.1. Benefical effect of senescence

Many studies, as detailed below, show that cellular senescence is important and beneficial to the organism during embryonic development, wound healing, and tumor suppression.

4.1.1. Embryonic development

It is widely known that senescence responds to various stresses in adult tissues. In November 2013, two studies showed a new role of senescence in the embryological development of mice. The presence of senescent cells was detected in many tissues using SA-β-Gal staining. These cells were also characterized by the absence of the marker associated with proliferation (Ki67)

and the increased markers of SAHF, such as H3K9me3, with an increase in cell cycle inhibitors (p16, p15 and p21) [239].

4.1.2. Wound Healing

After skin injury, cells enter senescence to repair and regenerate the tissue. Judith Campisi's team demonstrated the importance of senescent cells in this process by showing that healing processes are delayed in transgenic mice (p16-3MR) because the senescent cells are eliminated as soon as they appear [208]. Indeed, after a skin injury in wild-type (WT) mice, fibroblasts and ECs enter senescence to accelerate regeneration tissue by secreting SASP. Two important molecules in the healing process are secreted: PDGF-A, which promotes myofibroblast differentiation; VEGF, which promotes angiogenesis. The authors of this study then demonstrated a delay in the healing process in p16-3MR mice in the absence of senescent cells and/or these molecules at the site of injury.

4.1.3. Tumor suppression

Most of the main characteristics of senescent cells allows the cell to avoid tumorigenesis (apoptosis resistance, arrest proliferation). Thus, senescence is a process that was initially described as anti-tumor [240]. The senescent cell, for instance, strongly expresses p53 and p16, which are tumor suppressor genes [241]. Indeed, as described in the previous sections, these two proteins, by causing cell cycle arrest, oppose tumorigenesis, notably characterized by uncontrolled cell proliferation. Variations in the expression of these senescence genes are very often linked to the occurrence of cancer. Mutations altering the expression of p53 or p16 favor the occurrence of cancers (sarcomas, splenic lymphomas, melanoma) in mice [242, 243]. Conversely, mice expressing supernumerary copies of the p53 gene are naturally resistant to the development of cancers chemically induced by treatment with 3-methyl-cholanthrene [244]. Very interestingly, high-throughput genome analysis in humans reveals that malignant tumors (Serous ovarian and uterine corpus endometrial carcinoma) show an alteration in the expression of p53 [245].

4.2. Determinal effect of senescence

Initially, and more than 30 years after Hayflick's discovery, early studies show an increase in the number of senescent cells in the body during aging [246, 247]. In addition, an accumulation of cells presenting several markers of senescence such as $p16^{INK4a}$, $p21^{CIP1}$, SA-β-Gal, and telomere shortening, is also found in association with certain chronic pathologies associated with age, such as Alzheimer's disease, atherosclerosis, osteoarthritis, cancer, chronic

obstructive pulmonary disease (COPD), and idiopathic pulmonary fibrosis (IPF). However, the direct link between the development of the pathology and the involvement of senescent cells has only recently been established.

4.2.1. Cellular senescence and Aging

As previously described, inducing senescence can have beneficial effects and contribute to an individual's development. Paradoxically, the accumulation and persistence of senescent cells in the tissues (long-term senescence) can participate in developing of age-related pathologies and potentiate tumorigenesis. The various aging theories all point to the same notion: inflammaging. This latter is an age-related increase in pro-inflammatory markers in blood and tissues. It manifests like a chronic, sterile low-grade inflammation that develops with advanced age, in the absence of overt infection, and may contribute to clinical manifestations of age-related pathologies [248]. However, the precise cause of inflammation is unknown.

Studies on mice deficient for the mitotic checkpoint protein BUBR1 (encoded by the Bub1b gene) revealed that skeletal muscle, eye and adipose tissue are prematurely aged and accumulate a high number of p16-positive cells. The genetic inactivation of p16 in these mice allows for preventing of the appearance of senescent cells and reducing of aging phenotypes such as sarcopenia, lipodystrophy, and cataracts [249]. Another model mouse, INK-ATTAC, has shown that the specific elimination of p16-positive cells delays the development of geriatric pathologies and prolongs the lifespan of animals (Figure 17)[250, 251].

Figure 17: Representative image of C57BL/6 INK-ATTAC aged mice, with (+AP, senescent cells are cleared) and without (-AP, senescent cells are not cleared). Reprinted from (Baker et al., 2016) [251].

Finally, the last mouse model allows us to observe the accumulation of positive p16 cells with age, and this is the luciferase knockin mouse ($p16^{LUC}$), in which coding sequence for luciferase replaces one allele of p16. After the injection of its substrate, luciferin, the enzyme reflects the expression of p16 [252]. This model can be used to track the evolution of the p16 expression.

Additionally, it enables the observation of the involvement of the protein p16 during healing or tumor progression [252].

4.2.2. Cellular senescence and Age-related disease

Senescence has also been implicated in neurodegenerative diseases such as Alzheimer's, Parkinson's and amyotrophic lateral sclerosis. With age, the risk of developing pathologies, such as neurodegenerative diseases, increases significantly. Although no direct link has ever been demonstrated, the senescence of cells of the central nervous system could impact cognitive processes and play a role in Alzheimer's and Parkinson's diseases (the most common neurodegenerative pathologies) [253]. It has been demonstrated that with age, senescent cells accumulate within the cardiovascular system. They are found in cardiomyocytes and vascular cells and participate in the development of cardiovascular pathologies such as atherosclerosis [249]. The elimination of senescent cells led to a decrease in the formation of plaques and their progression [254].

4.2.3. Cellular senescence and Age-independent diseases

Senescent cells are not only implicated in promoting pathologies related to age but also participate in the occurrence of pathologies independent of it. Effectively, in a mouse model of obesity-induced either by a high-fat diet or by inactivation of the leptin receptor gene, the accumulation of senescent glial cells is detected at the level of the lateral ventricle [255].

4.2.4. Cellular senescence and tumorigenesis

Senescence can also increase the proliferative potential of cancer cells and contribute to the epithelial-mesenchymal transition, which makes invasive cells and promotes metastases appearance [256, 257]. Deleterious effects of SASP in aged tissues have also been observed, thus allowing a growth niche for the development of cancers [258]. The accumulation of senescent cells with aging creates fertile ground for the development of tumors. We must also point out that the increase in patient age seems to be correlated with a decrease in the survival rate of cancer patients [259]. In the case of cancers eliminating senescent cells allows us to see significant benefits. We can then observe a delay in the formation of tumors in mice [251] but also a reduction in the frequency appearance of metastases [260].

5. Role of Cellular senescence in pathogen infection

Despite the few available studies, mounting evidence suggests that viral infections activate senescence responses. Human respiratory syncytial virus (HRSV) has been shown to induce

senescence in A549 lung cancer cells, HEp-2 epithelial laryngeal carcinoma cells, and mouse epithelial lung cells *in vitro* and *in vivo* [261]. Similarly, the measles virus and HCMV induced senescence in normal human lung fibroblasts [262, 263]. Senescence markers such as SA-β-gal activity, p16, p21, and pro-inflammatory SASP factors, including IL-6 and IL-8, were upregulated in infected cells [261-264]. Tat and Nef HIV proteins induce the same senescence markers (SA-β-gal, p21, IL-6, and IL-8) in human microglia and bone marrow mesenchymal stem cells [265-267]. A recent study found that Tat protein induces senescence in microglial cells by increasing ROS levels [265]. Human papillomavirus E2 can induce senescence via pRb and p21-dependent pathways [268]. SARS-Cov-2 infection also causes senescence in lung cells. However, the presence of inflammatory factors and the inability to clear infected cells may result in a hyperinflammatory environment and the onset of ARDS [269]. Individuals who recover from SARS-Cov-2 exhibit other harmful symptoms in organs where senescence may play a role. For example, thrombotic complications are reported in approximately 30% of SARS-Cov-2 patients in intensive care units [270], and senescence is reported to promote clotting via the secretion of SASP molecules [271]. To alleviate viral pathologies, researchers are targeting cellular senescence and the SASP [272].

During virus-induced senescence (VIS), a DDR pathway was activated and caused an increase in mitochondrial ROS. Treating infected cells with the ROS inhibitor N-acetyl-L-cysteine prevented senescence induction [261, 266, 267]. Oxidative stress in VIS cells may activate cGAS-STING pathways. Although it has been reported that some viruses, including influenza and HRSV, stimulate the upregulation of ROS-generating enzymes such as NADPH oxidases and xanthine oxidase, the mechanism of ROS production in VIS cells remains poorly understood [273].

Senescence appears to regulate viral replication *in vivo*. When vesicular stomatitis virus was intranasally administered to mice, lower titres of the virus were observed in the lungs of mice treated with bleomycin, an inducer of senescence in the lung [274]. In these animals, NK and dendritic cell infiltrates were also found, implying a role for the SASP in immune-mediated viral clearance [275].

In addition to viral infections, bacterial infections can induce the cellular senescence of host cells. Bacterial lipopolysaccharide (LPS) is a powerful inflammatory inducer, it has been linked to the induction of cellular senescence in lung alveolar epithelial cells in a H2O2 dependent manner [276]. Another study found that repeated LPS stimulation can cause microglia senescence, leading to the inability to respond to detrimental stimuli and neurodegeneration

[277]. Furthermore, bacterial toxins play a role in cellular senescence. For example, the genotoxin colibactin, encoded by an Escherichia coli genomic island, can induce cellular senescence and promote tumor cell growth and colon cancer [278, 279]. Other microbes, such as Escherichia coli [280] and Helicobacter pylori [281], can cause DNA damage and cell cycle arrest. More resources should be dedicated to studying these pathogens' ability induce cellular senescence and the corresponding molecular mechanisms [278]. As for now, the roles of bacterial and viral infections in the induction of cellular senescence are still largely unknown [272].

Interestingly, the role of senescence during parasite infections has been recently described. In 2018, Guimarães-Pinto *et al*, demonstrated that infection of NIH-3T3 fibroblasts with *Trypanosoma cruzi*, an intracellular protozoan, induced a senescent-like phenotype, characterized by morphological changes, accumulation of SAHF, increased SA-β-gal activity and SASP. This phenotype enables these cells to act as reservoirs of parasites, during the early stages of the Chagas disease [282].

More intriguingly, senescence has been observed in both birds and humans during *Plasmodium* infection but it has not been explored during CM. Asghar *et al*, demonstrated telomere attrition in tissues (liver, lungs, kidney, spleen and brain) of *P. ashfordi* infected birds, and persistent chronic asymptomatic malaria infections results iin reduced lidespan, implying that a seemingly mild disease accelerates cellular aging [283, 284]. They then confirmed telomere attrition and increased of p16 expression in blood cells of *P. falciparum* malaria patients during an acute malaria infection[285]. In a recent study, the same team reported that a single *P. falciparum* infection accelerates cellular senescence in peripheral blood through high levels of inflammation and redox-imbalance, reversed after successful treatment and parasite clearance and in the absence of new infections [286].

By performing a differential gene expression profiling from mice with CM and control mice in our laboratory, (using the Affymetrix GeneChip® Mouse Expression Arrays), they noticed a up regulation of the senescence genes in the brain of mice developing CM compared to non-CM ones. Based on these findings, we propose that the senescence phenotype in the brain contributes to the pathogenesis of CM.

6. Astrocytes senescence

Senescent cells have been observed in both aged and diseased tissue, including the brain. Among the various cell types in the brain, proliferative cells like astrocytes, microglia and oligodendrocytes are subject to undergo senescence. As previously described in chapter 1, astrocytes account for approximately 20% of brain cells and play a major role in brain physiology and neuronal function. They support neuronal cells, regulate the content of the synaptic cleft, play an important role in maintaining ion homeostasis, and maintain BBB integrity. Acting as a part of the tripartite synapse, they control the concentration of glutamate, thus glutamatergic transmission, and secrete their glial transmitters. They also play a significant role in brain injury recovery by reducing wound-derived excitotoxicity, limiting damage, participating in scar formation and ensuring regeneration following brain injury [15, 287]. Astrocytes also have several immune functions, such as the presence of several pattern-recognition receptors and the ability to secrete cytokines and chemokines. In response to an acute injury, astrocytes are activated and undergo various alterations such as swelling, hypertrophy, proliferation, and increased expression of GFAP [288].

Astrocytes undergo cellular senescence during aging or respond to various factors and stimuli (below are some examples). They display specific phenotypes and the classic characteristics of other cell types. The key features are: cell cycle arrest, morphological change, increased GFAP and vimentin, formation of SAHFs, up expression of high-mobility group B (HMGB) proteins, reduced expression of laminB1, downregulation of neurotrophic growth factors, upregulation of SASP factors and increased SA-β-Gal activity (Figure 18) [17].

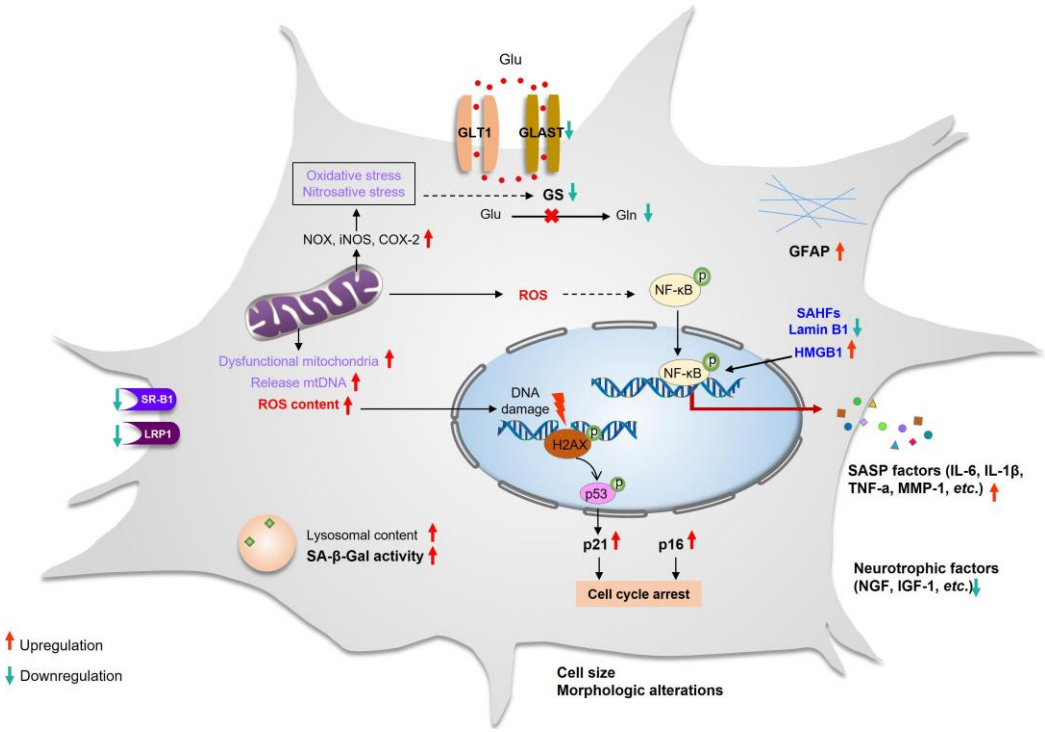

Figure 18: Characteristics of senescent astrocyte. Reprinted from (Han et al., 2020) [17].

In response to oxidative stress or proteasome inhibitor, murine and human astrocytes undergo a senescence program accompanied by increased expression of $p21^{WAF1/CIP1}$, p53, $p16^{INK4A}$ and SA-β-gal activity [289]. Another study showed that ammonia induced senescence in cultured astrocytes in an oxidative stress-dependent manner through p53-dependent transcription of cell cycle regulatory genes, $p21^{WAF1/CIP1}$ and GADD45α. Increased $p21^{WAF1/CIP1}$, p53, and GADD45α mRNA levels were also found in postmortem brain samples from patients with liver cirrhosis and hepatic encephalopathy [290]. Recently, it has been documented that treating astrocytes with sirtuins' inhibitor, tenovin-1 [291], or etoposide [292], increased the number of SA-β-gal-positive cell the expression of IL-6 and IL-1β as well as the cell cycle-related proteins. Others showed that X-irradiation caused senescence in human primary astrocytes, which confer vulnerability to glutamate toxicity on neurons [293]. In addition, the highly active antiretroviral therapy drug induces premature senescence of human astrocytes characterized by an increase in pro-inflammatory signaling [15]. These senescent astrocytes secrete IL-6, IL-8, CXCL-2, CXCL-10, TNF, TGFβ, GRO and Eotaxin [294]. According to another studies, obesity-induced senescent glial cell accumulation contributes to neurogenesis impairment and anxiety-like behavioral. Senolytics therapy restored neurogenesis and reduced anxious behavior [255].

Astrocytes senescence is implicated in the aging brain and neurodegenerative diseases such as Alzheimer, Parkinson and amyotrophic lateral sclerosis. During aging, astrocytes exhibit

cellular senescence characteristics, such as increased GFAP and vimentin expression, as well as SASP including, TNF-α, IL-1β and IL-6 [295]. This process play an important role in the neuroinflammation, degeneration of neurons, and accelerate the appearance of cognitive deficits with aging [295].

In Alzheimer's disease (AD), amyloid-β (Aβ) can activate pro-inflammatory signaling in astrocytes, and that inflammation has been associated with the severity of the disease [296]. A study demonstrated that astrocytes surrounding Aβ plaques are positive for the SASP component IL-6 [297]. Il-6 seems to be regulated by p38MAPK [298]. More profoundly, an increase in $p16^{INK4A}$ level was found in the frontal cortex area of old and AD patients compared to young subjects [298]. It has been proved that astrocytes become senescent in response to environmental toxins, such as herbicides paraquat and 2,3,7,8-tetrachlorodibenzodioxin, which contribute to Parkinson's disease (PD) in mice model [299, 300]. Senescent astrocytes were associated with loss of dopaminergic neurons, motor dysfunction, and reduced neurogenesis. Senescent cells depletion by treatment with senolytics drugs improves motor function and restores neurogenesis [299]. Another study showed increased p16 and p21 in astrocytes in the brains of patients with amyotrophic lateral sclerosis at the early stages of the disease [301].

During AD, human astrocytes expressed p16 and SASP constituents (MMP1 and IL-6) compared to healthy individuals of equivalent age [298]. Similarly, Senescent astrocytes and microglia accumulate in the mouse model $MAPT^{P301S}$PS19 of Tau-dependent neurodegenerative disease. Eliminating of senescent astrocytes using INK-ATTAC mouse model reduces gliosis and hyperphosphorylation of insoluble tau proteins, thereby limiting the degeneration of cortical and hippocampal neurons, allowing the maintenance of cognitive abilities such as object discrimination [302]. In addition, it has been demonstrated that the senescent astrocytes, during AD, cannot clear the glutamate released by neurons from the synapse, resulting in an accumulation of extracellular excitotoxic glutamate. In addition, the reduced secretion of neurotrophic growth factors by senescent astrocytes may lead to decreased neuronal growth. Furthermore, SASP secreted disrupts tight endothelial junctions and induces leukocyte transmigration, resulting in BBB disruption [17]. In our study, we are particularly interested in the role of astrocyte senescence during *Pb*A infection and its impact on the pathophysiology of CM. For that, different senescence markers were assessed in the brain of mice and human with CM.

7. Senescence of peripheral blood mononuclear cells (PBMCs)

Interestingly, peripheral blood is more useful in research on human aging and age-related diseases than tissue samples because of the ease of minimally invasive blood sampling [303]. In humans, the expression of the three cell cycle regulators (p53, p21 and p16) was found to vary with age and sex. In relatively healthy populations, cell cycle regulators p16, p53, and p21 expression increased with chronological age [304-307] The absence of association of p21 and p16 with age has been found in patients with COPD [308], in patients with psychosocial stress [309], as well as those under treatment conditions such as kidney transplantation [310]. As these disease contexts and treatments were found to induce the elevation of cell cycle regulators, the association between age and cell cycle regulators in peripheral blood cells is likely attenuated in the presence of other inducers of senescence.

Different diseases exhibit varying senescence profiles, which may differ across cell types. The level of p16 expression was found to be consistently higher in leukocytes and T cells from HIV-infected patients compared to healthy control patients [225, 311, 312]. At the same time, there was no difference in the expression of p53 and p21 between these two groups [312]. In neurodegenerative diseases, when PBMCs from AD patients were compared to healthy controls, p53 protein expression was higher, whereas p21 protein expression was lower [313-315]. The p21 protein level was consistently lower in monocytes isolated from AD patients compared to controls, while the p53 protein was undetectable [316]. In other studies, newly diagnosed PD patients had lower levels of p21 mRNA in leukocytes than healthy controls [317], while their CD8 T cells showed a p21 expression level similar to healthy controls. Furthermore, p16 mRNA in CD8+ T cells was lower in newly diagnosed PD patients compared to age and gender-matched controls [318]. In COPD, p21 expression is higher than p16 expression in the leukocytes [308]. Furthermore, p16 expression increases in leukocytes of participants suffering from anxiety, depression [319] and psycho-social stress[309]. The associations of p16, p53, and p21 mRNA expressions in PBMCs of patients with diabetes were contentious [320-322].

The role of higher cell cycle regulatory markers in human peripheral blood cells in the onset and/or disease progression is inconclusive. For example, lower levels of cell cycle regulators have been observed in the blood cells of patients with newly diagnosed PD and diabetes compared to healthy controls, possibly due to the migration of senescent cells to pathological sites [318, 320].

Increased p16 expression in leukocytes and T cells is associated with higher inflammatory levels of IL-6 in healthy older adults [306], patients with depression [319], or patients who have undergone coronary bypass surgery [305].On the other hand, antiretroviral therapy suppresses inflammation [305], which eliminates the relationship between p16 and IL-6 in HIV patients on treatment [323].

Chronic γ-radiation exposure induces downregulation of p16 and p21 but upregulation of p53 mRNA expression in PBMCs from radiation-exposed workers [324]. Radiation could cause DNA damage in blood cells and trigger a p53-mediated DNA damage response [325]. Another passive exposure to Sulphur mustard could cause oxidative stress, which is associated with premature senescence and results in the upregulation of p16 mRNA expression in leukocytes [326].

In recent years, research on the role of cellular senescence in aging and disease has advanced dramatically. However, the heterogeneity of this phenotype limits markers' utility to detect difficult senescence [166]. Cell cycle regulators are critical in mediating cell growth arrest, which is a defining feature of cell senescence. These could be detected in peripheral blood, which is a minimally invasive and clinically useful specimen. More research is needed to understand better the functions of senescent blood cells and how they contribute to immune response [303].

8. Elimination of senescent cells: Senotherapy

Baker *et al* conducted a fascinating study in which they show that the use of a model murine transgenic termed INK-ATTAC (INK-linked apoptosis through targeted activation of caspase), which allows, during the administration of a molecule (AP20178), this molecule that dimerizes the FKBP-CASP8 fusion protein, the elimination by apoptosis of cells that express the p16 gene, to delay the appearance of pathologies linked to aging such as cataract in the eyes, to delay sarcopenia in skeletal muscle, to limit the mass loss greasy in adipose tissue, to attenuate the hypertrophy of the cardiomyocytes, to reduce the renal glomerulosclerosis and to reduce inflammation and to prolong the lifespan of mice. However, a slowing down of the healing process was observed [250, 251]. However, this genetic manipulation in mice cannot be transposed to humans. Therefore, it is necessary to develop other strategies to eliminate senescent cells. As a result of these studies, a new category of molecules appears, the **senolytics**, which specifically target senescent cells to eliminate them by apoptosis. This approach was based on the observation that senescent cells are resistant to apoptosis [179].

➢ Dasatinib and Quercetin (D+Q)

In 2015, during a screening to identify senolytic molecules, the team of James L. Kirkland discovered that the combination of dasatinib (inhibitor of multiple tyrosine kinases with the ability to block ephrin-dependent receptor signaling, used as anti- cancer) with quercetin (a plant flavonoid, having many actions including that of inhibiting the PI3K pathway) (Figure 19), allows, as in the INK-ATTAC transgenic mouse model, specific elimination of senescent cells. The administration of this senolytic cocktail to different murine models, reduces vascular calcification and osteogenic signaling in aged and apoE-/- mice (a mouse model of atherosclerosis) [327, 328], improves cardiac functions in aged mice [328], enhances physical abilities (walking speed, grip strength and hanging endurance) in mice that were irradiated with the leg [328, 329], increase the lifespan of normal old mice and in a model progeria murine Ercc1$^{-/\Delta}$ (a mouse model of accelerated aging) [328, 329], reduce bone resorption in old mice [328, 330], improve lung function in a mouse model of IPF [255], and delay the onset of pathologies linked to aging in progeroid Ercc1$^{-/\Delta}$ mice [328]. D+Q could thus reduce the risk of developing many pathologies linked to aging, such as osteoporosis, hepatic steatosis, insulin resistance, neurodegeneration, vasomotor dysfunction, pulmonary fibrosis, chronic kidney disease and skeletal muscle dysfunction [140]. In 2019, the senolytic effect of the D+Q cocktail in patients with diabetic kidney disease showed a significant reduction in the number of senescent cells in adipose tissue and the skin, as well as a reduction of SASP markers in the blood of patients [331].

To date, the senolytic combination of D + Q has been tested in several human clinical trials for treating IPF, chronic kidney disease, skeletal health, hematopoietic stem cell transplant survivors and AD [332].

➢ Fisetin

Fisetin (3,3',4',7-tetrahydroxyflavone) is a flavonoid, a group of naturally occurring polyphenolic compounds. It is found in low concentrations in many fruits and vegetables, including apples, persimmon, grapes, onions, and cucumbers, with the highest concentration in strawberries [333]. Because of its hydrophobicity, Fisetin penetrates cell membranes and accumulates within cells to exert antioxidant effects [334]. Fisetin has also been shown to have anti-hyperglycemic, anti-hyperlipidemic, anti-inflammatory, neurotrophic, and anti-carcinogenic activities [333, 335-341]. Fisetin acts through various molecular targets and

signaling pathways, including BCL-2, PI3K/AKT, p53, NF-κB, and others [332, 342]. Various works have recently shown its advantages, among which we can name:

- Induce apoptosis in radiation-induced senescent HUVECs, oxidative stress-induced senescent MEFs, and genotoxin-induced senescent human fibroblasts [343, 344].
- Reduce senescence markers in progeroid *Ercc1*$^{-/\Delta}$ mice, aged WT mice and human adipose tissue explants.
- Improve the health and lifespan when administrated to aged animals [333, 345].

Fisetin has a terminal plasma half-life of just over 3 hours in mice, with its metabolites being excreted in feces and urine. Notably, no adverse effects of fisetin have been reported, even when given at high doses [346].

There are ongoing clinical trials for chronic kidney disease, skeletal health, osteoarthritis, COVID-19, childhood cancer survivors and frailty [332].

➢ Navitoclax

ABT-263, also known as Navitoclax (targeting the Bcl-2 family of anti-apoptotic factors) (Figure 19), have a senolytic effect dependent on cell type. It can selectively cause apoptosis in senescent HUVECs, IMR-90, and MEF cells but not in primary human preadipocytes [343]. Administration of navitoclax to sublethally irradiated mice reduces the burden of senescence in muscle satellite cells [343] and the bone marrow [347]. Navitoclax has also been shown to eliminate senescent macrophage foam cells in early atherosclerotic lesions [348]. Treatment with Navitoclax decreases the abundance of some but not all human and mouse senescent cell types *in vitro* [171] and reduces hematologic dysfunction caused by whole-body radiation [347]. ABT-263, on the other hand, has serious side effects such as thrombocytopenia and neutropenia [349]. A subsequent study focused on discovering two new senolytic agents capable of specifically inhibiting Bcl-xL. These molecules (A1331852 and A1155463) cause less hematological toxicity than Navitoclax [343].

➢ 17-DMAG

17-DMAG promoted apoptosis of senescent cells, in part, by disrupting the HSP90-AKT interaction to destabilize the active form of AKT (Figure 19) [350, 351]. HSP90, a family of ubiquitously expressed molecular chaperones, can promote cell survival via the stabilization of AKT or ERK. Using 17-DMAG induces the targeted death of senescent cells *in vitro* and *in vivo* in mice. It also limits the appearance of age-related pathologies and increases the survival of mice [350].

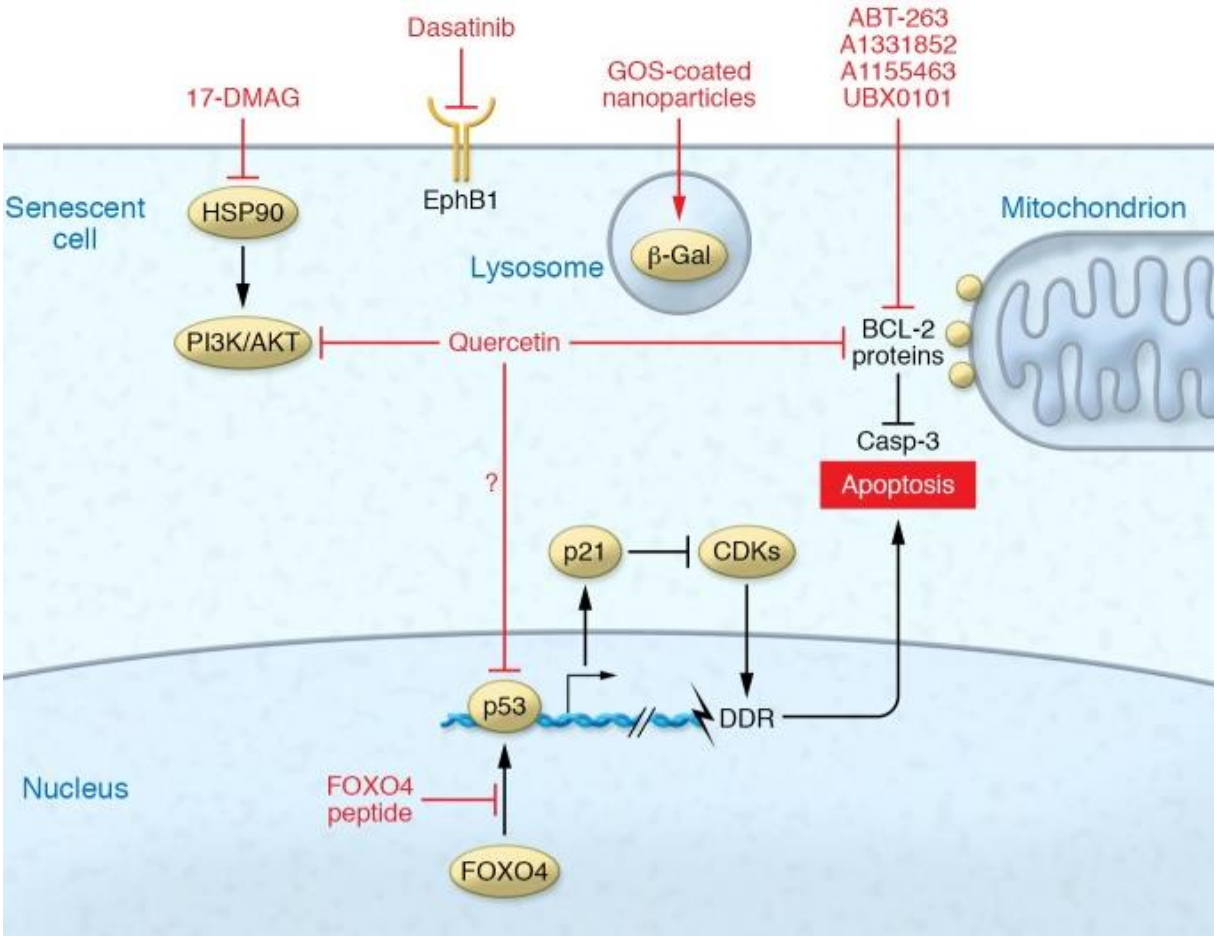

Figure 19 : Strategy targeting the senescent cells by use of senolytics drugs. Reprinted from (Ovadya et al., 2018) [351].

Strategies

Our first hypothesis was that cellular senescence and its SASP, composed of pro-inflammatory factors, could be a mechanism associated with the inflammatory response of astrocytes and microglia during *Plasmodium* infection and participate in the pathogenesis of CM. This hypothesis was comforted by several studies showing telomere attrition and an increase of the p16 senescence marker in the blood cells of *P. falciparum* malaria patients during the first three months post-infection [285]. Telomeres attritions were also confirmed in tissues of *P. ashfordi* infected birds and were associated with shortened lifespan [283, 284]. Additionally, a very recent study showed that the *P. falciparum* infection accelerates cellular senescence in peripheral blood through high levels of inflammation and redox imbalance, reversed after successful treatment and parasite clearance [286]. To validate our hypothesis, the senescence markers were assessed: 1) *in vivo* using CM-susceptible (CM^S) and CM-resistant mice (CM^R), 2) *in vitro*, using primary mouse cultures enriched in astrocytes and stimulated with *Plasmodium* parasite and 3) in post-mortem brain sections as well as in peripheral blood from CM patients. The role of this process in the CM pathogenesis was evaluated *in vivo* by administering senolytic drugs to *Pb*A infected mice.

Our second hypothesis was that astrocytes senescence was involved in cognitive deficits observed during an acute CM and long-term in chloroquine-rescued mice. For that, we 1) have compared the behavior of two mice models (susceptible and resistant to CM) before and after *Pb*A infection using: actimetry test for motor activity, elevated plus maze test for anxiety-like behavior, and tests to assess different types of memories; novel object recognition for recognition memory, spontaneous alternation for working memory and Y-maze for spatial orientation memory. Statistical analyses are ongoing to analyze of the relationship between senescence markers and cognitive deficits. 2) we evaluated the senescence markers and cognitive impairment in *Pb*A-infected mice treated with chloroquine. For the time being, we have only evaluated the p21 senescence marker in the brain. The other senescence markers, as well as behavioral tests, are being conducted. Finally, to evaluate the effect of age on CM development, we assessed mortality, parasitemia, behavioral and cerebral damage in mice of different ages: adult (6-month-old) and old (12-month-old), compared to young adult (2-month-old) after infection with *Pb*A.

Materials and methods

1. *In vivo* studies

1.1. Mice

For the first project, we used 8-10 weeks-old C57BL/6 mice (B6) (Janvier laboratories, C57BL/6JR) and B6.WLA-*Berr2* congenic mice strain (L28) generated in our Lab on the B6 background expressing the $Berr2^{WLA}$ allele that confers the resistance to CM [30]. All mice were kept in standard conditions in the animal facility of the Pasteur Institute of Lille. These experimental mice were performed following institutional guidelines for animal care and use. Approvement was given by the French Committee for Animal Health Care "Ministère de l'Agriculture et de la Peche n°A 75485.

1.2. Parasites and Infection

Mice were infected intraperitoneally with 10^6 RBCs infected by *Pb*A, clone 1.49L (provided by Dr. D. Walliker, Institute of Genetics, Edinburgh, UK). Same-age-non-infected mice were used as negative controls. Between 6 to 10 days post-infection, B6 infected mice develop neurological symptoms such as hind-limb paralysis, deviation of the head, motor coordination impairment, convulsions and coma. Unlike L28, which develops none of the symptoms and dies later from hyperparasitemia (Figure 20). These mice have shown a reduced parasite sequestration and BBB disruption with low infiltration of CD8 in the brain along with altered glial cell response upon *Pb*A infection compared to B6 mice [30]. Mice were monitored twice a day following infection, and parasitemia was determined by Giemsa-stained blood smears from the tail vein every 3 days. All mice were euthanized between days 6 and 8 post-infection when the **B6 CM-susceptible mice** (**CM^S**) showed neurological signs. **B6.WLA-*Berr2* CM-resistant mice** (**CM^R**) not developing ECM were used as controls.

All the mice's brains, spleens and sera were collected to evaluate the different senescence markers.

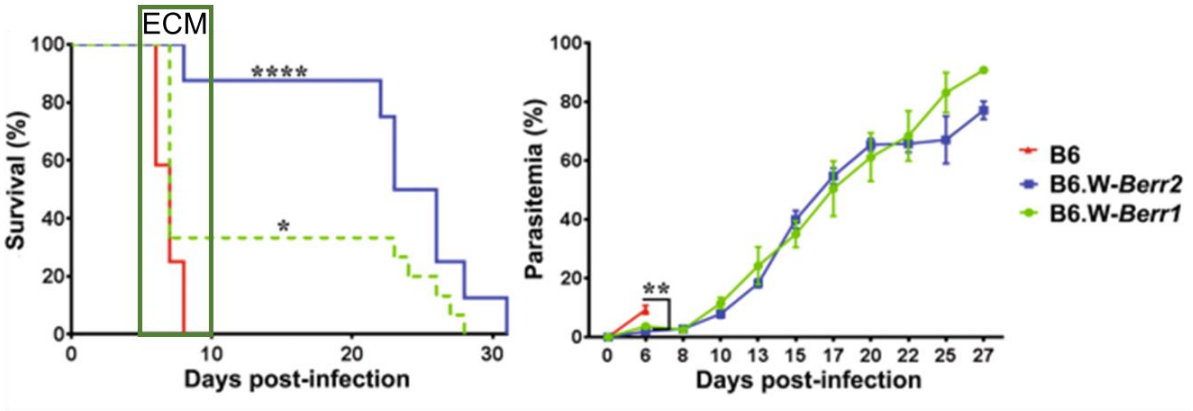

Figure 20: Survival and parasitemia in B6 and B6.W-Berr mice after PbA infection. Reprinted from (Keswani et al., 2020) [30].

1.3. Isolation of brain astrocytes and microglia

We used a bank of RNA obtained from astrocytes and microglial cells isolated from brains of control and infected mice, which were available and carried in the laboratory. Cells were isolated using the Neural Tissue Dissociation kit (Miltenyi Biotec, 130-093-231), and were stained with anti-ITGAM/CD11b (eBioScience, 12–0112-81) and anti-SLC1A3/GLAST (Miltenyi Biotec, 130–095-814) fluorescent antibodies. Astrocytes (ITGAM/CD11b^{-} SLC1A3/GLAST^{+}) and microglia (ITGAM/CD11b^{+} SLC1A3/GLAST^{-}) were then sorted by FACSAria (Becton Dickinson), and analyzed by RT-qPCR as described previously [27].

1.4. Treatment of infected mice with senolytic drugs

CM^{S}-infected mice were treated by oral gavage from day 1 to 8 post-infection with a senolytic cocktail: 5 mg/kg Dasatinib (D) (Sigma, SML2589) + 50 mg/kg Quercetin (Q) (Sigma, Q4951) or 50 mg/kg Navitoclax (MedChemExpress, HY-10087) or 100 mg/kg Fisetin (CliniSciences, F356025), dissolved in 10% ethanol, 30% polyethylene glycol 400 (Sigma, 25322-68-3) and 60% Phosal 50 (CliniSciences, HY-Y1903). All mice were randomly allocated to each group for treatment.

Mortality was monitored daily and parasitemia was assessed every 3 days. Half of the mice were used to monitor parasitemia and mortality, while the remaining half were sacrificed at 11 dpi, after passing the window period for ECM (6-10 dpi). Brains, spleens, and sera were collected.

2. *In vitro* studies

2.1. Isolation of *Pb*A-iRBCs

Severe combined immune deficiency mice (SCID; Institut Pasteur de Lille, Lille, France) were injected intraperitoneally with parasitized RBCs (*PbA* clone 1.49L). The parasitemia rate was between 40 and 50% at 15 days post-infection. The total blood was collected from these mice in 50 µl heparin (Sanofi-Synthelabo, France). *Pb*A-iRBCs were separated from other cells by a 40% Percoll gradient (Sigma, France) by centrifugation at 2,500 rpm for 30 min after being washed twice in phosphate-buffered saline (PBS) (Gibco, France), and centrifugated at 1600rpm for 5 minutes at room temperature (RT). The parasitized RBC were then washed in PBS and re-suspended in Dulbecco's Modified Eagle Medium (DMEM) (Gibco, France) containing 10% fetal bovine serum (FBS; Dutscher, S181B-500). Giemsa-stained blood smears from the tail vein showed a purity of 90–100% *Pb*A-iRBCs.

2.2. Primary cultures of mouse astrocytes

In vitro experiments were carried out by I. Leleu, IE CNRS, in our laboratory. Primary glial cells were gently dissociated and isolated from the brains of 1-2-day-old newborn C57BL/6 mice. Brains were isolated under sterile conditions; meninges were peeled off and kept for subsequent cell isolation. Single-cell suspensions of each brain were obtained by gently dissociating brain tissues in a dissection medium [PBS, 45% glucose, 2% penicillin/streptomycin] followed by two washes in DMEM at 900 rpm for 10 minutes. Cells (2.5×10^6) were seeded in cell-culture flasks that had been pre-coated for 2 hours with poly-L-ornithine hydrobromide (Sigma, France) in a cell-culture medium [DMEM supplemented with 10% FCS, 1 g/l D-glucose, 0.1% penicillin/streptomycin] and maintained at 37°C in a 95% air/5% CO2 humidified incubator. After 7 days, the culture medium was replaced and the cells were incubated for an additional 7 days before being used in further experiments.
Cultures were enriched in astrocytes by gently shaking for 24 hours and kept in DMEM containing 10% FBS.

2.3. Parasite stimulation

For stimulation, 10^6 astrocytes per petri dish were seeded two days before, in cDMEM. *Pb*A-iRBCs were recovered from SCID mice, were put in contact with astrocytes at a ratio of 10:1 for 24 hours and were removed. Then, cells were resuspended in the medium for 4,7,10, or 15

days post-stimulation, with the addition of a new medium on day 7. Unstimulated astrocytes were cultured in the same conditions and used as controls.

For autophagy inhibition, the astrocytes were treated with 10 nM Bafilomycin A_1 (BAF A_1; MedChemExpress, HY-100558) from the beginning of the *Pb*A-iRBCs stimulation to 10 days post-stimulation.

2.4. siRNA silencing

Astrocytes were plated on a 12-well plate at 5.10^5 cells/well and then transfected for 6 hours with *Rubin/Rubicon* or *Atg5* siRNA (Horizon Discovery; Dharmacon; RUBCN/rubicon 100,502,698; ATG5 11,793) or control siRNA at 25 nM using the HiPerfect transfection reagent (Qiagen, 301,704). The medium was then replaced with a fresh culture medium, and 48 h later, cells were stimulated with *Pb*A-iRBCs. After 10 days, different senescence markers were evaluated. These silencing experiments were realized by I. Leleu

3. Human studies

3.1. Ethics statement

The study was conducted according to the guidelines in the Declaration of Helsinki. It was approved by the Institutional Human Ethics Committee of SCB Medical College, Cuttack, and the Institutional Review Board of all three collaborating institutes: (a) the Institute of Life Sciences, Bhubaneswar, India (b) the Tata Institute of Fundamental Research, Mumbai, India and (c) Institut Pasteur de Lille, Lille, France. The National Health Office Ethics Committee in India approved the study design.

All blood samples were collected after obtaining written consent from participants or their accompanying relatives in the case of comatose patients.

3.2. Study Site

The study was conducted at SCB Medical College and Hospital, Cuttack, Odisha, India, between 2008 and 2011. According to WHO, India accounted for 27% of malaria cases outside of Africa, and 65% of malaria in the Southeast Asian region in 2008. In the same year, over 82% of the population was living in a malaria-endemic zone [352]. The central and eastern regions are the most vulnerable. In 2009, Odisha recorded 24% of malaria cases, of which 40% were caused by *P. falciparum*.

Malaria transmission in Odisha is annual, with some climate-related fluctuations. Thus, a transmission peak occurs during and just after the rainy season [from June to October], then decreases during the winter [from November to February]. Blood samples were collected from infected patients during the period of high malaria transmission.

Figure 21: Localization of Cuttack in India

3.3. Participants and blood collection

All participants involved in the study were recruited as they passed through the outpatient and medical department interns at SCB Medical College between 2008 and 2011. *P.falciparum* infection was screened by an immune chromatography test (SD Bio Standard Diagnostics, India) and Giemsa-stained blood smears as previously described [353]. After validation of the diagnosis, all patients received appropriate treatment. Only individuals infected with *P. falciparum* were included in the study, a total of 252 patients, aged over 15 years.

Patients were categorized as uncomplicated malaria MM (Mild Malaria) (n=60), patients having a fever without complication with evidence of *P. falciparum* infection, or Severe Malaria (SM) (n=192), patients having at least one laboratory or clinical feature of severe malaria reported by the WHO. SM cases were very heterogeneous. Patients with SM were categorized into MOD (Multiple Organ Dysfunction), CM and CM-MOD. CM was defined as patients with fever and altered sensorium, unarousable coma with a Glasgow Coma Scale (GCS) of ≤10) after exclusion of other causes of encephalopathy such as encephalitis, meningitis, and metabolic encephalopathy by biochemical investigations in the CSF. MOD patients had at least two damaged organs, including ARF, hepatopathy, ARDS, systolic shock

CNS (GCS≤10), respiratory distress, renal failure and hepatic dysfunction (ALT/AST ≥3 times normal, prolonged prothrombin and albuminemia). When more than a single organ failure was associated with CM, patients were considered CM-MOD. Patients co-infected with other *Plasmodium* species or with a chronic disease like tuberculosis or cirrhosis were excluded from the study. Peripheral blood was collected (5 mL) on the day of recruitment, before treatment initiation.

Several studies were carried out in our laboratory on these 252 patients in order to determine specific biomarkers that may be associated with the disease. For that, circulating levels of several cytokines, chemokines and biological parameters were quantified in the plasma of all participants [97, 354, 355]. In this study, we decided to randomly choose roughly ten patients per group to check the senescence markers. 37 patients were investigated: 11 patients with MM, 5 patients with MOD, 14 patients with CM and 7 patients with CM-MOD.

3.4. Post-mortem brain tissue

Paraffin-embedded human brain tissue sections derived from patients who died from CM and from non-infected healthy controls who died for a reason other than malaria, coming from Ivory Coast, were evaluated by confocal microscopy to evaluate senescence markers.

Figure 22: Localization of Ivory Coast in Africa.

4. Identification of senescence biomarkers:

4.1. Affymetrix GeneChip Analysis

In collaboration with Cécile LECOEUR, statistical analysis was carried out on the affymetrix results carried out in our laboratory. Briefly, total RNA was extracted from the cell lysates of the brains of control and *Pb*A-iRBCs infected CM^S and CM^R mice using a Trizol® Plus RNA Purification Kit (Invitrogen, 15596026) according to the manufacturer's instructions. A Nanodrop spectrophotometer and an Agilent bioanalyzer were used to determine RNA integrity and concentration. The Genopole Institut Pasteur's Technologic Platform treated equal RNA concentrations from each of the four animal groups (n = 3 per group) using the Affymetrix protocol (Paris). The Affymetrix GeneChip® 1.0 ST Array Mouse was used as previously described [345].

4.2. Real-time quantitative PCR

Before RNA isolation, the brains and spleens of control and infected mice were homogenized in RLT Lysis Buffer (Qiagen, 79216) with a Polytron homogenizer. The Nucleospin RNA kit (Machery Nagel, 740,955,250) was used to extract RNA from organ supernatant homogenates, astrocytes isolated in vivo from mouse brains; frozen pellets of primary astrocyte cultures control or after PbA-contact, and whole blood for all study participants. Complementary DNA (cDNA) synthesis was done using the SuperScript VILO kit (Invitrogen, 11,754,250) in a C1000 Thermal Cycler (Bio-rad, France) with the following program: 10 min at 25 °C; 60 min at 42°C and 5 min at 85°C. Then, RT-qPCR was performed by mixing, in the final 10µL volume, 2.5 ng cDNA with primers (Table 2, 3; Eurogentec) and SYBR Green Master Mix (ThermoFisher Scientific, 4,385,612). The QuantstudioTM 12 K Flex Real-Time PCR system (ThermoFisher Scientific) was used for the RT-qPCR, which consisted of a 10-minute run at 95°C, followed by 40 cycles of 15 seconds at 95°C and 1 minute at 60°C. Relative expression of genes of interest was quantified using ΔΔCt or ΔCT (for the human cDNA samples). The data were normalized to Hprt1 or Gadph gene expression and expressed as a fold-change of gene expression versus the control condition.

Name of primer	Forward Sequence	Reverse Sequence
HPRT1	5'-TCC-TCC-TCA-GAC-CGC-TTT-T-3'	5'-CCT-GGT-TCA-TCA-TCG-CTA-ATC-3'
P21	5'-ATT-CCA-TAG-GCG-TGG-GAC-CT-3'	5'-TCC-TGG-GCA-TTT-CGG-TCA-C-3'
P53	5'-CCT-GGC-TGT-AGG-TAG-CGA-CT-3'	5'-ACT-CCT-CCA-TGG-CAG-TCA-TC-3'
P38	5'-GCG-TCT-GCT-GAA-GCA-CAT-GAA-ACA-3'	5'-ATG-GGT-CAC-CAG-GTA-CAC-GTC-ATT-3'
P16	5'-AAT-CTC-CGC-GAG-GAA-AGC-3'	5'-GTC-TGC-AGC-GGA-CTC-CAT-G-3'
pRb	5'-AAA-CAA-GGA-AAA-GTG-AGG-AC-3'	5'-GAT-CTG-CAC-AAG-ATT-CTC-AAT-CC-3'
GADD45γ	5'-TCT-ACG-AGT-CCG-CCA-AAG-TC-3'	5'-GCT-ATG-TCG-CCC-TCA-TCT-TC-3'
IL-6	5'-GCT-ACC-AAA-CTG-GAT-ATA-ATC-AGG-A-3'	5'-CCA-GGT-AGC-TAT-GGT-ACT-CCA-GAA-3'
CCL-2	5'-CAT-CCA-CGT-GTT-GGC-TCA-3'	5'-GAT-CAT-CTT-GCT-GGT-GAA-TGA-GT-3'
CXCL10	5'-GCT-GCC-GTC-ATT-TTC-TGC-3'	5'-TCT-CAC-TGG-CCC-GTC-ATC-3'
BCL-2	5'-CTC-GTC-GCT-ACC-GTC-GTG-ACT-TCG-3'	5'-CAG-ATG-CCG-GTT-CAG-GTA-CTC-AGT-C-3'
BCL-X	5'-TGG-ATC-TCT-ACG-GGA-ACA-ATG-C-3'	5'-GTG-GCT-GAA-GAG-AGA-GTT-GTG-G-3'
BCL-W	5'-CGA-GTT-TGA-GAC-CCG-TTT-CCG-CC-3'	5'-GCA-CTT-GTC-CCA-CCA-AAG-GCT-CC-3'
MCL-1	5'-GCT-CCG-GAA-ACT-GGA-CAT-TA-3'	5'-CCA-GTT-TGT-TAC-GCC-ATC-T-3'
LC3	5'-GAC-CAG-CAC-CCC-AGT-AAG-AT-3'	5'-TGG-GAC-CAG-AAA-CTT-GGT-CT-3'
Rubcn/Rubicon	5'-CTC-ATC-CAT-GAC-CAG-GTG-TG-3'	5'-GTC-GCT-CTC-ATG-CAA-ACT-GA-3 '
Atg5	5'-ATA-TCA-GAC-CAC-GAC-GGA-GCG-3'	5'-CAG-CAT-TGG-CTC-TAT-CCC-GTG-3'

Table 3: List of mouse primers and sequences used for RT-qPCR

Name of primer	Forward Sequence	Reverse Sequence
GAPDH	5'-GAA-GGT-GAA-GGT-CGG-AGT-C-3'	5'-GGA-GGG-ATC-TCG-CTC-CTG-GAA-3'
P21	5'-GAC-TCT-CAG-GGT-CGA-AAA-CG-3'	5'-GGC-TTC-CTC-TTG-GAG-AAG-ATC-A-3'
P16	5'-TGC-CTT-TTC-ACT-GTG-TTG-GA-3'	5'-GCC-ATT-TGC-TAG-CAG-TGT-GA-3'

Table 4: List of human primers and sequences used for RT-qPCR

4.3. Western blot analysis

Brain lysate, extracted from CM^S control and infected mice, was resuspended and crushed in lysis buffer (RIPA lysis buffer, Interchim, R0278-500 mL) with a Protease Inhibitor Cocktail (Roche, 04693159001). After centrifugation, the total protein concentration was measured with the BCA protein assay kit (Interchim, UP40840A). Each sample was resuspended in Laemmli buffer (Bio-Rad, 1,610,747) at a 1 mg/ml protein concentration. Brain protein extracts were

separated on a standard SDS-PAGE in a 5, 10, or 15 % polyacrylamide gel (BioRad, 1,610,148) and electro-transferred into 0.2 µm nitrocellulose membranes (ThermoFisher Scientific, 88,018) using the semi-dry electrotransfer method. Membranes were blocked for 2 hours at RT in 1X PBS-0.2% Tween 20® (Euromedex, 2001-B) and then incubated overnight at 4°C with the primary antibodies (diluted in PBS-0.2% Tween 20®) using a Cassette Miniblot System (Immunetics). Details of the primary antibodies used are listed in table 4. A Precision Plus Protein All Blue Standard (Bio-rad Laboratories, 161-0373) was used to track the separation of proteins. After two washes with PBS-0.2% Tween 20®, the immunoreactivity profile was detected by incubating the membrane with the secondary antibodies (Table 5) diluted in PBS-0.2% Tween 20® for 2 hours. Blots' Revelation was done using the Clarity™ Western ECL Substrate (Bio-Rad, 170-5061). Blots' images were captured and analyzed by the Molecular Imager ChemiDoc™ XRS+ system (Bio-Rad) using Image Lab™ software (Version 5.2, Bio-Rad). For each independent experimental replicate, the relative protein levels were determined by densitometry (ratio of the intensity of the phosphorylated protein band to the total protein within the same membrane) using the ImageJ/FIJI software (version 1.53; ImageJ™ software, National Institutes of Health). The protein levels in the brains of CM^S-infected mice were normalized to CM^S control mice's protein levels.

4.4. Immunofluorescence staining

Brain tissues from control and *Pb*A-iRBCs-infected CM^S mice were snap-frozen and stored in Neg50 (Epredia, 65029). Serial coronal sections were cut at 5 µm thick and mounted onto Super-frost plus slides (Thermo Fisher, J1820AMNZ). Brain sections were then fixed for 10 min in 4% paraformaldehyde (PFA, Electron Microscopy Sciences, 15,713 R7G5). Following permeabilization with 0.1% Triton X-100 (Sigma-Aldrich, T8787) diluted in PBS 1X, slides were blocked with 5% FBS for 30 min at RT and incubated overnight at 4°C in a humidified chamber with anti-GFAP-Alexa Fluor 488 antibody. The following day, sections were washed in several changes of PBS before being incubated for 2 hours at room temperature with anti-p21, anti-pp53, or anti-Bclx antibodies. The nature, source and dilution of all antibodies are listed in table 4. After being washed, slides were incubated with the appropriate conjugated secondary antibodies (listed in Table 5), diluted in 5% FBS, for 2 hours at RT in the dark.

Paraffin-embedded sections of human brain samples were dewaxed using a standard protocol as described earlier [356]. Sections were deparaffinized in xylene and rehydrated in an alcohol gradient series. After antigen retrieval (in 10 mM citrate buffer, pH 6.0 for 30 min at 100°C),

slides were permeabilized, blocked, and stained with anti-GFAP-Alexa Fluor 488 and anti-p21 antibodies as described for mouse sections. Primary and secondary antibodies are the same as those listed for mouse immunofluorescence.

Astrocyte Primarycultures, stimulated with PbA-iRBCs, were plated on glass slides as described. After washing with PBS, it was fixed with 4% PFA for 20 min. Cells were then permeabilized with 0.2% Triton X-100 diluted in PBS 1X for 5 min, washed and incubated with anti-GFAP-Alexa Fluor 488 antibody, diluted in 10% FBS, for one hour at RT. After washing with PBS, cells were incubated with the following antibodies: anti-p21 and anti-LC3 (detailed in table 4) for 1h at RT. Washed slides were then incubated with appropriate conjugated secondary antibodies (detailed in table 5) for 30 min at RT and washed again.

For all sections, the cell nucleus was stained with DAPI (Invitrogen, D1306) for 30 min, and slides were mounted with Perma-fluor mounting medium (Thermo-Fisher, TA-030-FM).

Target	Source	Reference	Dilution	Application (WB/IF)
GFAP- Alexa 488	Thermo- Fisher	53-9892-80	1/400	IF
P21- Alexa	Santa cruz biotechnology	Sc-817	1/1000 1/100	WB IF
P53	Santa cruz biotechnology	Sc-126	1/200	WB
P-p53	Santa cruz biotechnology	Sc-516-90	1/100 1/100	WB IF
P38	Biolegend	622403	1/200	WB
P-p38	Santa cruz biotechnology	Sc-166182	1/100	WB
ATM	Santa cruz biotechnology	Sc-135663	1/100	WB
P-ATM	Biolegend	BLE651201	1/300	WB
Bcl-x	Santa cruz biotechnology	Sc-8392	1/100	IF
LC3	Medical & Biological Laboratories	PM036	1/100	IF
CXCL-10	R&D	AF-466-NA	1/100	IF

Table 5 : Primary antibody list for immunofluorescence (IF) and/or western blot (WB)

Target	Source	Reference	Dilution	Application (WB/IF)
Anti-mouse IgG (Alexa Fluor 594)	Invitrogen	A11005	1/200	IF
Anti-mouse IgG (Alexa Fluor 633)	Invitrogen	A21050	1/200	IF
Anti-goat IgG (Alexa Fluor 633)	Invitrogen	A21086	1/200	IF
Mouse IgG (HRP)	Ab6728	Abcam	1/10000	WB
Rabbit IgG (HRP)	Ab97051	Abcam	1/10000	WB

Table 6: List of secondary antibodies used in IF and/or WB

4.5. Imaging and image processing

Fluorescent slides were scanned using the Zeiss AxioScan.Z1 slide scanner (Zeiss, Jena, Germany) using 20x magnification (0.22µm/pixel) and auto-estimated exposure times. Using 4 epi-fluorescent filters (DAPI, Alexa 488, Cy3, Cy5), the whole slide scan was imaged. These experiments were done in strong collaboration with N. SAISI, PhD student.

Images were complemented with image deconvolution using Huygens Essential software (Scientific Volume Imaging, http://svi.nl/) to enhance the spatial allocation of image signals and help improve the segmented cell objects by minimizing artifactual external neighboring signals. Then, the segmentation of individual cells is finally performed by the Imaris Surface creation module (v9.1 .2, BitPlane, http://www.bitplane.com) to extract data for cellular marker quantification.

4.6. SA-β-Gal Assay

The SA-β-Gal staining procedure was performed as previously described [138]. Sections (5 µm) of snap-frozen brain tissue derived from control and infected CM^S mice were fixed with 2% formaldehyde (Sigma, F1268) -0.2% glutaraldehyde (Merck, 432VV351439) for 5 min at RT, washed with PBS and then incubated with SA-β-Gal staining solution (1 mg/ml X-gal, 40 mM citric acid/sodium phosphate buffer pH 6.0, 5 mM potassium ferrocyanide, 5 mM potassium ferricyanide, 150 mM sodium chloride and 2 mM magnesium chloride) overnight at

37°C. SA-β-Gal brain sections were scanned by the Zeiss LSM710 confocal microscope (ZEISS microscopy GmbH) using an Airyscan super-resolution module (0.325µm/pixel) with a 20X oil immersion lens. The Senescence Counter is written in the ImageJ macro language. In brief, areas measured from each image were used for SA-β-Gal positive cells; we analyzed 6 images from 3 independent experiments. We selected type 8-bit images and used the "adjust," "threshold max," and "measure" commands in ImageJ (National Institutes of Health, Bethesda, MD, USA). The "% area" results were used as the stained level of SA-β-gal [357, 358].
Astrocytes were plated on glass slides and stimulated with PbA-iRBCs as previously described for in vitro SA-β-Gal staining. They were then fixed and stained with SA-β-Gal solution as described for brain sections at days 0,4,7,10 and 15 post-stimulations. Images were captured using a Zeiss Axioplan2 microscope with a 20X lens, and SA-β-Gal positive cells were manually counted in random microscopic fields (at least 200 cells/field) by counting 1) the total number of cells and 2) blue-staining^{+} cells corresponding to SA-β-Gal^{+} cells. The data is representative of two independent experiments (N=4-5 per condition).

4.7. Enzyme-linked immunosorbent assay (ELISA)

Cytokines and chemokines were quantified in sera of control CM^{S}, infected CM^{S} and treated-CM^{S} mice using ELISA Kits for IL-6 (Biolegend, 431,301), CCL2 (Biologend, 432,704) and CXCL-10 (R&D Systems, DY-466-05) in triplicates.

5. Behavioral assessment

For project 2, we used male and female B6 and L28 mice aged 2, 6 and 12 months, called young adult, adult and old mice. All mice were infected with 10^{6} *Pb*A-iRBCs. Mortality and parasitemia were evaluated. The following behavioral tests were conducted: actimetry, elevated plus maze, Y-maze spatial, spontaneous alternation in Y-maze and novel object recognition test. The number of animals used for behavioral tests ranged from 14 to 15 per group. All tests were performed on the same mice before and after the *Pb*A infection.

5.1. Actimetry

The actimetry test allows for the evaluation of animals' spontaneous locomotion in an open field using an infrared actimeter (Bioseb). Mice were transferred to the behavior testing room 1hour before the test began. Each mouse was placed in a transparent Plexiglass enclosure 45 x 45 cm

in size, surrounded by two rows of infrared sensors 1 cm thick (Figure 23). The first row of sensors measures all horizontal motor movements (distance traveled, speed, and type of movement), while the second row of sensors (located at 7 cm in height) counts the number of times the animal straightens up (rearing). Each test lasts 10 minutes, and the mice are free to explore the compartment during that time. The variables used are the distance traveled (in cm), the percentage of time spent resting, the percentage of time spent moving slowly and the percentage of time spent moving quickly.

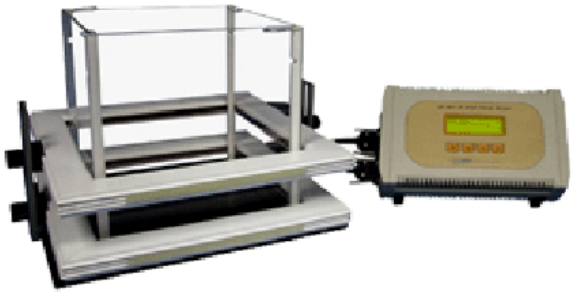

Figure 23: Actimetry arena.

5.2. Elevated plus maze (EPM)

EPM is a straightforward and well-validated test for studying anxious behavior in rodents. It is based on the animal's internal conflict between a natural desire to explore unknown environments and the anxiety caused by open spaces and heights [359]. It entails positioning the mouse in the center of a cross, forming a raised labyrinth 50 cm above the floor. This labyrinth has four arms, two of which are closed by 14.5 cm high walls and two of which are open (Figure 24). The labyrinth's arms are 36.5 cm long and 6 cm wide. As a result, the mouse will have the option of exploring either arm. The brightness above the open arms is restricted to no more than 200 Lux. The mouse placed them in the middle of the maze and allowed them to explore the maze for ten minutes. She is then returned to her cage, and the maze is cleaned with ethanol before the next mouse enters it. The installation includes infrared sensors linked to a camera and the preconfigured Ethovision XT 7.0 (Noldus, Wageningen, Netherlands) software for detecting animal movements and measuring the percentage of time spent in the open arms versus the total time of the experiment.

Figure 24: Elevated plus maze.

5.3. Y-Mase Spatial

The Y-maze is used to assess the spatial reference memory of rodents. The Y-maze had arms that were each 28 cm long, and 6.2 cm wide, and had opaque walls that were 15 cm high. The walls around the room were covered with various extra maze cues (Figure 25). The mice had free access to two of the three arms during the acquisition phase (5 min). The mouse is returned to the maze after 2 minutes and has free access to all three arms for 5 minutes (Test phase). The amount of time the mouse spent in each arm of the maze was recorded using EthovisionXT (Noldus Information Technology, Wageningen, The Netherlands) during both phases. The percentage of time spent in each arm (familiar and new) during the 5-min test phase was calculated.

Figure 25: Y-Maze spatial test.

5.4. Novel object recognition (NOR)

The NOR, or novel object recognition test, is based on rodents' natural preferences to explore a new object over a familiar one. This test was performed as previously described [360]. The

experimental device was a square enclosure (50 x 50 cm) surrounded by black partitions to limit the mice's visual field to the test arena (Figure 26). The test was conducted over three days and included the following: a habituation phase of 10 minutes per day for the first two days; the first day in an empty enclosure; the second day in the same enclosure with two identical training objects; and the third day with a first acquisition phase of 15 minutes with two identical objects (different from those used on the second day); and the second phase of 10 minutes for the retention test with a retention interval of one hour. During the retention test, the arena contained a familiar object (which was present during the 15 min acquisition phase) and a new object. Movements were recorded using the Ethovision XT 7.0 software (Noldus, Netherlands), and the time spent exploring the objects (new and familiar) was measured. To be included in the protocol, animals must explore the objects for at least 20 seconds during the acquisition phase. The main result was the discrimination index (DI), which was calculated as (TB – TA) / (TB + AT). Where TB is the exploration time of the novel object A (TA) and the familiar object B (TB).

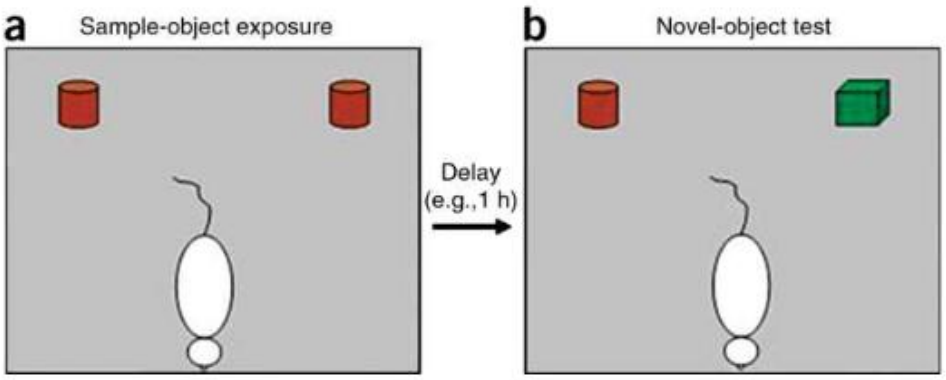

Figure 26: Novel object recognition.

5.5. Spontaneous alternation

The spontaneous alternation test measures working memory, which is the ability to retain information in the short term and use it immediately to express appropriate behavior in a given situation. This test took place in a 30 x 8 x 15 cm Y-shaped maze with identical arms separated by a 120° angle (Figure 27). The three arms are rated A, B, and C, and the animals are allowed to explore them for 8 minutes. The number of visits to each arm and the number of alternations is recorded. A spontaneous alternation is defined as three consecutive entries into the maze's three arms (ABC/BCA/ACB...). Mice with fewer than 10 visits were excluded from the test.

An alternation score is calculated from this sequence of visits using the following formula: (Number of alternations/ Total number of visits-2) * 100

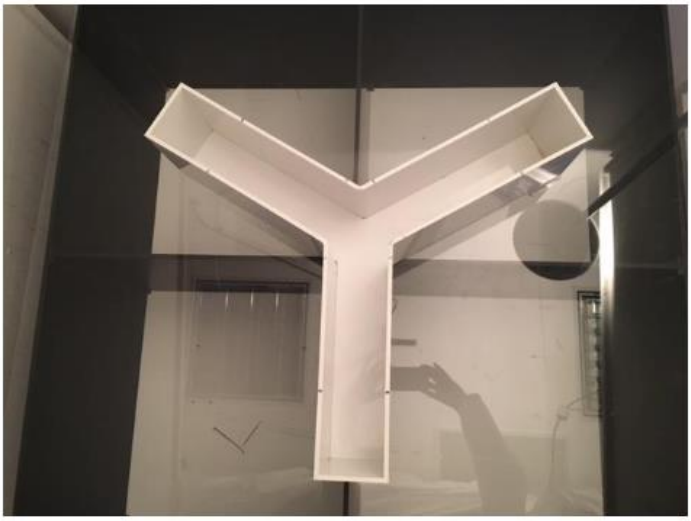

Figure 27: Spontaneous alternation y-maze apparatus.

6. Magnetic resonance imaging (MRI)

MRI experiments were only performed on B6 mice aged 6 and 12 months, after and before infection, as previously described [3]. Three MRI sequences were performed: T-2-weighted (T2W), diffusion-weighted images (DWI), and proton magnetic resonance spectroscopy (^{1}HMRS). Animals were anesthetized with isoflurane before being placed in a dual-coil small animal restrainer with a volume coil for transmission and a surface quadratic coil for signal reception. The electromagnetic interaction between the coils was actively decoupled. A force transducer was used to continuously monitor respiration rates and waveforms. The rectal temperature was kept at 37 °C by a feedback-controlled circulating water pad.

6.1. T2W images sequence

The fast spin-echo TurboRARE (rapid acquisition relaxation-enhanced) pulse sequence was used to acquire anatomic T2W images in the axial and sagittal planes with the following parameters: repetition time, 5000 ms; echo time, 77 ms; matrix size, 256 x 256 pixels; field of view, 20 x 20 mm; and the number of excitations, 4. Each T2W sequence took 10 minutes to acquire. Non-overlapping 0.5 mm-thick slices were acquired for axial and sagittal images.

6.2. DWI sequence

DWI was carried out on a single axial slice that was positioned in the cortical and subcortical regions. The DWI sequence was run in three directions [1, 0, 0], [0, 1, 0], and [0, 0, 1], with 6 b values used to characterize signal decay. The following b values were defined: 100, 200, 400, 600, 800, and 1000 s/mm^2. The sequence parameters were as follows: 20 x 20 mm field of view; 128 x 128 matrix size; 1 mm slice thickness; 3000 ms repetition time; 33 ms echo time; and an 8-minute acquisition time. The apparent diffusion coefficient (ADC) is a measurement of the movement of water molecules within tissues[361]. Tissue ADCs were obtained by fitting a mono-exponential model to the data set. This post-processing was carried out using the Paravision 5.1 software (Bruker, Ettlingen).

6.3. ^{1}H-MRS sequence

T2W axial and sagittal brain images were used to position the 1 H-MRS voxel. The point-resolved spatial selection protocol was used in conjunction with outer volume suppression and the following parameters to perform single voxel (4.0 x 0.8 x 3.8 mm^3) volume localized ^{1} H-MRS in the cerebral cortex: 20-millisecond echo time; 2.5-second repetition time; 4000-Hz spectral width; 512 averages; 20-minute acquisition time.

To quantify ^{1}H-MRS metabolites in vivo, the TARQUIN (totally automatic, robust quantitation in nuclear magnetic resonance) method was used. The TARQUIN algorithm consisted of three steps: (1) preprocessing (removal of post-acquisition residual water by Hankel singular value decomposition, automatic phasing); (2) basis set simulation (quantum mechanical simulation of ^{1}H-nuclear magnetic resonance signals from small molecules); and (3) solution of a nonlinear least squares fitting problem (modeling of the experimental data as a linear combination of modified basis signals and, after all segments were adjusted, re-stimulation of the basis set and synthesis at the new frequencies) [362, 363].

7. Statistical analysis

Statistical analyses and plots were done with R version 1.4.2 (http://www.rstudio.com/). To compare the Affymetrix microarray data between the CM^S and CM^R infected mice we performed a T test and computed a FDR adjusted pvalue. The other data of gene expression and plasmatic level were compared between the groups with a Kruskal-Wallis test followed by a Conover post-hoc test available in the R package PMCMRplus (FDR pvalue computed

according to Benjamini-Hochberg method) when significant. , protein level or activity) To test the difference between the 4 PMCMRplus. To make graphs, we used ggplot2. ggpubr, ggsignif, rstatix packages and GraphPad Prism (Version 5, GraphPad software, Inc.). For all experiments, error bars represent the SEM. The sample size and the number of replicates for each experiment are mentioned in the corresponding figure legend. The Mann-Whitney test was used to compare two groups. Analyses of variance for cell culture analysis (ANOVA), followed by Tukey's multiple comparisons or Bonferroni posthoc tests, were used to compare kinetics groups and treatment groups. For survival analyses, we used the log-Rank (Mantel-Cox) test. *P* values, for each experiment were reported as significant as *P<0.05; **P<0.01; ***P<0.001, ****P<0.0001. To look for relationship between the studied cytokines/chemokines and the markers of senescence we used the software Cytoscape v 3.9.0 and the database STRING for the mouse. Thanks to N SAIDI. An enrichment analysis based on the GO terms and the significantly differentially expressed genes from the transcriptomic data was done with the R package ClusterProfiler. Then pvalues were adjusted by the false discovery rate method. And we used the R package mixOmics to perform the discriminant analyse on the human data.

Results project 1

Title : Non canonical autophagy promotes p21-dependent senescence in astrocyte during *Plasmodium* infection that participate in CM pathogenesis

1. Increased expression of cell senescence-related markers together with resistance to apoptosis are observed in the brain during CM.

To get insight into the cellular and molecular mechanisms involved in CM pathogenesis, we used CM^S and CM^R mice infected with *Pb*A. The senescence markers were evaluated at days 6 and 8 post-infection when the B6 CM-susceptible mice (CM^S) showed neurological signs. First, we used Affymetrix GeneChip mouse expression arrays to compare whole-brain transcriptomic profiles from CM^S and CM^R *Pb*A-infected and control mice. Of the 1781 genes showing a difference between at least two groups of mice, 660 showed significant differences in expression when comparing CM^S with CM^R mice (false discovery rate (FDR)-adjusted p-value <0.05). The log2 fold-change ranged from -1.44 to 0.84. In this CM^S vs CM^R comparison, we found that 320 genes were significantly upregulated and 340 were downregulated. Next, we used the R package Cluster Profiler to perform a Gene Ontology (GO) enrichment analysis. Seventy-eight GO terms were found significantly enriched (FDR adjusted p value <0.05). Of the 141 genes classified in GO's *Mus musculus* senescence pathways (Table 6), we identified three genes (*Cdkn1a/p21, PML* (coding for the promyelocytic leukaemia protein) and *Calr* (coding for calreticulin)) that were upregulated in *Pb*A-infected CM^S mice, relative to *Pb*A-infected CM^R mice (Figure 28). Next, we used real-time qPCR to quantify the mRNA levels expression of six selected senescence biomarkers *p53*, $p21^{WAF1}$, *GADD45γ*, *p38MAPK*, $p16^{INK4}$ and *pRB* in whole brain and the spleen extracts from uninfected and *Pb*A infected CM^S compared to CM^R mice. A significant increase of $p21^{WAF1}$ (***P<0.001), *GADD45γ* (***P<0.001), *p38MAPK* (***P<0.001) and *pRB* (***P<0.001) was observed in the brain of CM^+ mice (*Pb*A-infected B6 mice developing CM) (Figure 29a), in contrary to $p16^{INK4}$ which was significantly reduced (**P<0.01). No significant difference was observed for *p53*. The link between $p21^{WAF1}$ and CM is reinforced by the significant diminution of its expression in the brain of *Pb*A-infected CM^R (****P<0.0001) as well as for *GADD45γ* (****P<0.0001) and *p38MAPK* (***P<0.001) when the expression of *p53* (*P<0.05) and $p16^{INK4}$ (**P<0.01) were significantly express (Figure 29a). In addition, anti-apoptotic gene expression such as *Bcl-x*

(**P<0.01*)* was significantly augmented in infected CM^S compared to control mice when no difference was observed for *Mcl-1*, *Bcl-w* and *Bcl-2* (Figure 29b). All these markers were exclusively expressed in the brain of CM^+ mice but not in the spleen (Figure 30). Quantitative western blot analysis performed on brain extract from same experimental mice confirmed increase at protein level in the brain of CM^+ compared to uninfected control of ~0.5-fold for $p21^{WAF1}$ (**P<0.01), 2-fold for p-p53/p53 ratio (*P<0.05) and ~2-fold for p-p38MAPK/p38 ratio (**P<0.01), (Figure 29c). Note that the ratio of p-ATM/ATM proteins (***P<0.01) was increased in the brain of CM^+ mice (Figure 29c) confirming DNA damages in parallel of anti-apoptotic processes characterized a high expression of Bcl-2 anti-apoptotic protein family [170]. In addition, we observed a higher percentage of SA-β-gal-positive cell staining (3-fold *P<0.05) on frozen coronal brain sections from CM^+ compared to uninfected mice (Figure 29d) [13]. Altogether, these data reveal an early senescence process in the brain of CM^+ mice characterized by a p21-dependent cell cycle arrest.

NCBI Gene ID	Gene Name	Gene symbol	P-value[1]
12575	Cyclin-dependent kinase inhibitor 1A	Cdkn1a	0.014
18854	Promyelocytic leukemia	PML	0.020
12317	Calreticulin	Calr	0.001

Table 7: Results of senescence genes up regulated in the brain of CM^S compared to CM^R infected mice identified by Affymetrix GeneChip.

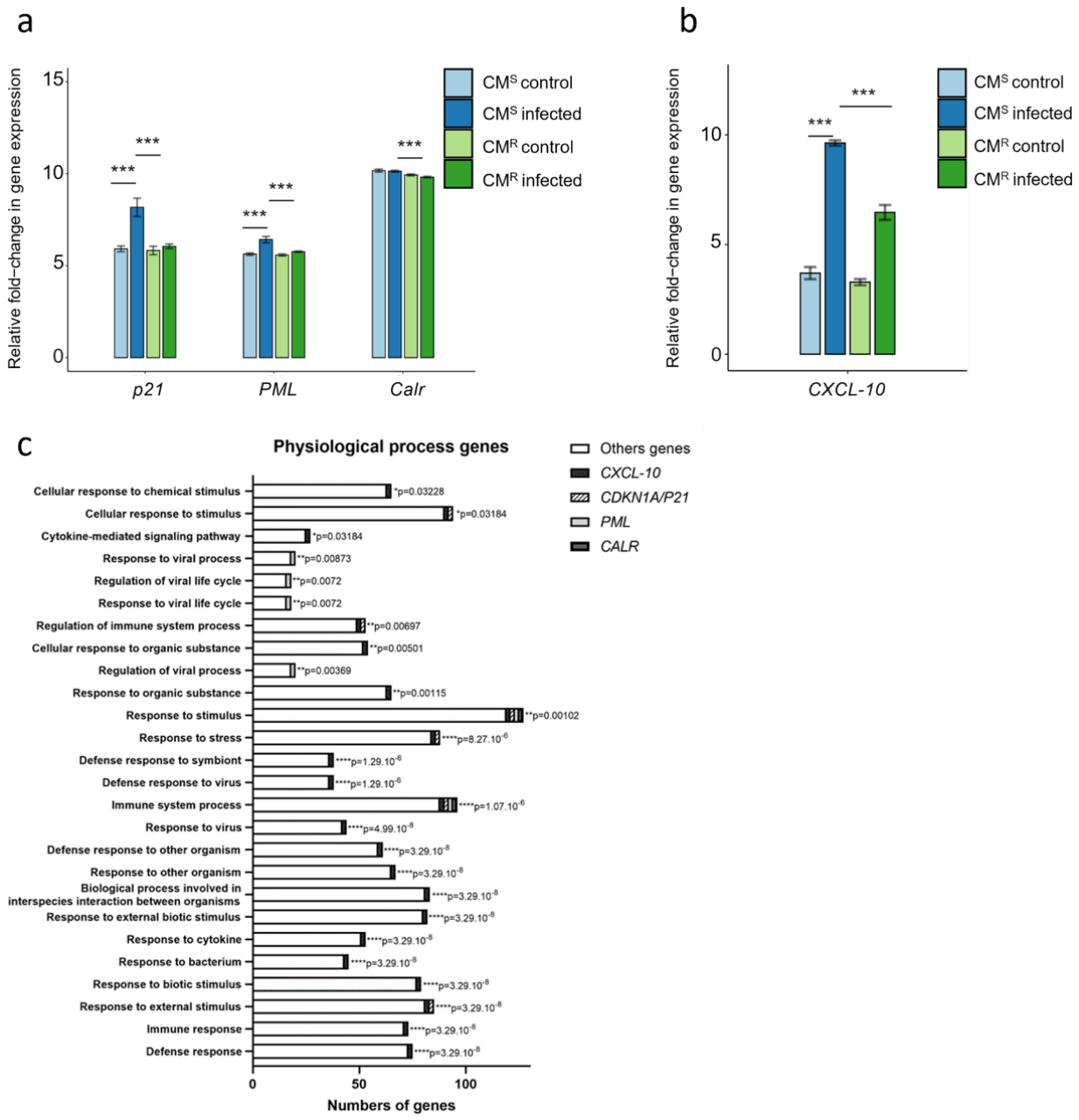

Figure 28: Senescence signature associated with ECM in the brain .

Relative fold-change in gene expression of (a) senescence markers (p21, PML and Calr) and (b) SASP chemokines CXCL-10, obtained from the brains of control and infected CM^S and CM^R mice in transcriptomic studies using Affymetrix GeneChip Mouse Expression Arrays. Data represented as mean±SEM. Values (n=3 per group) were compared to the control group or between selected groups using Benjamini–Hochberg False Discovery Rate. ***$p < 0.001$. (c) Contribution of senescence genes in physiological processes during ECM.

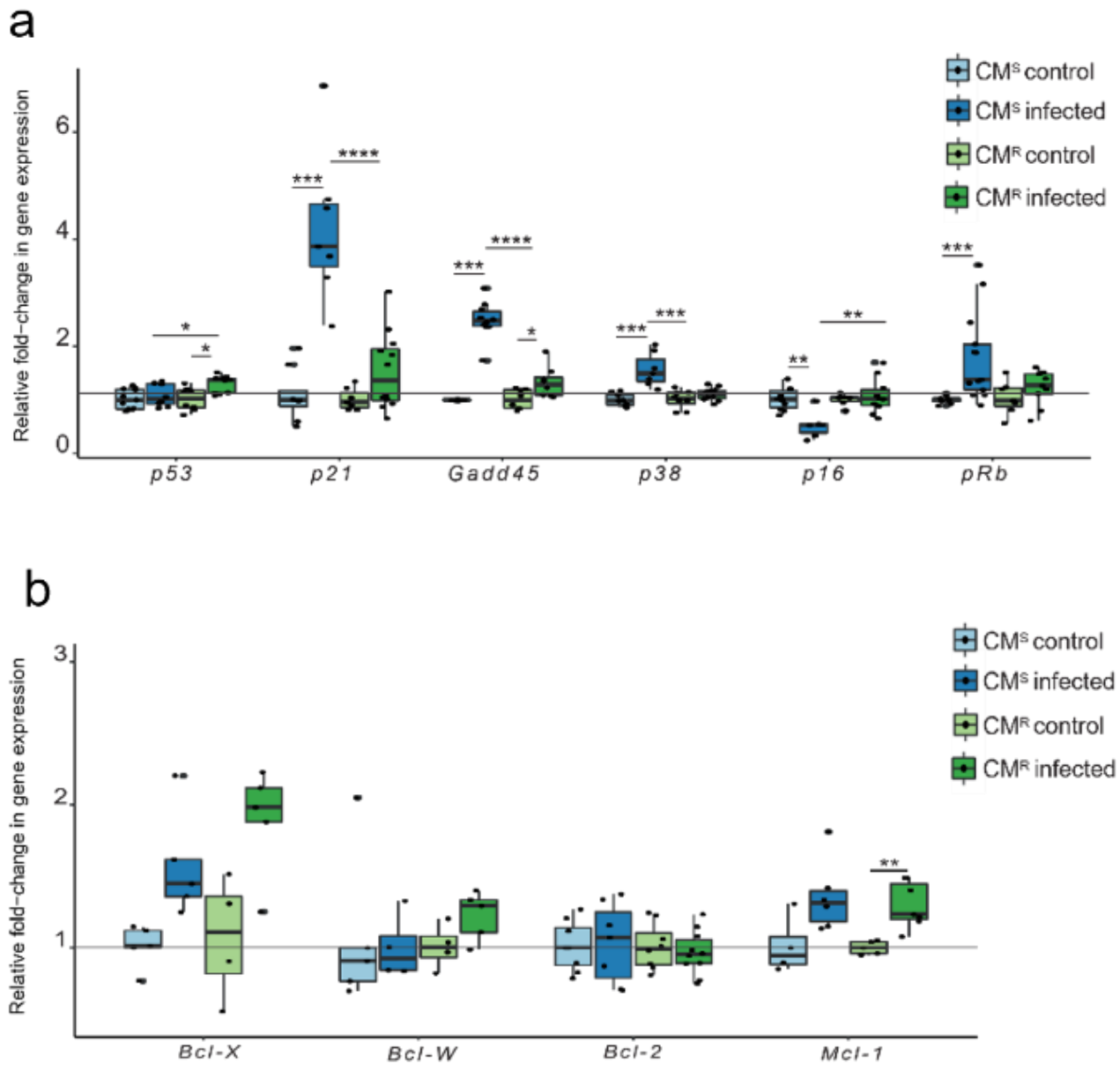
a
Relative fold-change in gene expression
0
2
4
6
CMS control
CMS infected
CMR control
CMR infected
*
*
***
****
***
****
*
***
***
**
**
***
p53
p21
Gadd45
p38
p16
pRb
b
Relative fold-change in gene expression
1
2
3
CMS control
CMS infected
CMR control
CMR infected
**
Bcl-X
Bcl-W
Bcl-2
Mcl-1

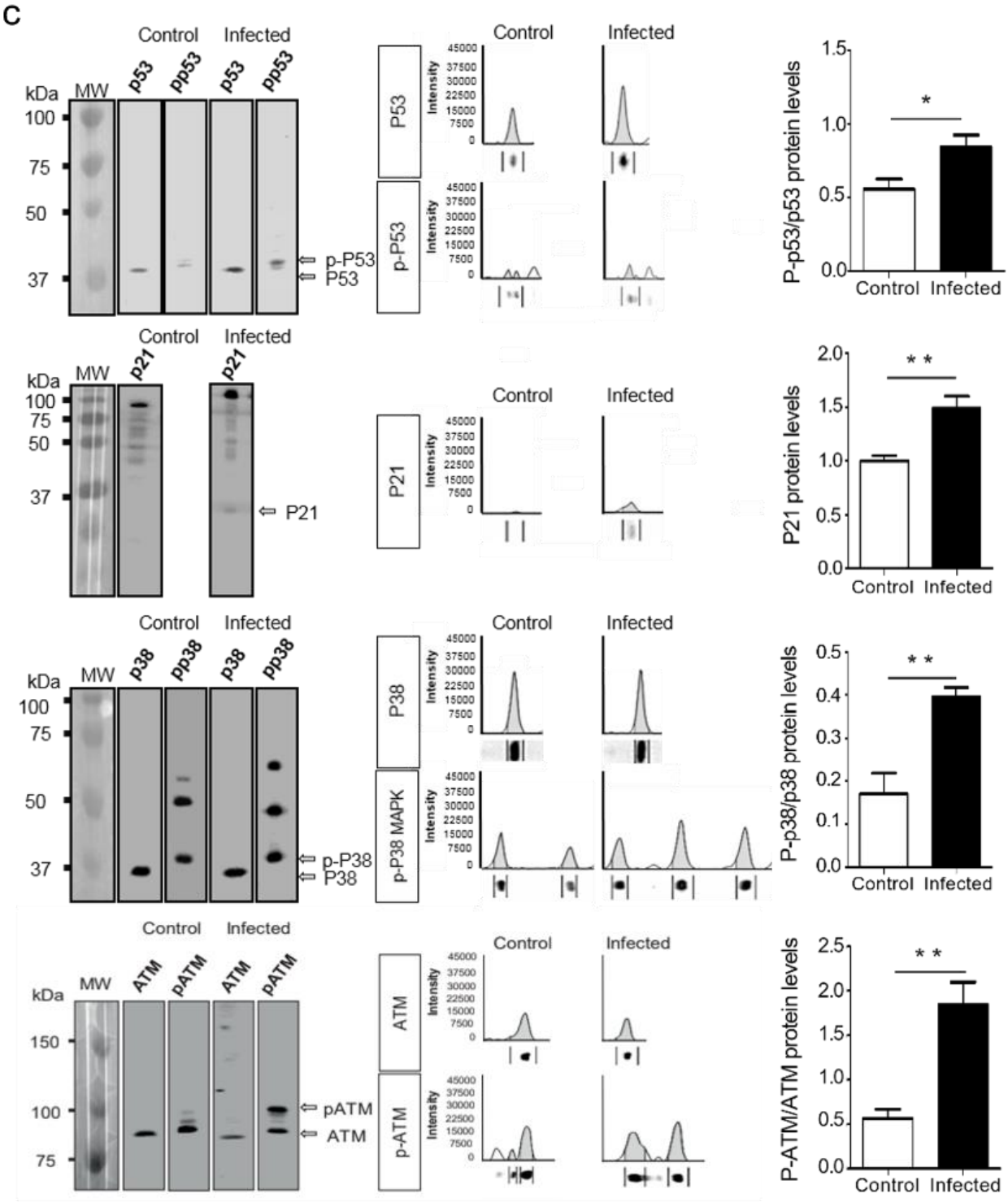
C
Control
Infected
kDa
MW
p53
pp53
100
75
50
37
p-P53
P53
P53
p-P53
Intensity
45000
37500
30000
22500
15000
7500
0
P-p53/p53 protein levels
1.5
1.0
0.5
0.0
*
Control
Infected
p21
P21
P21 protein levels
2.0
1.5
1.0
0.5
0.0
* *
p38
pp38
p-P38
P38
P38
p-P38 MAPK
P-p38/p38 protein levels
0.5
0.4
0.3
0.2
0.1
0.0
ATM
pATM
150
100
75
pATM
ATM
p-ATM
P-ATM/ATM protein levels
2.5
2.0
1.5
1.0
0.5
0.0

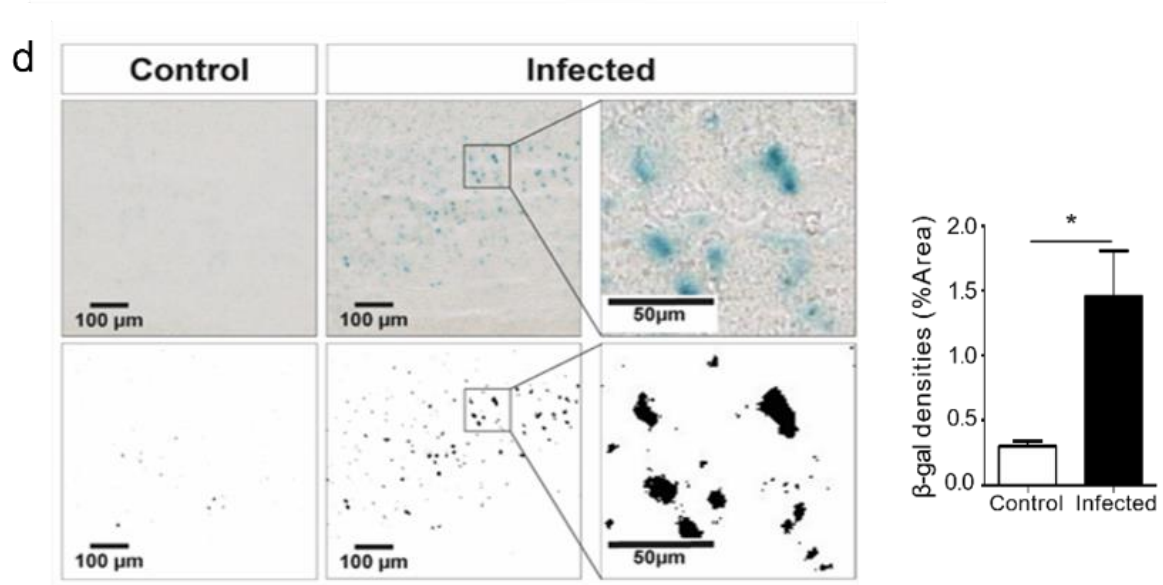

Figure 29: Senescence markers are expressed in the brain during ECM.

Fold relative expression of (a) p53, $p21^{WAF1}$, GADD45γ, p38MAPK, $p16^{INK4}$, pRB, cell cycle arrest and (b) Bcl-x, Bcl-w, Bcl-2 and Mcl-1 anti-apoptotic genes was quantified by RT-PCR in whole-brain of control and infected CM^S and CM^R mice. Relative mRNA levels in the infected groups were normalized to the respective control group. Data are presented as mean ± SEM. Values (n= 3-10 per group) were compared to the control group or between selected groups using a Mann–Whitney test. *p < 0.05; **p < 0.01; ***p < 0.001; ****p < 0.0001. (c) Western blot analysis of S15-phosphorylated and total p53(p-p53 and p53), $p21^{WAF1}$, Thr180/182-phosphorylated and total p38MAPK (p-p38 and p38), phosphorylated and total ATM (P-ATM and ATM) protein expression in the total brain lysates of control and infected CM^S mice. phosphorylated p53, p38 and ATM were quantified using imageJ software and normalized against total p53, p38 and ATM. Relative p-p53/total p53, p-p38/total p38 and p-ATM/total ATM protein levels were shown as mean ± SEM of at least three independent experiments. Total p21 was quantified using imageJ software and normalized to the control. The relative p21 protein levels was shown as mean ± SEM of at least three independent experiments. Values were compared to the control group using Student's t-test (*p < 0.05; **p < 0.01). (d) Representative SA-β-Gal staining in coronal brain sections, from control and infected CM^S mice. Scale bars= 100µm. The graph shows the results of quantitative analysis of SA-β-Gal staining. Data are representative of three independent experiments and shown as the mean ± SEM. Values were compared to the control group using Student's t-test *p < 0.05.

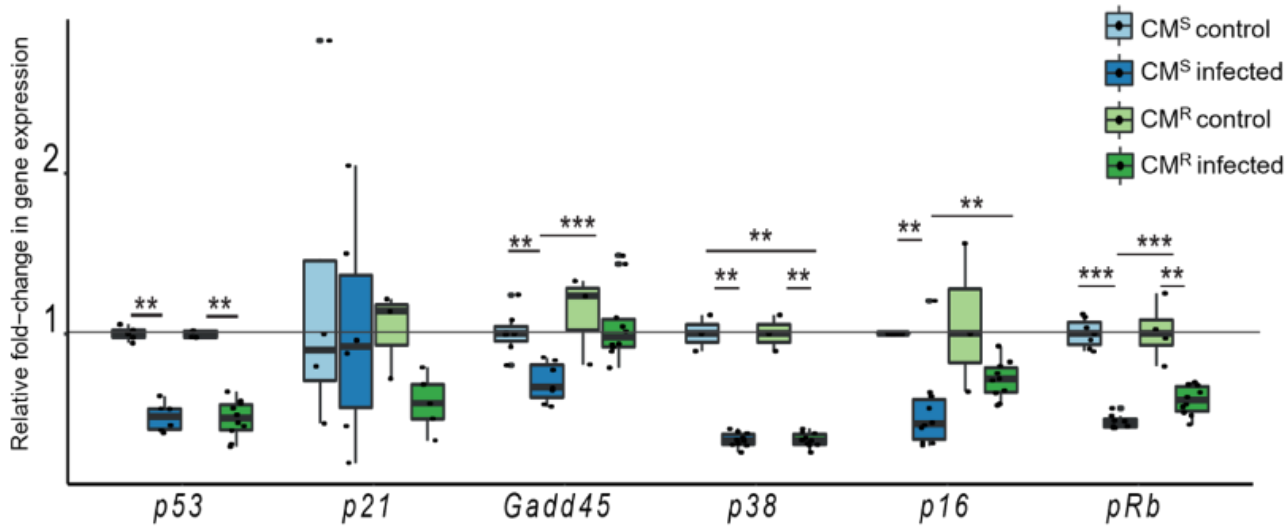

Figure 30: Expression of senescence markers in spleen.

Fold relative expression of (a) *p53*, *p21*^{WAF1}, *GADD45γ*, *p38MAPK*, *p16*^{INK4} , *pRB*, cell cycle arrest genes was quantified by RT-PCR in whole-spleens of control and infected CM^S and CM^R mice. Relative mRNA levels in the infected groups were normalized to the respective control group. Data are presented as mean ± SEM. Values (n= 3-10 per group) were compared to the control group or between selected groups using a Mann–Whitney test. ***p < 0.001; ****p < 0.0001.

2. Astrocytes are the brain cells most affected by senescence during CM.

In order to determine which subpopulation(s) of glial cells underwent senescence during ECM. For that, we first quantified by RT-qPCR the expression of the senescence markers by astrocytes and microglial cells isolated from brain of *Pb*A-infected CM^S and CM^R. A significant increase of $P21^{WAF1}$ (*P<0.05), *Gadd45γ* (**P<0.01) and *Bcl-x* (*P<0.05) genes expression was found in astrocytes isolated from CM^S mice but not in astrocytes from CM^R mice or microglial cells isolated from CM^S or CM^R mice (Figure 31a,b). These data were then confirmed on brain section stained with different immunofluorescent-labelled antibodies specific for $p21^{WAF1}$, p-P53 and BCL-X (for senescence markers), in addition to DAPI for cell nuclei and GFAP for reactive astrocytes. Confocal microscopy analysis showed a high number of $GFAP^+$ activated astrocytes expressing P21 (~40%) in the cortex of CM^+ mice brain compared to uninfected control (~15%) (***P<0.001) (Figure 31c). We also noticed an increase of $GFAP^+$ $p\text{-}P53^+$ astrocytes (~36%) in CM^+ mice compared to 13% for control mice (*P<0.05) (Figure 31d) and of $GFAP^+BCL\text{-}X^+$ astrocytes (~42%) in CM^+ mice compared to uninfected controls (<20%) (**P<0.01) (Figure 31e). Of note, activation of SA-β-Gal expression in similar areas on coronal brain sections was observed in CM^+ mice (Figure 32). Thus, astrocytes seem to be particularly affected by a P21-mediated senescence process induced by the parasite in the brain during CM.

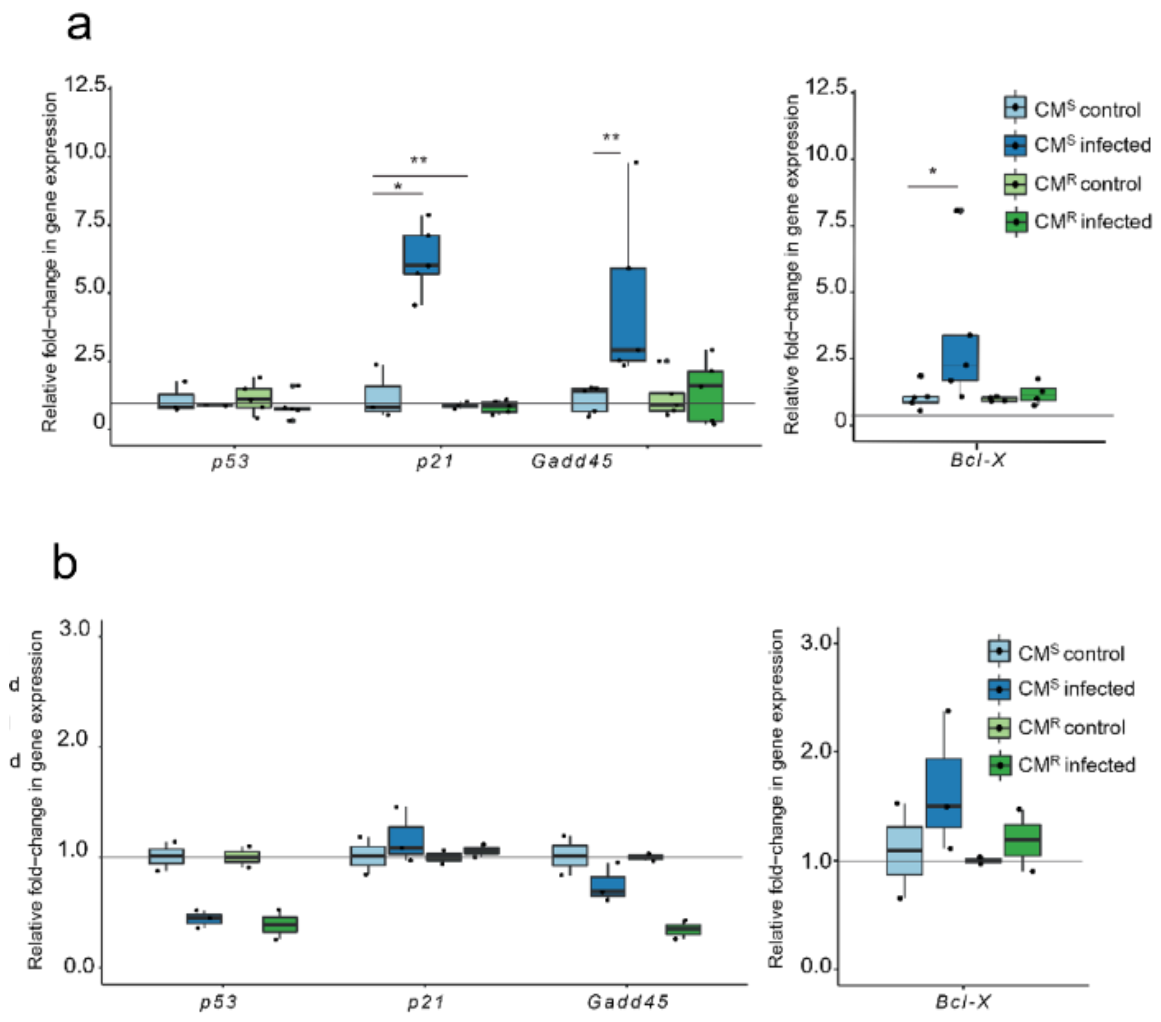
a
Relative fold-change in gene expression
12.5
10.0
7.5
5.0
2.5
0
**
*
**
p53
p21
Gadd45
*
Bcl-X
CM^S control
CM^S infected
CM^R control
CM^R infected
b
d
d
3.0
2.0
1.0
0.0
p53
p21
Gadd45
Bcl-X

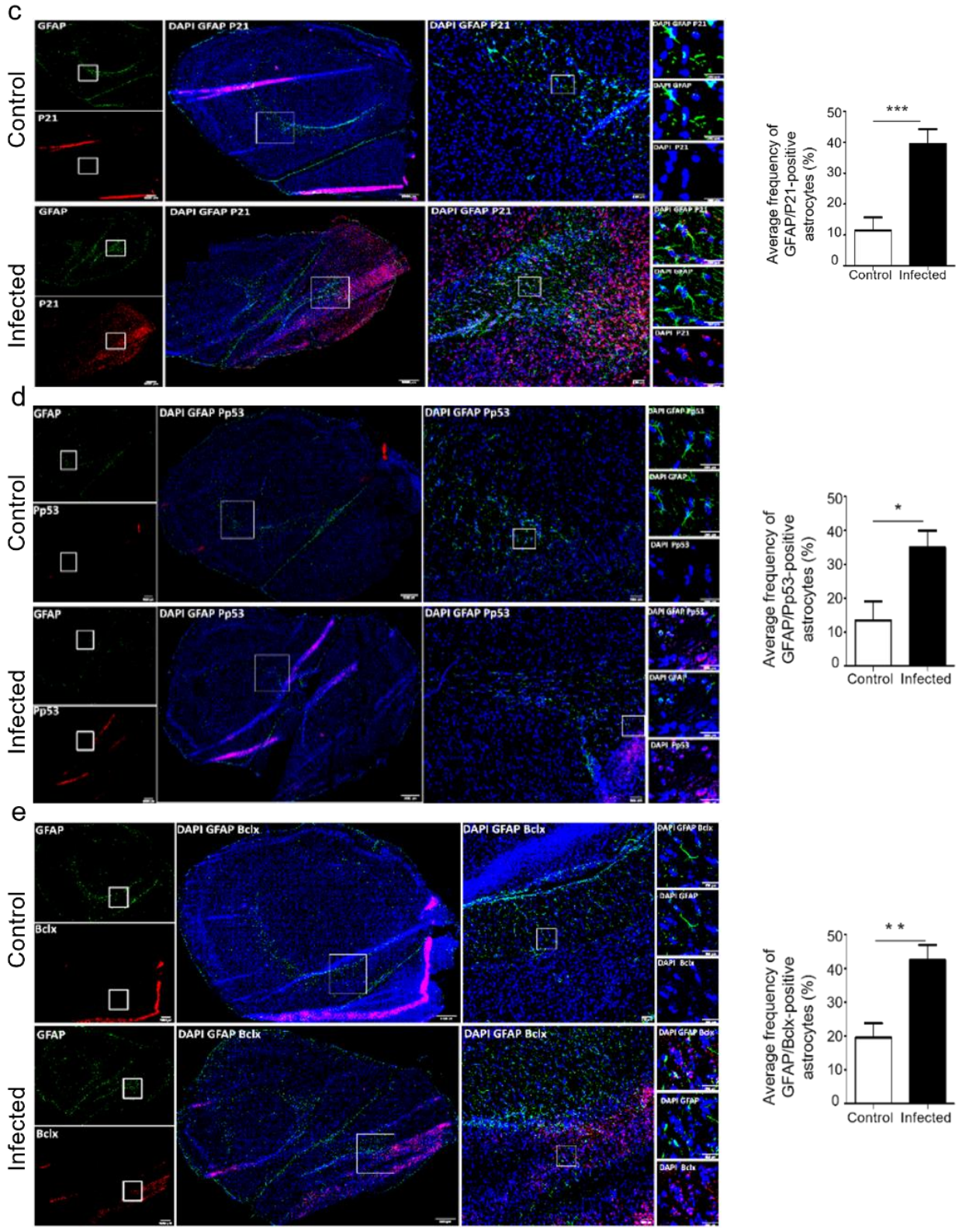

Figure 31: Astrocytes during ECM developed a senescence-like phenotype.

Relative mRNA levels of *p53*, *p21*^{WAF1} and *GADD45γ* and *Bcl-x* in the sorted (a) Astrocytes and (b) Microglia of control and infected CM^{S} and CM^{R} mice. Representative immunofluorescence images showing (c) p21 or (d) p-p53 or (e) Bcl-x protein levels (red) in GFAP^{+} astrocytes (green) in the brain of infected CM^{S} mice compared to control. scale bar represents 2000µm. White boxes show magnified

regions (scale bars,100µm). Graphs shows quantification of the percentage of activated astrocytes (GFAP+ cells) expressing senescence markers (p21 or p-p53 or Bcl-x). Data are presented as mean ± SEM. Values (n= 3 mice) were compared to the control group using Student's t-test. *p < 0.05; **p < 0.01; ***p < 0.001.

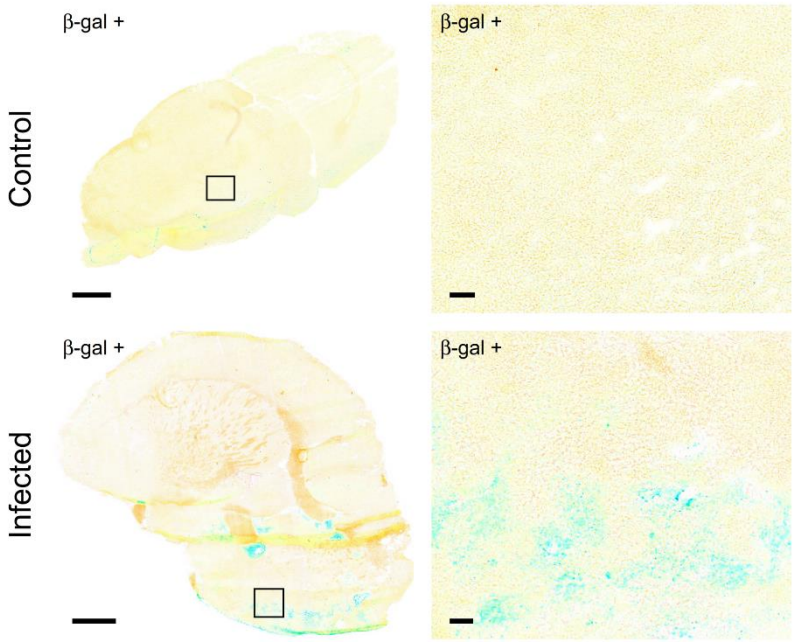

Figure 32: Representative SA-β-Gal staining in whole coronal brain sections, from control and CM⁺ mice. Scale bars= 1000; 50µm.

3. Astrocyte senescence is triggered by direct interaction with the parasite.

To determinate the molecular events implied in the induction of senescence, primary culture of astrocytes derived from CM^S mice were incubated *in vitro* with *Pb*A-iRBCs at a ratio 1:10 for 24 hours. Induction of senescence was followed up at 4, 7, 10 and 15 days after removal of *Pb*A-iRBCs by measuring SA-β-Gal activity by confocal microscopy. As shown in the figure 33a, a significant elevated percentage of SA-β-Gal^+ cells were observed in parasite stimulated cells from day 4 (~30% of SA-β-Gal^+ cells; **P<0.01) compared to the unstimulated cells (~10% of SA-β-Gal^+ cells). Maximum SA-β-Gal^+ cells was obtained at day 10 (~40% of SA-β-Gal^+ cells; *P<0.05) and maintained at day 15 (~37% of SA-β-Gal^+ cells; **P<0.01) post-stimulation. Induction of SA-β-Gal activity was correlated with morphological changes in astrocytes such as a cytoplasm enlargement and a low nucleus/cytoplasm ratio on day 10 post stimulation (Figure 33b), and a rise in the expression of $p21^{WAF1}$ (***P<0.001) (Figure 33c). Confocal microscopy imaging revealed that 18% astrocytes co-expressed GFAP and P21 in stimulated cultures compared to 6% in unstimulated control (*P<0.05) (Figure 33d). This suggests that direct stimulation by *Pb*A-iRBCs can induce a P21-senescence-like phenotype in astrocytes.

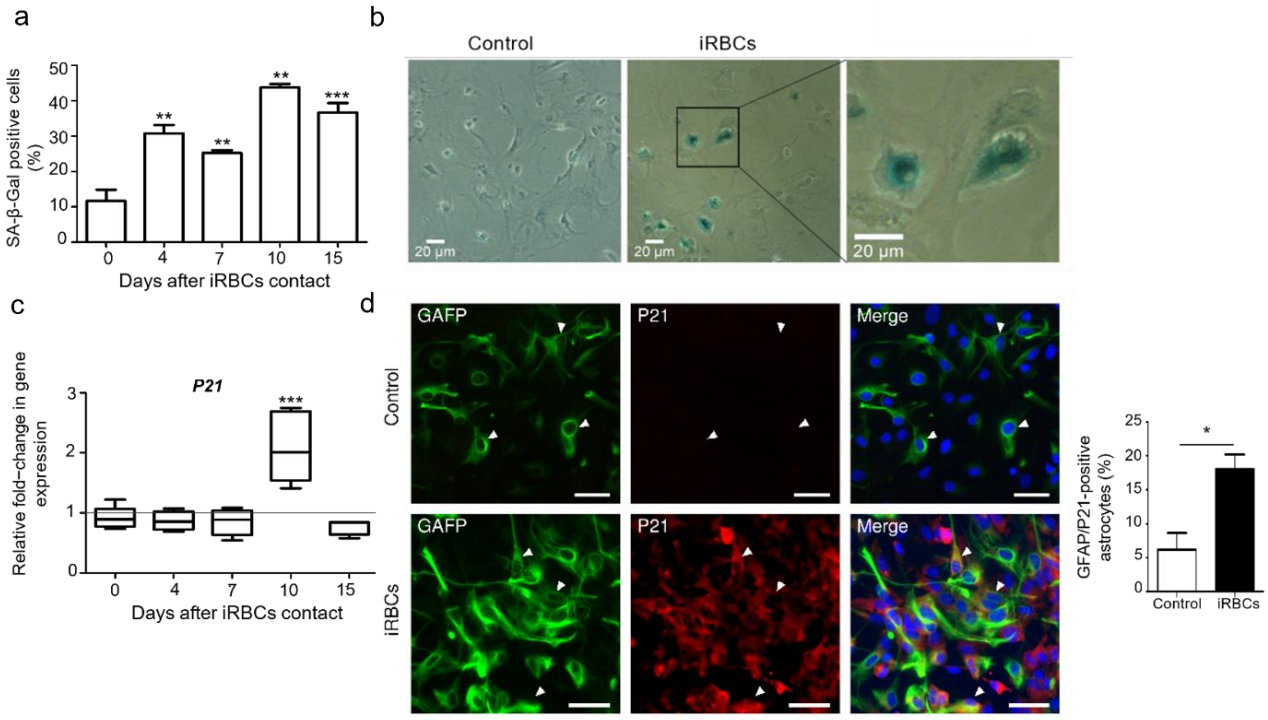

Figure 33: Astrocytes undergo premature senescence after direct contact with PbA-iRBCs.

Primary astrocyte cultures were incubated with *Pb*A-iRBCs at a ratio of 1:10 for 24 h. *Pb*A-iRBCs were removed after 24h and the astrocytes were incubated further for 4 or 7 or 10 or 15 days. (a) Graph shows quantification result of SA-β-gal positive astrocytes after contact with *Pb*A-iRBCs at different timepoint (0,4,7,10 and 15 days) (n = 3-5 per condition). (b) Representative images of SA-β-gal staining in astrocytes stimulated or not with *Pb*A-iRBCs at day 10. (Scale bar: 20µm). (C) Quantification by RT-qPCR of relative $p21^{WAF1}$ gene expression at different time points (4,7,10 and 15 days) post stimulation by *Pb*A-iRBCs as compared to unstimulated controls. (n = 4-7 per group) (d)Representative images of double immunofluorescence showing p21 protein levels (red) and GFAP astrocytes (green) in astrocytes stimulated with *Pb*A-iRBCs at day 10 as compared to that of unstimulated cells. (Scale bar: 20µm). Graphs shows quantification of the percentage of GFAP/P21 positive astrocytes (n= 3-5 per group). All data are presented as mean ± SEM. Values were compared to the control group using Student's t-test. *p < 0.05; **p < 0.01; ***p < 0.001.

4. Astrocyte senescence induced by *Pb*A is triggered by a LC3-dependant non-conventional autophagy.

We then assessed if P21-induced senescence process by *Pb*A-iRBCs in stimulated astrocytes could be linked with the LC3-associated phagocytosis (LAP) evidenced during the transfer and the degradation of *Pb*A-microvesicles in astrocytes [94]. Immunohistochemistry and confocal microscopy analysis of *Pb*A-iRBCs stimulated and unstimulated astrocytes cultures showed $GFAP^+$ astrocytes (in green) coexpressing $P21^+$ (in red) and MAP1LC3/$LC3^+$ (in magenta) (~16% in stimulated cells compared to ~7% for controls; **P<0,01) (Figure 34a). To confirm the link between LC3 and P21, we used RNA silencing strategy by targeting *Rubcn/Rubicon* and *Atg5* known to be essential for the LAP of *Pb*A-microvesicles in astrocytes. After switching off *Rubcn* and *Atg5*, at day 10 post stimulation in astrocyte cultures, the expression of $p21^{WAF1}$ was strongly diminished concomitantly with *Map1Lc3/Lc3*, *Rubcn* and *Atg5* a in cultures treated with si*Rubcn* and si*Atg5* compared to iRBCs-stimulated control (Figure 34b). No effect was observed on $p16^{INK4}$ expression. We also analyzed by confocal microscopy the effect of the autophagy inhibitor bafilomycin A_1 (BAF A_1) on the induction of senescence by *Pb*A in astrocytes. In BAF A_1 treated cultures, the percentage of $GFAP^+$ and $P21^+$ astrocytes were decreased (~5%) (**P<0.01) compared to untreated parasite stimulated cultures (~20%) (Figure 34c). Altogether, these data strongly suggest a link between the autophagy process induced by the astrocyte-*Pb*A interaction.

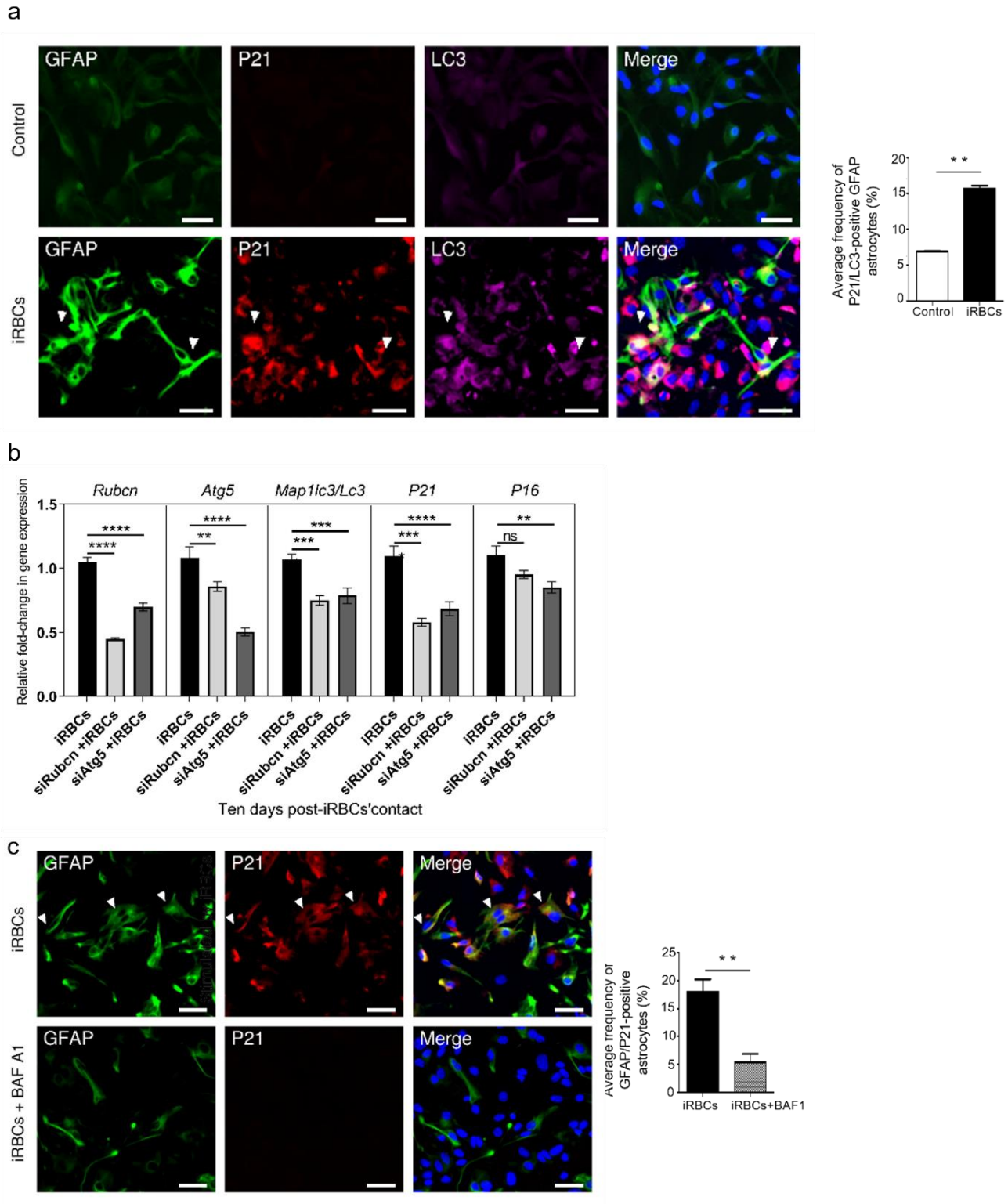

Figure 34: Autophagy promote astrocyte senescence after contact with PbA parasite.

Primary astrocyte cultures incubated with *Pb*A-iRBCs, were transfected or not with 25nM siRubcn/Rubicon or siAtg5 RNA from the time of contact to 10 days. (a) Confocal immunofluorescence images labeling for GFAP astrocytes (green), p21 (red) and LC3 (magenta) in astrocytes stimulated with *Pb*A-iRBCs at day 10 as compared to that of unstimulated cells. (Scale bar: 20µm). Graphs shows quantification of the percentage of GFAP/P21/LC3 positive astrocytes. Data are presented as mean ± SEM. Values (n= 2-5 per group) were compared to the control using Student's t-test **P < 0.01. (b)

Quantification by RT-qPCR of relative *Rubcn*, *Atg5*, *Map1lc3/Lc3*, *p21* and *p16* genes expression in untreated, siRubcn/Rubicon-, and siAtg5- transfected astrocytes at 10 days after stimulation by *Pb*A-iRBCs (n = 3-5 per group). Data are mean fold-change ± SEM of genes expressed. One-way ANOVA with Tukey's multiple comparison test was used for statistical analysis, with data considered significant at **P < 0.01; ****P < 0.0001. (c) Primary astrocyte cultures were incubated with *Pb*A-iRBCs for 24 h and treated or not with 10 nM of BAF A1. Confocal immunofluorescence images labeling for GFAP astrocytes (green) and p21 (red) in BAF A1-treated astrocytes, compared to the untreated cells. (Scale bar: 20µm). Graphs shows quantification of the percentage of GFAP/P21 positive astrocytes. Data are presented as mean ± SEM. Values (n= 2-5 per group) were compared to the infected untreated group using Student's t-test **P < 0.01.

5. Parasite-induced senescence is correlated with the production of pro-inflammatory cytokines/chemokines by astrocytes.

We next looked at the expression of CXCL-10, especially in senescent astrocytes, to confirm that senescent cells can play a significant role in the induction of inflammation in the brain during CM. CXCL-10 is one of the main pro-inflammatory factors significantly increased in the differential transcriptomic (Figure 28b) (***P<0.001) as well as by RT-qPCR quantification (****P<0.001) in the brain of CM^S/CM^R infected mice compared to controls (Figure 35a). We also found a high *Cxcl-10* gene expression in *ex vivo* astrocytes isolated from CM^+ brain compared to CM^R group (Figure 35b) as well as in CM^+ mice plasma (Figure 35c). These findings attested to the astrocytes' involvement in the neuroinflammatory response to ECM. Immunohistochemistry and confocal microscopy analysis of brain sections from CM^+ and control mice labelled with an anti-GFAP (in green), anti-CXCL-10 (in magenta), anti-P21 (in red) and DAPI (in blue) shown that 36% of activated $GFAP^+$ astrocytes co-express P21 and CXCL-10 in CM^+ compared to 4% in uninfected control mice (**P<0.01) (Figure 35d). Following on from our recent observation whereby CXCL-10 secretion by *Pb*A-iRBC-stimulated astrocytes from CM^S mice is associated with LC3 non-canonical autophagy[94], we next looked at whether CXCL-10 secretion by senescent astrocytes is linked to autophagy in primary astrocyte cultures treated with bafilomycin A_1 (BAF A_1).. Ten days after contact with *Pb*A-iRBC, the proportion of $GFAP^+P21^+$astrocytes producing CXCL-10 (in magenta: ~14%) was significantly greater than in non-stimulated cells (~2.8%; *P<0.05). There was no difference between control cell cultures treated with BAF A_1 (~2%) and non-stimulated cells (Figure 35e). These data were confirmed in 10 days post-stimulated primary astrocytes cultures after silencing *Rubcn* and *Atg5* genes in which *Cxcl-10* expression was downregulated (*P<0.05) in astrocytes (Figure 35f). No difference was found between stimulated astrocytes control or after silencing *Atg5* alone (Figure 35f). Furthermore, p21-dependent senescence interactions between *P38*, *P53*, *P21* and *CXCL-10* expressed in brain of CM^+ mice were also revealed by the STRING database (Figure 36a). CXCL-10, p21 and LC3 were positively associated, albeit not significantly (Figure 36b). The production of two others pro-inflammatory factors, Il-6 and Ccl-2 were also increasing *ex vivo* in astrocytes isolated from brain of CM^+ mice and *in vitro*, after *Pb*A stimulation (Figure 37-38). We observed interactions between senescence factors (such as P38 and P53) and two pro-inflammatory factors (IL-6 and CCL2) (Figure 36a,b). The fact that *IL6* and *CCL2* expression was elevated in *Pb*A-stimulated

astrocytes silenced for *Rubcn* suggested that IL-6 and CCL2 production was not related to LAP (Figure 38). These data strongly suggest that CXCL-10 secretion by senescent astrocytes depends (at least in part) on the autophagy of *Pb*A-MVs.

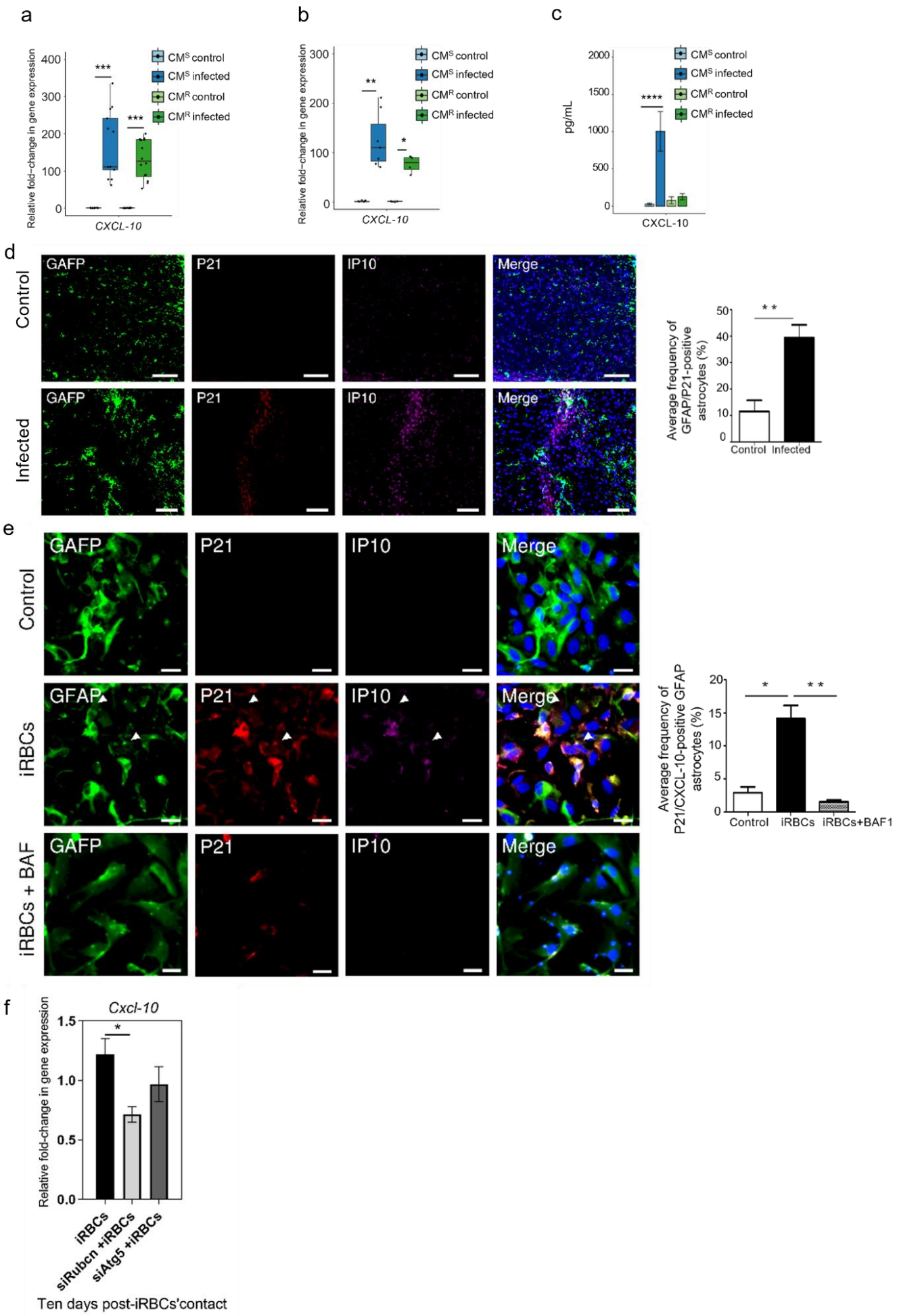
a
b
c
Relative fold-change in gene expression
CXCL-10
CM^S control
CM^S infected
CM^R control
CM^R infected
pg/mL
CXCL-10
d
Control
Infected
GAFP
P21
IP10
Merge
Average frequency of GFAP/P21-positive astrocytes (%)
Control
Infected
e
Control
iRBCs
iRBCs + BAF
Average frequency of P21/CXCL-10-positive GFAP astrocytes (%)
Control
iRBCs
iRBCs+BAF1
f
Cxcl-10
Relative fold-change in gene expression
iRBCs
siRubcn +iRBCs
siAtg5 +iRBCs
Ten days post-iRBCs'contact

Figure 35 : Senescent astrocytes secrete CXCL-10 during ECM.

(a)Relative expression of *CXCL-10* genes in the brains of control and infected CM^S and CM^R mice (n= 11-16 per group) and in (b) the sorted astrocytes (n= 4-7 per group). (c) CXCL-10 protein levels in the plasma of CM^S and CM^R mice with and without *Pb*A infection were measured by ELISA (n= 5 per group). Values were compared to the control group or between selected groups using a Mann–Whitney test. *p < 0.05; **p < 0.01; ***p < 0.001; ****p < 0.0001. (d) Representative immunofluorescence images showing p21 (red) and CXCL-10 (magenta) protein levels in $GFAP^+$ astrocytes (green) in the brain of infected CM^S mice compared to control. scale bar represents 2000µm. Graphs shows quantification of the percentage of GFAP/P21/CXCL10 positive astrocytes (n= 3 per group). Data are presented as mean ± SEM . Values were compared to the control group using using Student's t-test **P < 0.01. (e) Confocal immunofluorescence images labeling for GFAP astrocytes (green), p21 (red) and CXCL-10 (magenta) in stimulated astrocytes treated or not with BAF1 A1, compared to that of unstimulated cells. (Scale bar: 20µm). Graphs shows quantification of the percentage of GFAP/P21/CXCL-10 positive astrocytes. Data are presented as mean ± SEM. Values (n= 2-5 per group) were compared to the infected untreated group using Student's t-test *p < 0.05; **p < 0.01. (f) Quantification by RT-qPCR of relative *CXCL-10* genes expression in untreated, siRubcn/Rubicon-, and siAtg5- transfected astrocytes at 10 days after stimulation by *Pb*A-iRBCs (n = 3-5 per group). Data represents median fold-change ± SEM of genes expressed. Statistical analysis was performed using one-way ANOVA with Dunnett's multiple comparisons post-test, with data considered significant at *P < 0.05.

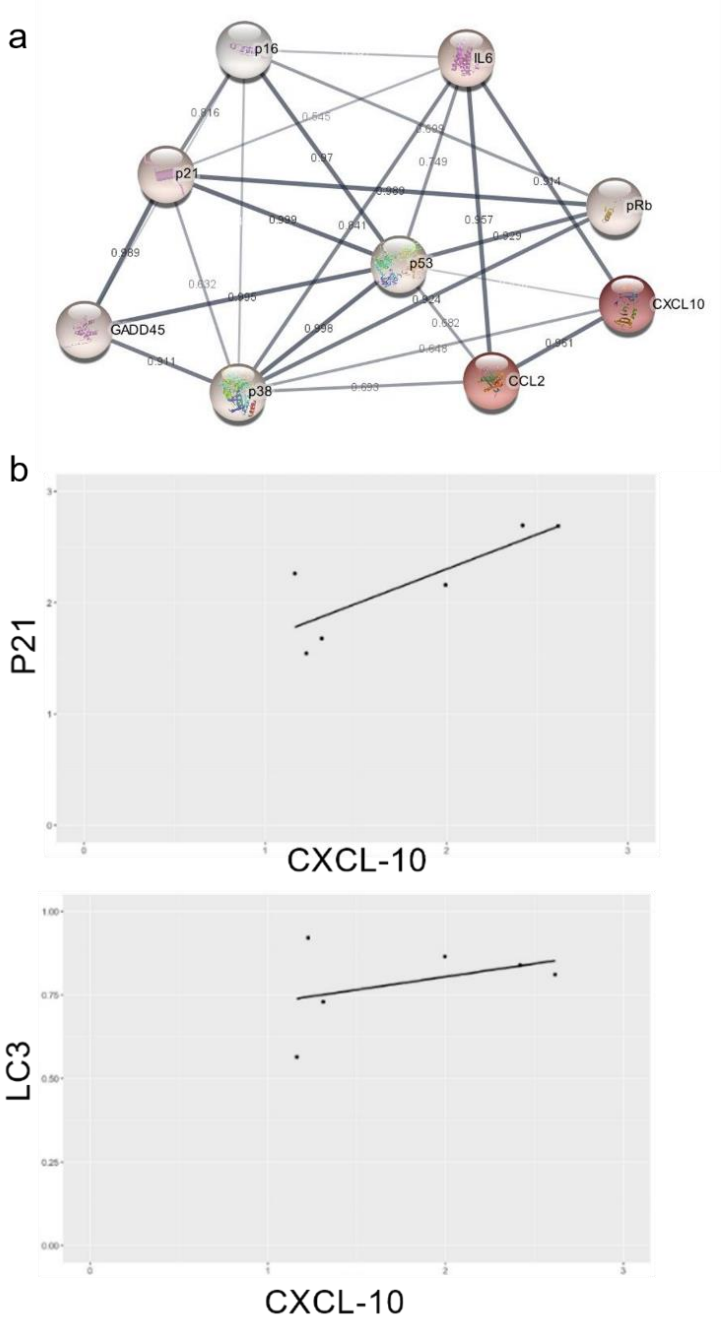

Figure 36: Interaction between cell cycle arrets regulators and SASP factors during ECM.

(a) Cytoscape analysis was performed to show the interaction between cell cycle arrest genes (p53, p38, p21, pRb, GADD45 and p16) and SASP factors (IL-6, CXCL-10 and CCL-2). The intensity of node coloring reflects the mean level of gene expression in the brain of CM^S infected mice, the transparency and thickness of the edges are linked to the confidence in the interaction. (b) Relationship between p21 or LC3 and CXCL-10 in *Pb*A stimulated astrocytes in vitro.

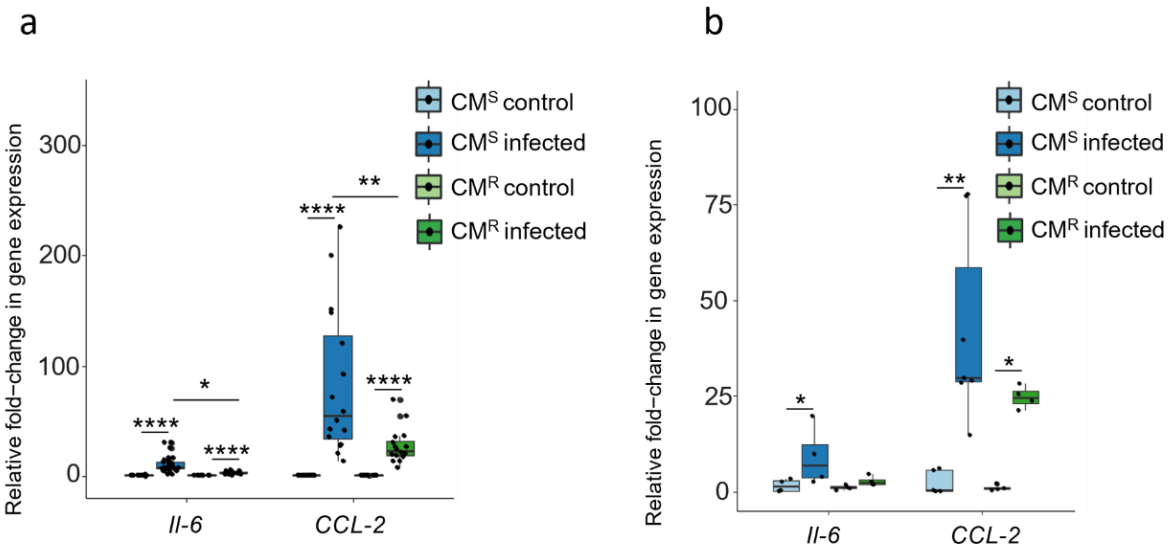

Figure 37: Expression of IL-6 and CCL-2 in the brains and sorted astrocytes.

(a) Relative expression of *IL-6* and *CCL-2* genes in the brains of control and infected CM^S and CM^R mice (n= 11-16 per group) and in (b) the sorted astrocytes (n= 4-7 per group). Data are presented as mean ± SEM, compared to the control group or between the selected groups using Mann–Whitney test; **P < 0.01; ***P < 0.001; ****p < 0.0001.

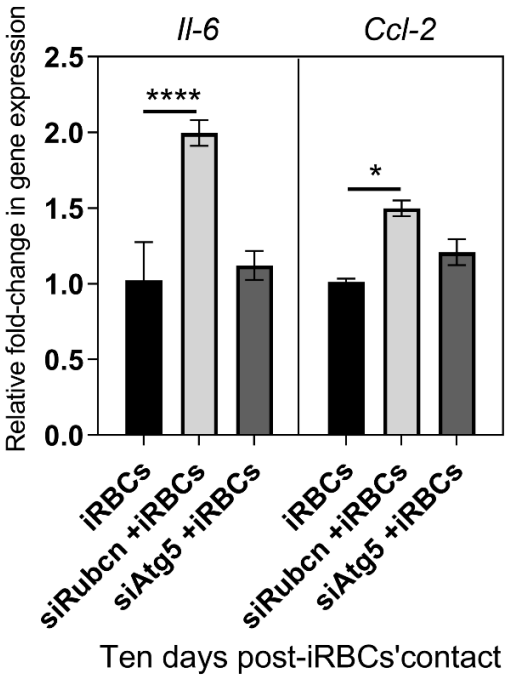

Figure 38: Expression of Il-6 and CCL-2 in stimulated astrocytes treated or not by Rubcn/Rubicon or Atg5 siRNA.

Quantification by RT-qPCR of relative *IL-6* and *CCL-2* genes expression in untreated, siRubcn/Rubicon-, and siAtg5- transfected astrocytes at 10 days after stimulation by *Pb*A-iRBCs (n = 3-5 per group). Data represents median fold-change ± SEM of genes expressed. Statistical analysis was

performed using One-way ANOVA with Tukey's multiple comparison test, with data considered significant at *P < 0.05; ****p < 0.0001.

6. Treatment with senolytic drugs prevents the accumulation of senescent astrocytes in the brain and the development of ECM by reducing the inflammatory response

To confirm the impact of astrocytes senescence in the pathophysiology of ECM, we treated CM^S mice before infection with a cocktail of two senolytic drugs, Dasatinib and Quercetin (DQ), that eliminate the senescent cells by inducing apoptosis [364]. Oral administration of DQ to CM^+ mice from day 1 to 8 post-infection resulted in a 60% survival from ECM (**P<0.01), mice died 30 days later from hyperparasitemia (Figure 39a). Parasitemia level was not affected by the treatment (Figure 39b). A significant decrease in the mRNA expression of $p21^{WAF1}$(**P<0.01), *GADD45γ* (*P<0.05), and *pRB* (*P<0.05), confirming the elimination of senescent astrocyte in infected and treated mice. No significant difference was observed for *p53*, *p38MAPK* and *p16* (Figure 39c). In line with these observations, the percentage of $GFAP^+$ activated astrocytes expressing P21 were also decreased on brain section of infected and treated mice (~28%) compared to infected untreated mice (~40%) (*P<0,05) (Figure 39d).

We also evaluate the impact of the DQ senolytic drugs on the inflammatory response induced in the brain after infection by quantifying CXCL-10 expression. We observed a significant reduction of *Cxcl10* gene expression (*P<0,05) in the brain of infected treated mice compared to infected non-treated mice (Figure 39e). This was associated with a significant decrease in the production of CXCL-10 (****P < 0.0001) in the sera of infected but untreated CM^+ mice (Figure 39f). Altogether, these data suggest that the inflammatory response during ECM is linked to astrocyte senescence.

However, treatment with Navitoclax and Fisetin, two others senolytic drugs, had no effect on the development of ECM (Figure 40).

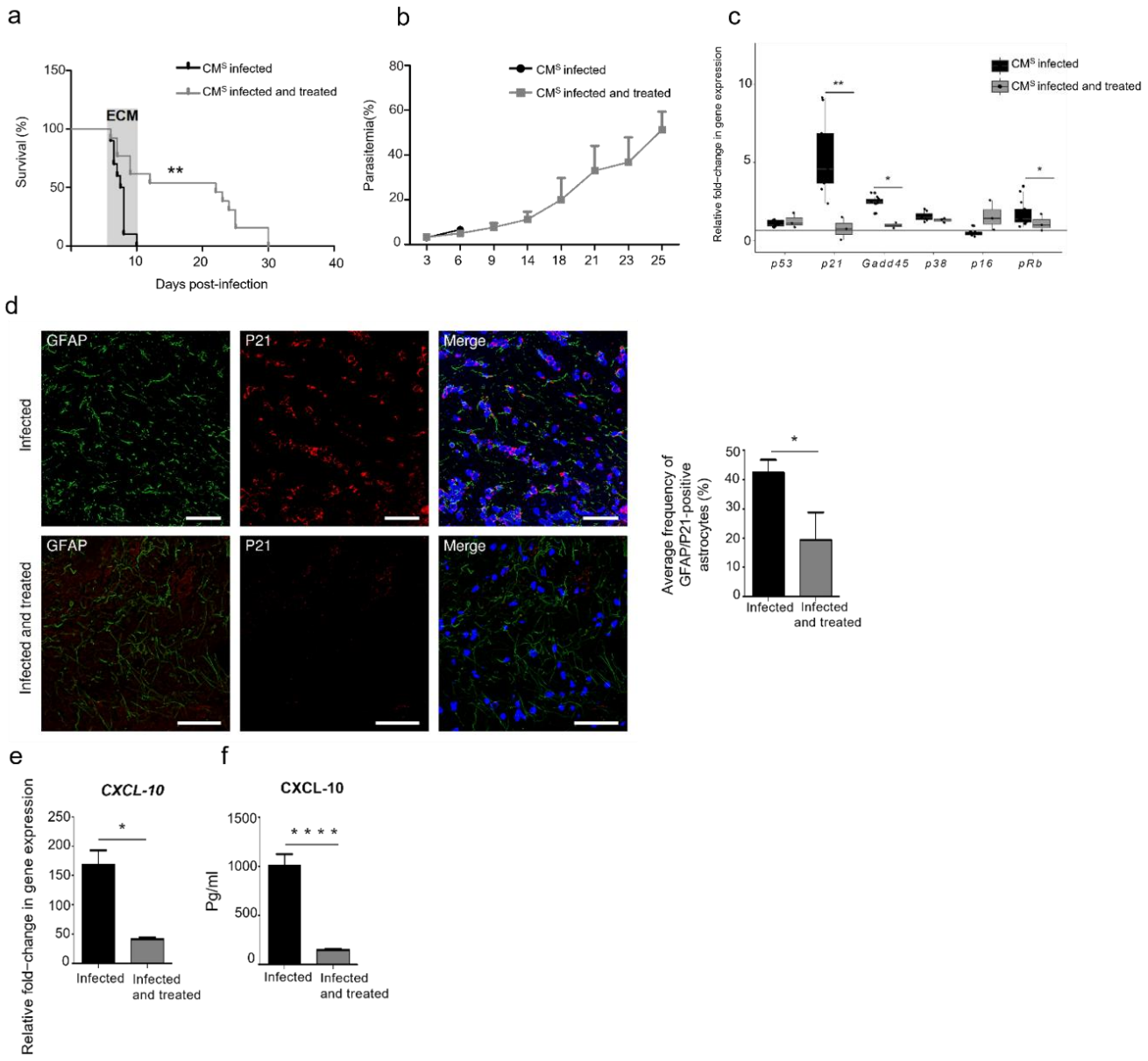

Figure 39: Dasatinib plus Quercetin prevented ECM, and was effective in eliminating senescent astrocytes.

(a)Survival and (b) Parasitemia rate of mice infected with *Pb*A and treated with Dasatinib plus Quercetin. Data are results from n = 10–13 mice that were compared using a Mantel-Cox test (a) or a Mann–Whitney test (b). (c) Expression of *p53*, *p21*, *GADD45γ*, *p38MAPK*, *P16* and *pRB* genes was quantified by RT-qPCR in brain at day 6.5 post infection for *Pb*A group and day 11 post infection for infected and treated group. (d) Representative immunofluorescence images showing p21 protein levels (red) in GFAP$^+$ astrocytes (green) in the brain of infected and infected treated mice. scale bar: 400µm. Graphs shows quantification of the percentage of GFAP/p21 positive astrocytes. (e) Expression of *CXCL-10* was quantified by RT-qPCR in the brain of mice (n =3-16 per group). (f) CXCL-10 protein levels in the plasma of infected and infected treated mice were measured by ELISA (n =5 per group). Data are mean fold-change ± SEM. Values in c-f were compared to the infected group using Mann–Whitney test; *P< 0.05; **P < 0.01; ***P < 0.001; ****p < 0.0001.

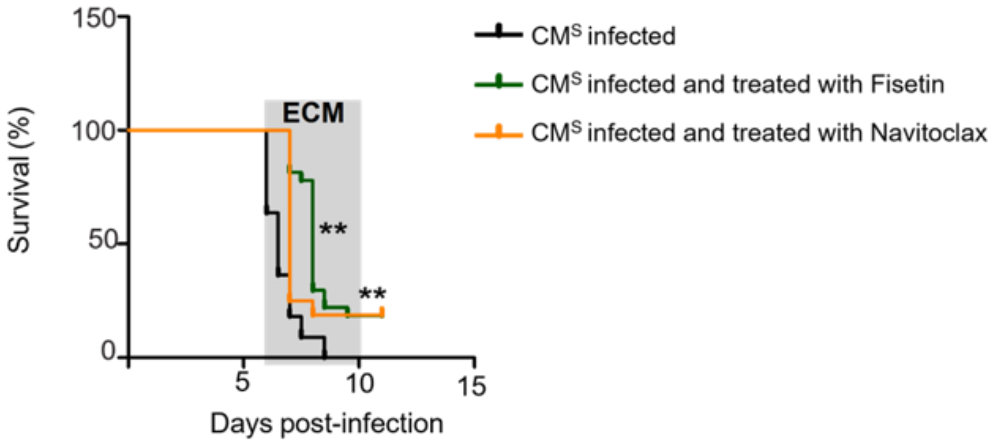

Figure 40: Survival rate of mice infected with* Pb*A and treated with Navitoclax or Fisetin.

Data are results from n = 13–27 mice that were compared using a Mantel-Cox test.

7. Relevance to *P. falciparum*-induced human CM

We extended our study to human by assessing the expression of P21 (using confocal microscopy) in the brains of patients from the Ivory Coast infected with *P. falciparum* and had died from CM.

In line with our findings in the mouse, the percentage of activated astrocytes expressing $GFAP^{+}p21^{+}$ was higher in brain samples from the CM patients (~27%) than in samples from healthy individuals (~15%) (**P<0.01) (Figure 41a). Furthermore, we detected sequestered *P. falciparum* iRBCs in the microvasculature of the same brain regions (Figure 41b).

Next, we used RT-qPCR to quantify the mRNA expression of $p21^{WAF1}$ and $p16^{INK4}$ in total peripheral blood mononuclear cells (PBMCs) from patients from India with mild malaria (MM), isolated CM, multi-organ failure (MOD) and (CM-MOD). We observed significantly greater expression of $p21^{WAF1}$ in the CM (*P<0.05) and CM- MOD relative to the MM groups (**P<0.01). The difference in p16 expression between the MM and MOD groups was not significant (Figure 41c). However, the p16 expression in the CM group (**P<0.01) and the CM-MOD group (**P<0.01) was significantly lower than in the MM group, and there was no difference in p16 expression between the CM and CM-MOD groups (Figure 41d). These results suggested that p21-driven senescence also occurs in the PBMCs and brain cells of patients who have died of CM.

Finally, we evaluated the relationship between the expression of senescence markers P16 and P21 with plasma levels of SASP including CXCL-10 [97]. To that end, we tested the ability of cytokine and chemokine plasmatic levels and p21 and p16 expression levels to discriminate between different malaria severity groups among the patients from India. As observed on Figure 41E, the MM and the CM-MOD groups are disjointed. Interestingly, p21 appeared to be associated with death (Figure 41f).

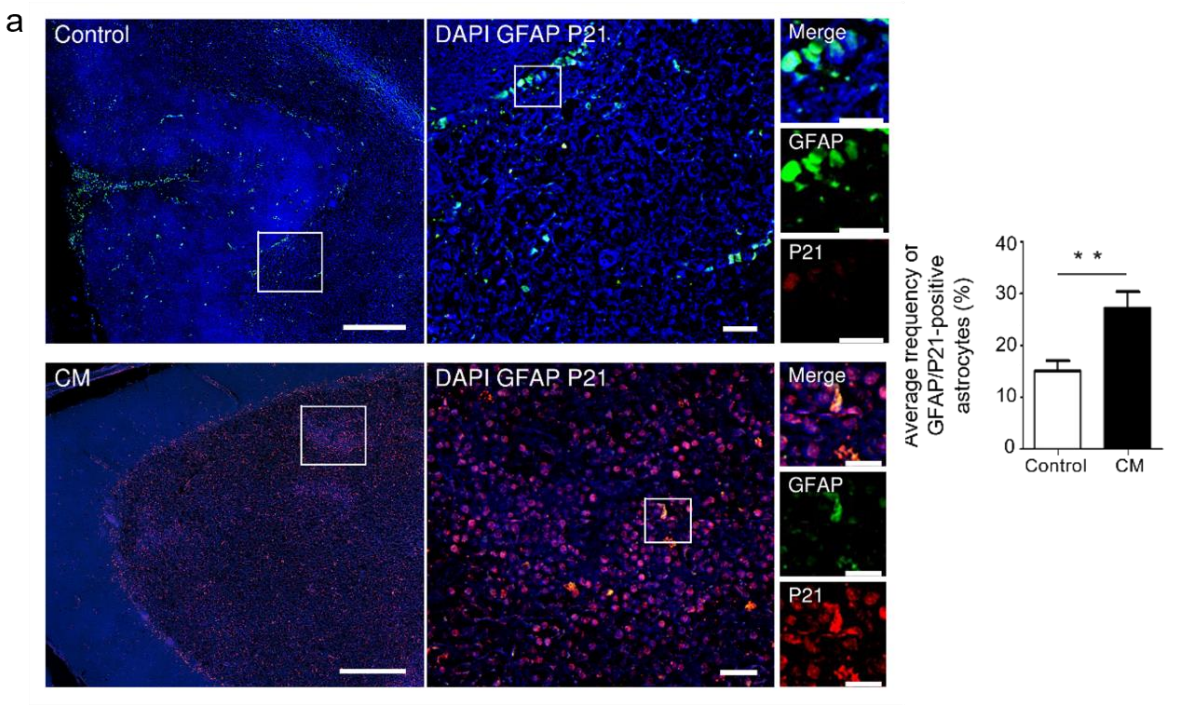
a
Control
DAPI GFAP P21
Merge
GFAP
P21
CM
DAPI GFAP P21
Merge
GFAP
P21
Average frequency of GFAP/P21-positive astrocytes (%)
40
30
20
10
0
* *
Control
CM

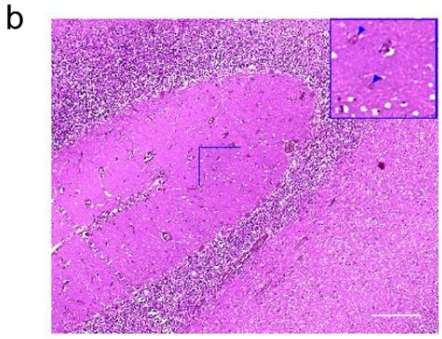
b

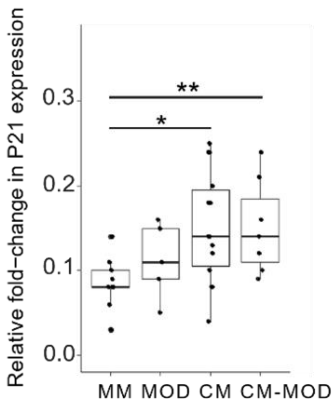
c
Relative fold−change in P21 expression
0.3
0.2
0.1
0.0
**
*
MM MOD CM CM-MOD

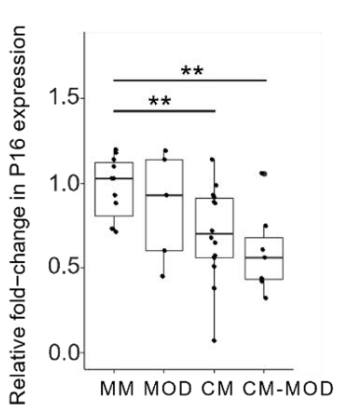
d
Relative fold−change in P16 expression
1.5
1.0
0.5
0.0
**
**
MM MOD CM CM-MOD

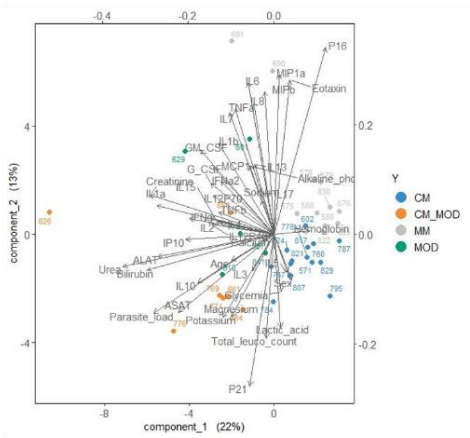
e
component_2 (13%)
component_1 (22%)
P16
MIP1a
IL6
MIP1
Eotaxin
TNFa
IL7
IL1b
GM_CSF
G_CSF
MCP1
IL13
IFNa2
Alkaline_phos
Creatinine
IL15
IL1a
Soluble_IL7
IL12P70
IL2
Haemoglobin
IP10
ALAT
Urea
Bilirubin
IL10
Age
IL3
Glycemia
ASAT
Parasite_load
Potassium
Magnesium
Lactic_acid
Total_leuco_count
P21
Y
CM
CM_MOD
MM
MOD

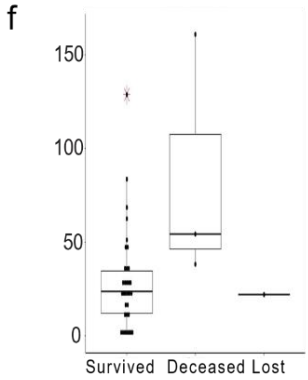
f
150
100
50
0
Survived
Deceased
Lost

Figure 41: p21 is expressed in peripheral blood and in brain of CM patients.

(a) Representative images of double immunofluorescence for GFAP (Green) and p21 (Red) in the human brain sections of CM patients compared to controls. Graphs represents quantification of the percentage of GFAP/p21 positive astrocytes. Values were compared with controls using Student's t-test; **P < 0.01. Results obtained were presented as median ± SEM. (b) Hematoxylin and eosin stained sections of the brain of CM patients .Scale bar represents 100µm. Quantification by RT-qPCR of relative (c) p21 and (d) p16 genes expression in peripheral blood of Malaria patients : Mild Malaria (MM) , Multiple organ dysfunction (MOD), Cerebral malaria (CM) and CM-MOD. Values were compared to the MM group or between the selected groups using Mann–Whitney test; *P< 0.05; **P < 0.01. Error bars show the median ± SEM. (e) Principal component Analysis showing the contribution of senescence markers, cytokines and chemokines and parasite load in different patients groups (f) Distribution of the parasitic load according to the issue from the treatment.

Results project 2

Title: Impact of senescent astrocytes on premature aging of the brain and associated cognitive deficits during CM

1. Old mice are resistant to ECM

To assess the role of senescent astrocytes, which accumulate with normal aging, on CM development, we compared the mortality and parasitemia rates in *Pb*A-infected mice aged 6 and 12 months (6 and 12M) to young adult mice aged 2 months (2M). We observed that in contrast to the 2- and 6-months-old mice, which died between 6 to 10 days post-infection, the B6 12-months-old mice did not develop ECM and survived for more than 20 dpi before succumbing to hyperparasitemia (Figure 42).

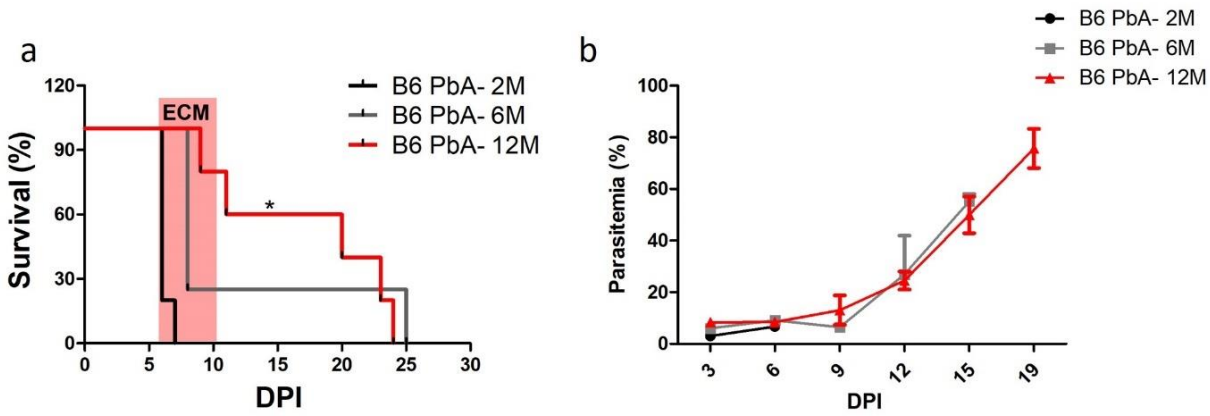

Figure 42: Old mice are resistant to CM.

(A) Survival and (B) parasitemia percentage (%) of mice infected with *Pb*A aged 2, 6 and 12 months. Data are results from n = 10 mice that were compared using a Mantel-Cox test. *p < 0.05.

2. Expression of senescence markers in the aging brain

The presence of senescent cells in the brain of old mice was then assessed using established senescence markers including cell cycle arrest and SASP, by RT-qPCR. The findings confirmed the induction of senescence in old mice's brain, as evidenced by increased expression of *p16*, *p38* and *Rb* in the brain of old (12M) compared to young adult mice (2M) (Figure 43). There was no significant difference in the expression of *p21*, *p16*, *p38* or *GADD45* in the brain of old mice after *Pb*A infection, but there was a significant decrease in the expression of *Rb* (Figure 43). These results suggest that the *Pb*A infection in old mice did not influence the senescence process in the brain.

For the moment, we evaluated the expression of five cytokines and chemokines of SASP: *MCP-1*, *IL-6*, *CXCL-10*, *IFN-γ* and *TNF-α*. There was no significant difference in the expression of these markers in the brain of old mice compared to young adult mice (Figure 44). Augmented expression of *MCP-1* and *TNF-α* was observed in the brain of old mice after *Pb*A infection (Figure 44). Interestingly, we observed that the *Pb*A-infected old mice showed decreased expression of *MCP-1*, *IL-6*, *CXCL-10*, *IFN-γ* and *TNF-α* in the brain when compared to the *Pb*A-infected young adult mice. These results suggest that the protection from CM in old mice was associated with a decrease in brain inflammation.

Other markers will be conducted to determine whether and how the aging brain's senescence can play a protective role in ECM.

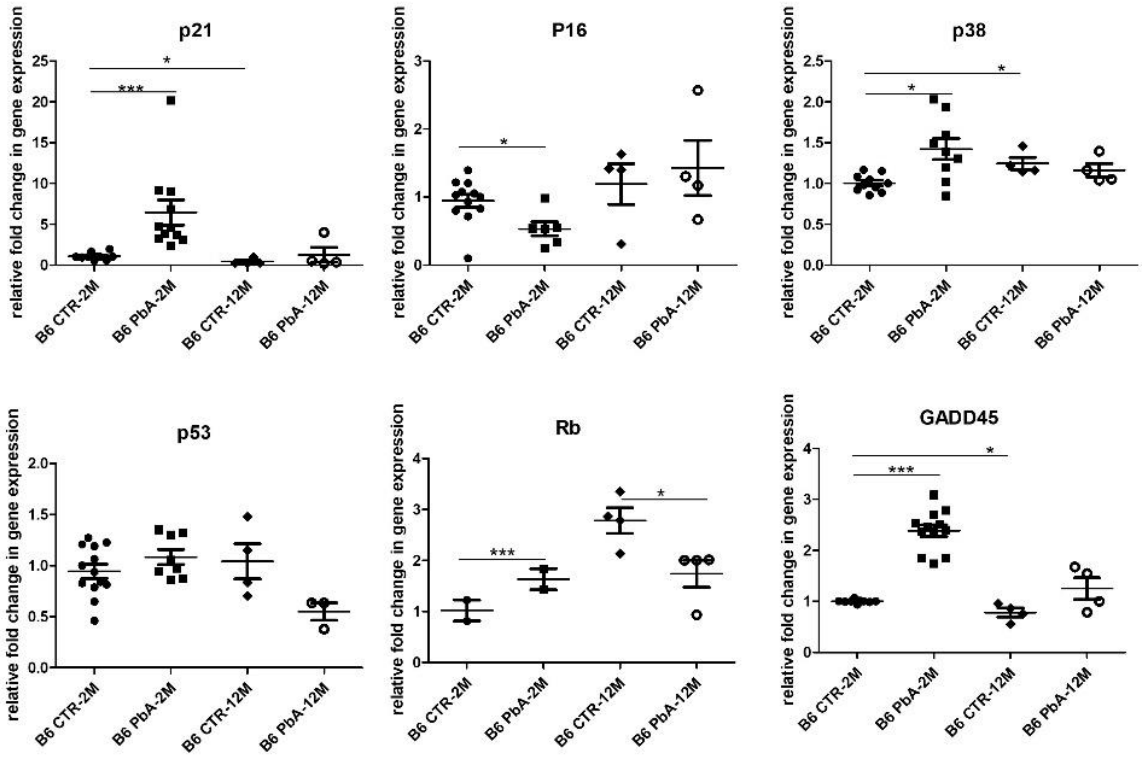

Figure 43: Relative expression of senescence markers in the brain of young adult and old mice, before and after PbA infection.

Fold relative expression of *p21*, *p16*, *p38*, *p53*, *Rb* and *GADD45* was quantified by RT-PCR in whole-brain of control and infected B6 mice (young adult (2M) and old mice (12M)). Relative mRNA levels in the infected groups were normalized to the respective control group. Data are presented as mean ± SEM. Values (n= 3-10 per group) were compared to the control group or between selected groups using a Mann–Whitney test. *$p < 0.05$; **$p < 0.01$; ***$p < 0.001$; ****$p < 0.0001$.

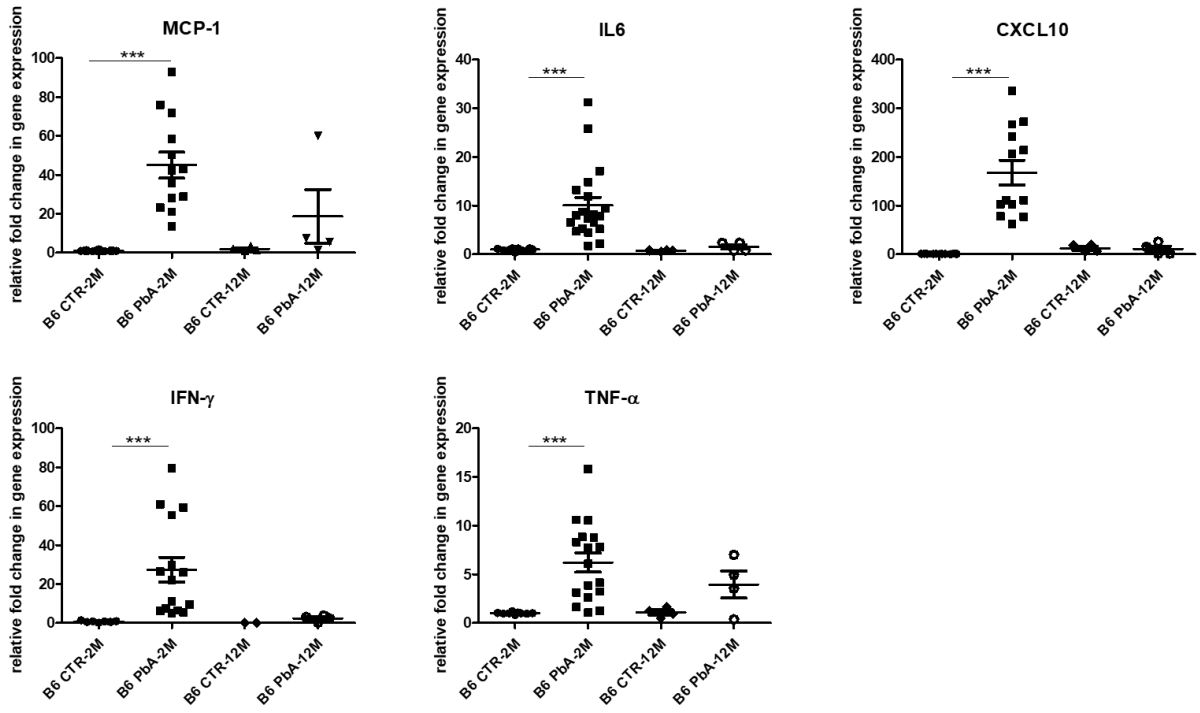

Figure 44 : : Relative expression of SASP markers in the brain of young adult and old mice, before and after PbA infection.

Fold relative expression of *MCP-1, IL6, p38, CXCL10, IFN-γ* and *TNF-α* was quantified by RT-PCR in whole-brain of control and infected B6 mice (young adult (2M) and old mice (12M). Relative mRNA levels in the infected groups were normalized to the respective control group. Data are presented as mean ± SEM. Values (n= 3-10 per group) were compared to the control group or between selected groups using a Mann–Whitney test. *p < 0.05; **p < 0.01; ***p < 0.001; ****p < 0.0001.

3. *Pb*A infection impair locomotive activity and increase anxiety-like behavior without affecting memory in old mice.

Several studies have shown that ECM is associated with increased of cognitive impairment [11, 12]. Herein, we compared the behavior of young adult, adult and old B6 and L28 mice (aged 2,6 and 12M) before and after *Pb*A infection. Various behavioural tests were performed. First, we used an open-filed infrared actimeter to compare the spontaneous locomotive activity of mice before and after *Pb*A infection (test was performed at 3.5dpi for B6 mice and 4dpi for L28 mice). We did not observe a significant difference in total distance traveled by B6-2M mice (Figure 45a) and the percentage of time spent resting before and after *Pb*A infection (Figure 45b). But we showed a significant increase in the percentage of time spent moving slowly for *Pb*A infected mice compared to controls (~40% versus ~31%, *P<0.05), and a decrease in the percentage of time spent moving quickly (~49% versus ~58%, **P<0.01) (Figure 45c-d). However, for L28-2M mice, we were unable to recover the data because the data file was damaged. These findings indicate that *Pb*A infection does not significantly impair locomotion of young adult mice. Additionally, there were no significant differences in locomotive activity between old (12M) and young adult (2M) B6 mice before infection (Figure 45a-d). L28 old mice, on the other hand, have a significant increase in locomotive activity compared to young adult mice. They traveled significantly longer distance (~4715cm) than younger mice (2M) (~3760cm). In addition, when compared to young adult mice, they spent less time moving slowly (Figure 45e-f) and spent 61% of their time moving quickly, compared to young adult mice (~45%) (Figure 45g). Furthermore, *Pb*A-infected B6 and L28 old mice (12M) have impaired locomotion activity, as evidenced by a significant decrease in total distance traveled, an increase in the percentages of time spent resting and moving slowly, and an increase in the percentage of time spent moving quickly when compared to controls of the same age (Figure 45a-h). These results suggest that the *Pb*A infection impair locomotion of old mice.

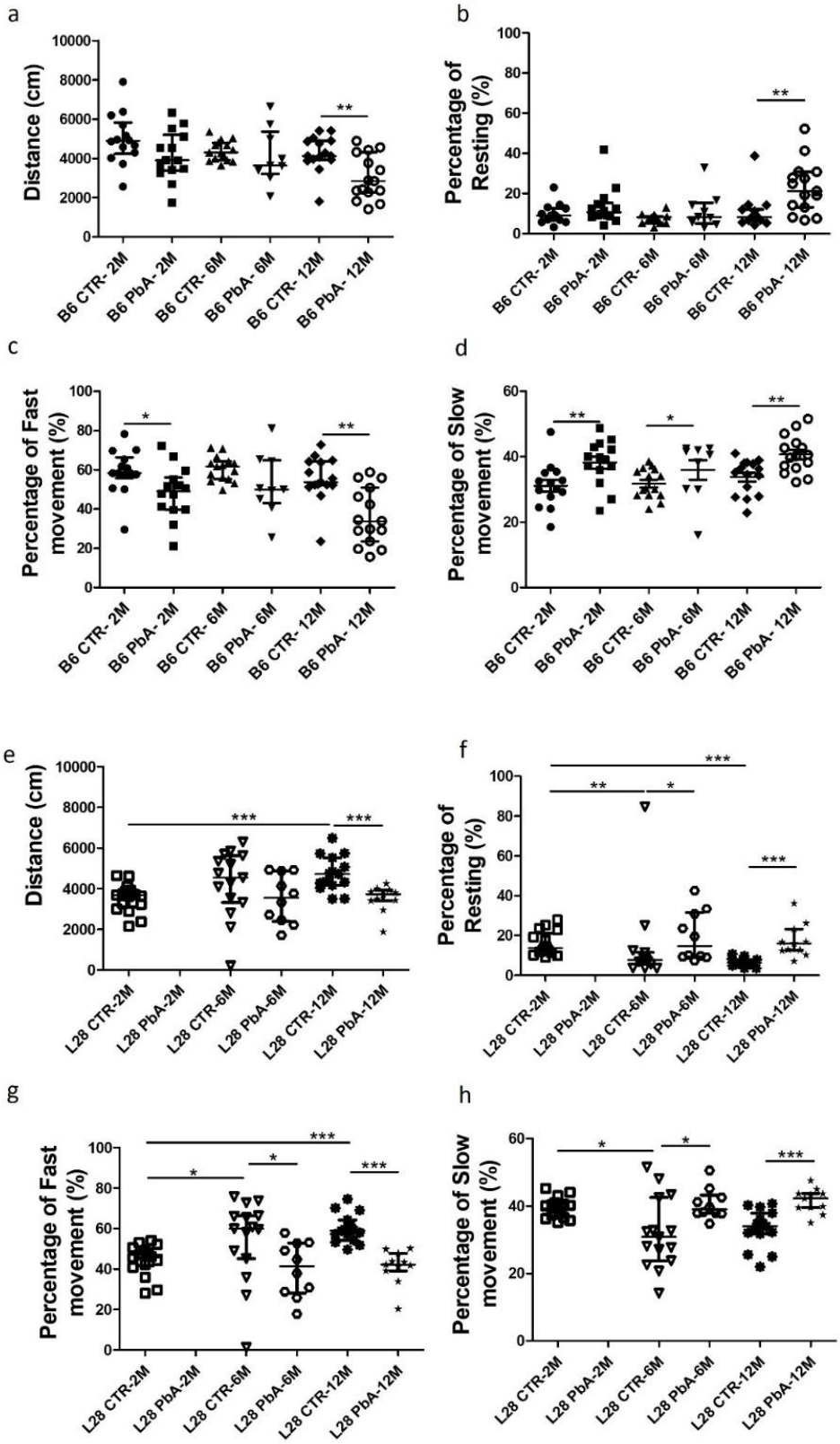

Figure 45: Effect of PbA infection on spontaneous locomotion in actimeter at day 3.5 post infection.

The graphs show the locomotive activity parameters of B6 (a-d) and L28 mice (e, h): the distance traveled, (b ,f) the percentage of time spent resting, (c, g) the percentage of time spent moving slowly and (d, h) the percentage of time spent moving quickly of *Pb*A-infected and control mice at different ages: 2, 6 and 12 months. Results were

expressed as the median ± SEM from 14-15 animals per group. Values were compared to the control group using a Mann–Whitney test. *P < 0.05; **P < 0.01; ***P < 0.001.

The EPM test was then used to determine the mice's level of anxiety (test was performed at 4dpi for B6 mice and 5dpi for L28 mice). In line with what has been described in the literature, we found that after *Pb*A infection, B6 mice aged 2M spent significantly less time in the open arms than controls (17% versus 11%, **P<0.01) (Figure 46a). Similar results were observed for *Pb*A-infected L28 mice aged 2M (~23% versus ~7%, ***P<0.001) (Figure 46b). These results suggest that *Pb*A infection induces an anxiety-like behavior. We also found that both B6 and L28 old mice (12M) spent significantly less time in the open arms than young adult mice (2M) (Figure 46a-b). These results suggest that aging is associated with an increase in anxiety-like behavior. Moreover, B6 and L28 mice (12M) presented a significant decrease in the percentage of time spent in open arms after *Pb*A infection when compared to controls (Figure 46a-b), suggesting that the *Pb*A infection increases anxiety-related behavior in old mice.

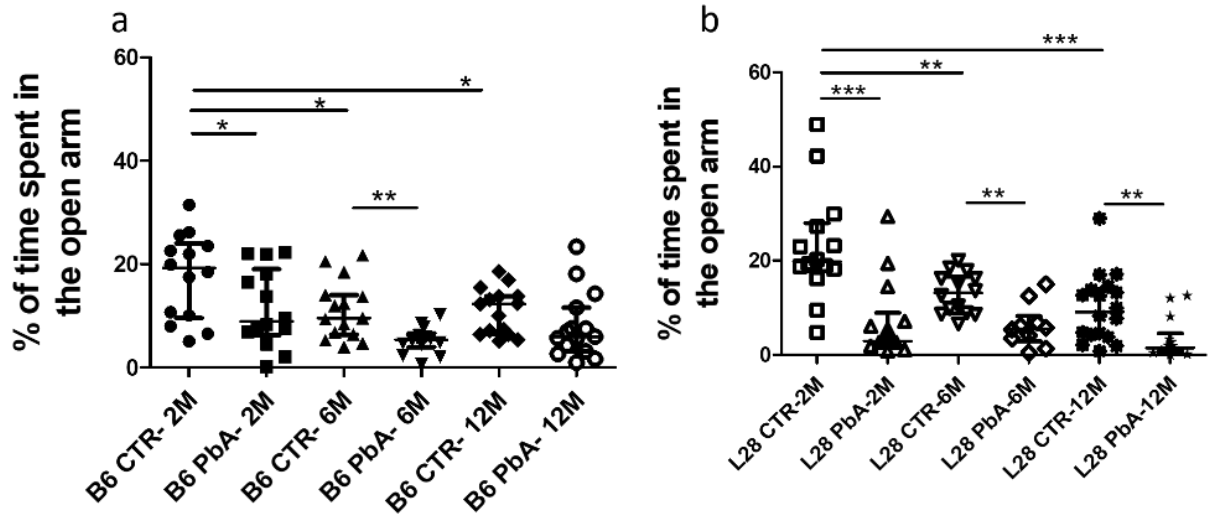

Figure 46 : Effect of PbA infection on anxiety behavioral in elevated plus maze test.

The graphs show the percentage (%) of time spent in the open arm for (A) B6 and (B) L28 mice before and after *Pb*A infection at different ages: 2, 6 and 12 months. Results were expressed as the median ± SEM from 14-15 animals per group. Values were compared to the control group using a Mann–Whitney test. *P < 0.05; **P < 0.01; ***P < 0.001.

Next, we examined the spatial memory function of mice before and after *Pb*A infection, using y-maze spatial test (test was performed at 5dpi for B6 and 12dpi for L28 mice). We found that *Pb*A-infected B6 mice (aged 2M) exhibited a tendency to spend less time in the new arm than controls (~60% versus ~68%, respectively) (Figure 47a). Similar result was observed for infected L28 mice (aged 2M) (~55% versus ~64 %, respectively) (*P<0.05) (Figure 47b). These results suggest that *Pb*A infection may impairs spatial memory in young adult mice. Furthermore, when compared to young adult mice (2M), B6 and L28 old mice (12M) showed a significant decrease in the percentage of time spent in the new arm, indicating that the spatial memory performance declines with age (Figure 47a-b). Moreover, no difference in the percentage of time spent into the novel arm was observed in B6 and L28 old mice before and after *Pb*A infection (Figure 47), suggesting that the *Pb*A infection in old mice has no effect on spatial memory.

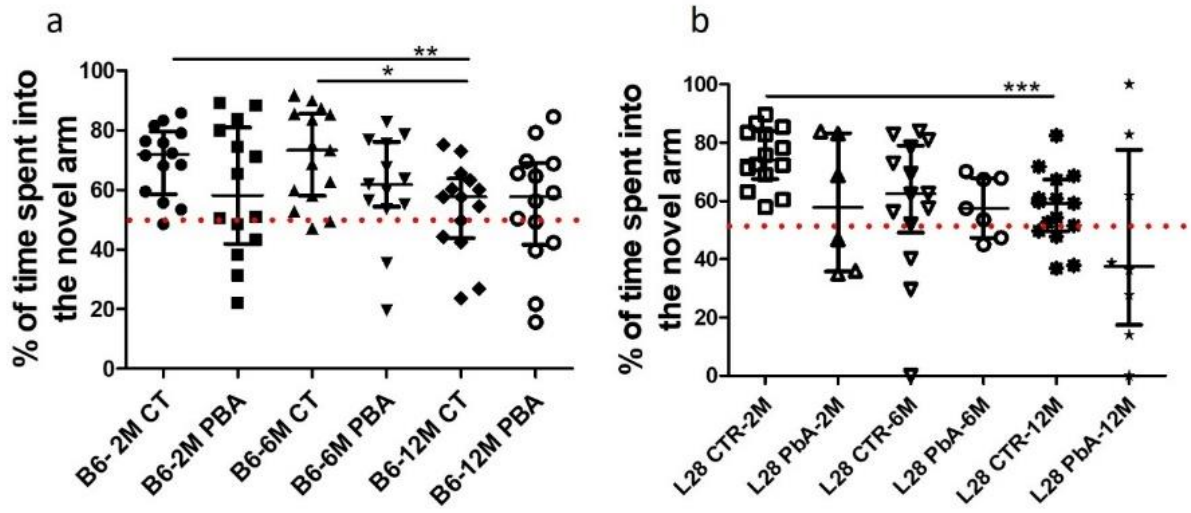

Figure 47 : Effect of PbA infection on mice's spatial memory in the Y-maze.

The graphs show the percentage (%) of time spent in the novel arm for (a) B6 and (b)L28 mice before and after *Pb*A infection at different ages: 2, 6 and 12 months. Results were expressed as the median ± SEM from 14-15 animals per group. Values were compared to the control group using a Mann–Whitney test. *P < 0.05; **P < 0.01; ***P < 0.001.

Y-maze spontaneous alternation test was then used to access mice working memory before and after *Pb*A infection (test was performed at 6dpi for B6 mice and 14dpi for L28 mice). In this test, all mice scored above ~60% of alternation, with no significant differences between groups (Figure 48a-b). These results suggest that the *Pb*A infection has no impact on working memory. There was no difference in the spontaneous alternation rate with age in B6 and L28 mice, indicating that working memory is not affected with age (Figure 48a-b). Similarly, *Pb*A infection in old mice did not exhibit impairment in the working memory.

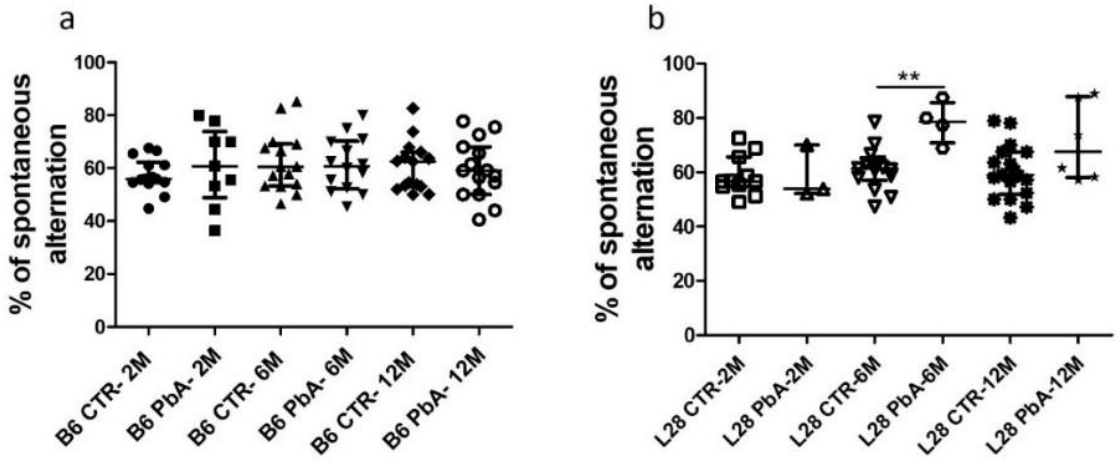

Figure 48: Percentage of spontaneous alternation during the Y-maze test.

The graphs show the percentage (%) of spontaneous alternation for (a) B6 and (b) L28 mice before and after *Pb*A infection at different ages: 2, 6 and 12 months. The results were presented as the median ±SEM of 9-15 animals per group. Values were compared to the control group using a Mann–Whitney test. **P < 0.01.

Finally, we performed the NOR test to assess visual recognition memory in L28-2M mice before and after *Pb*A infection (at 7 to 9 dpi). No difference was seen between groups on the discrimination index, ~0.18 and ~0.12 for the control and infected groups respectively, indicating that recognition memory was not impaired after *Pb*A infection in L28 mice (Figure 49). This test was not performed on B6 mice because they died before the test.

This test cannot be analyzable on L28 mice aged 6 and 12M, because the mice did not sufficiently explore the objects during the acquisition phase.

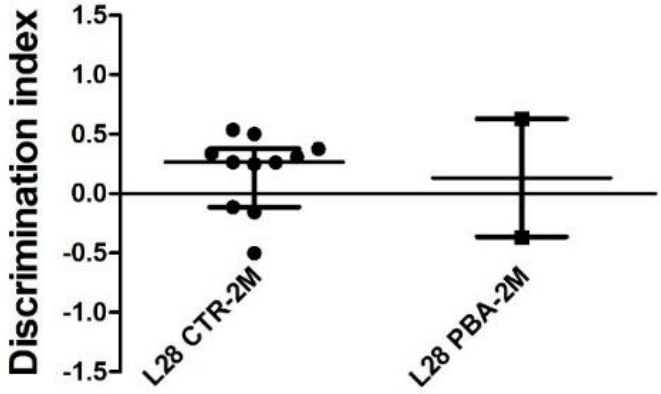

Figure 49: The discrimination index during the novel object recognition (NOR) test.

The graph shows the discrimination index in young adult L28 mice before and after *Pb*A infection. Results were expressed as the median ± SEM from 5-10 animals per group. Values were compared to the control group using a Mann–Whitney test...

4. *Pb*A infection did not cause tissue damage in the corpus callosum or the olfactory bulb in old mice.

Interestingly, in a previous study conducted in our lab, they found a lesion in the corpus callosum and olfactory bulbs in young adult mice after *Pb*A infection, as well as an increase in the levels of metabolites such as taurine, glutamine and glutamine to glutamate [3]. Glutamate is the main neurotransmitter in hippocampus where it plays a crucial role in spatial memory. However, spatial memory alterations could be the consequences of hippocampal glutamate homeostasis modification [365]. Based on that, we interested to correlate the behavior alterations with brain damage and change in metabolites levels in the brain after *Pb*A infection. Axial and sagittal T2W images from *Pb*A-infected B6 mice aged 6 and 12M showed no tissue damage in the corpus callosum or the olfactory bulb (Figure 50). In addition, *Pb*A infection did not cause brain edema, because there was no difference in ADC in the cortex or brain width between control and *Pb*A infected mice at these ages (Figure 50). Furthermore, according to the ^{1}H-MRS analyses of the cortex, the *Pb*A infection in old mice had no significant effect on taurine, NAA, choline and glutamine to glutamate levels (Figure 51). Interestingly, we show an increase in glutamine to glutamate levels in old mice, similar to what we observed in adult mice developing CM. This result suggests that the *Pb*A infection during CM shares some similarity with brain aging at the metabolites levels.

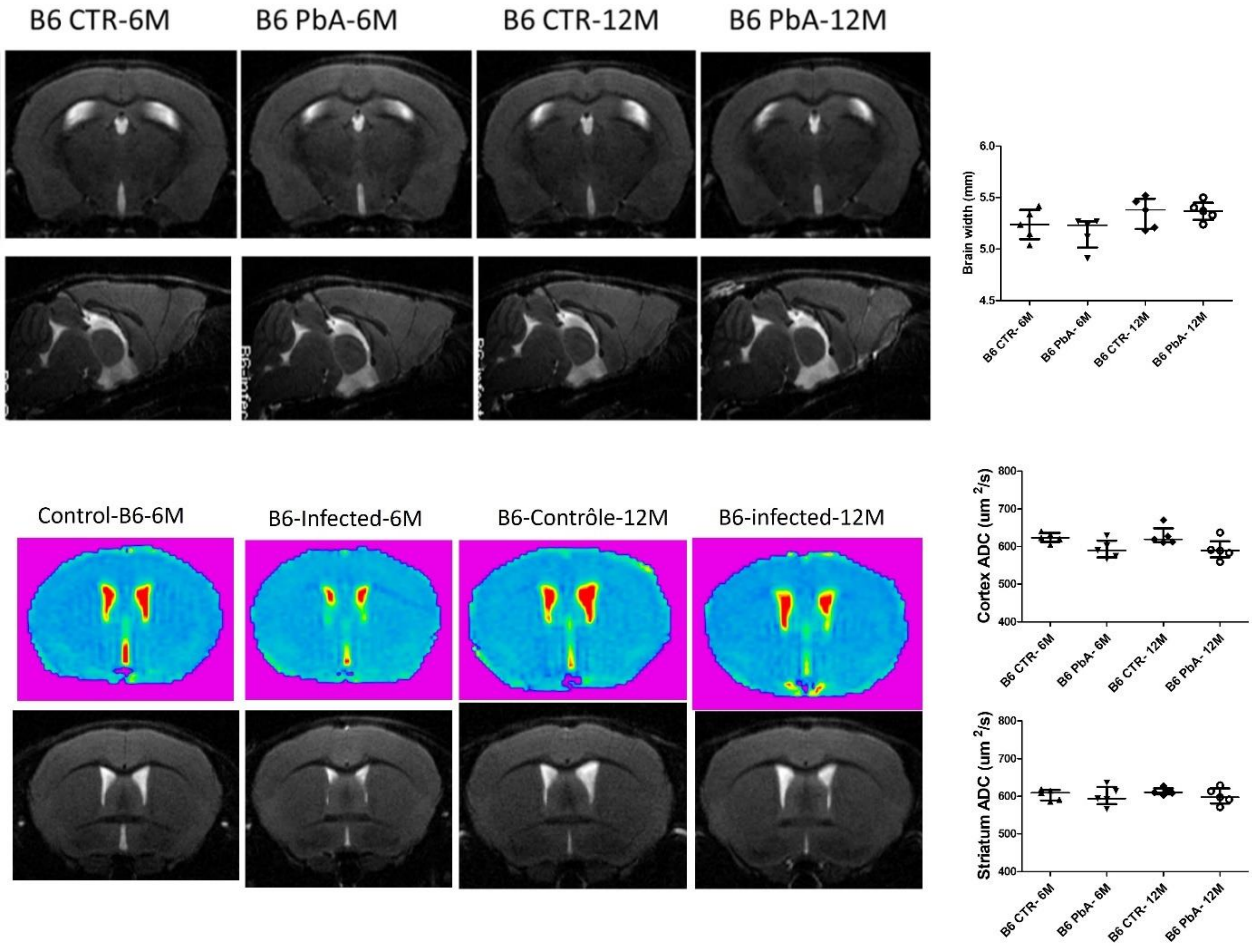

Figure 50: There was no change in the corpus callosum or olfactory bulb in adult or aged mice after PbA infection.

Sagittal and coronal sections of T2W MRI images from control and *Pb*A-infected B6 mice aged 6 and 12 months on day 6–7 post-infection. The white arrows indicate the difference in the brain width, in the corpus callosum and olfactory bulb between infected mice and controls at 2 months of age. Data represented as median ± SEM. Values were compared with the control group or between the selected groups using Mann–Whitney test.

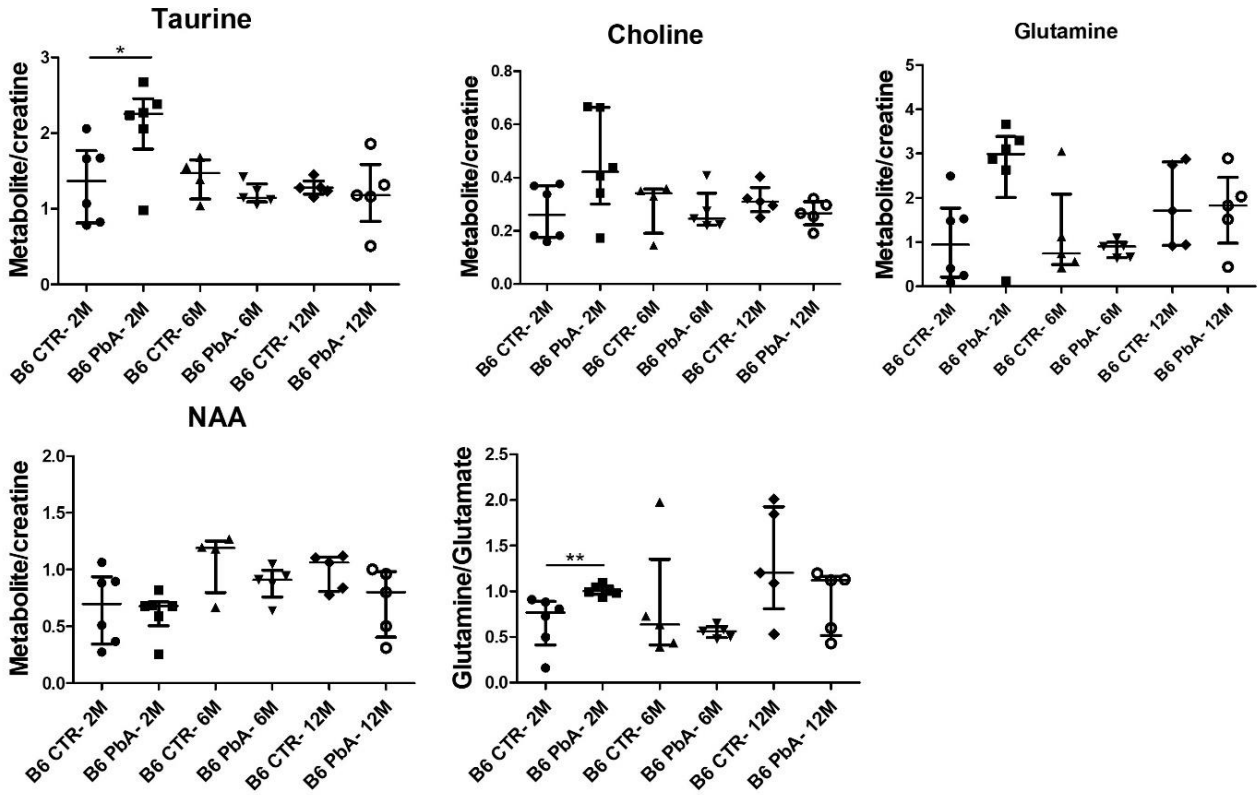

Figure 51: Brain metabolites quantified by [1] H-magnetic resonance spectroscopy in the cortex of control and PbA infected mice at day 6-7 post-infection, at age of 6 and 12 months.

Taurine, choline, Glutamine, N-acetylaspartate (NAA), and Glutamine to Glutamate metabolites levels were quantified by brain [1] H-MRS, and were expressed as the relative area of each metabolite compared to the area of creatine. Data represented as median ± SEM. Values were compared to the control group or between selected groups using a Mann-Whitney test. *P < 0.05; **P < 0.01; ***P < 0.001.

5. Senescent astrocytes may be a mechanism involved in cognitive impairments during CM

In the project 1, we demonstrated that senescent astrocytes participate in the pathogenesis of CM. It would be interesting to determine whether this process contributes to cognitive deficits. As described in literature, our results indicate that *Pb*A infection does not impair locomotion but does cause anxiety and alteration in spatial memory in young adult mice (2M). Interestingly, statistical analysis is ongoing to determine the correlation between the senescence markers (SASP and cell cycles arrest genes upregulated during CM) and cognitive parameters.

The following hypothesis sought to determine whether long-term cognitive impairment in mice after *Pb*A-infection and treatment with chloroquine is caused by astrocyte senescence. To confirm this, we planned to examine senescence markers as well as conduct behavioral tests on mice infected and treated with chloroquine. Because the behavioral manipulation fell during the confinement period, we had to sacrifice the mice and recover the organs for the RT-qPCR and confocal analysis. For the time being, we only examined p21 expression by RT-qPCR. Interestingly, we found a significant increase in their expression in the brains of infected and chloroquine-treated mice compared to control mice (Figure 52).

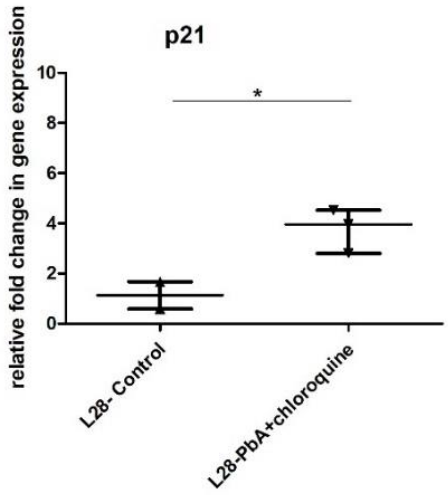

Figure 52 : Fold relative expression of p21 in the brain of control and chloroquine-treated PbA-infected mice.

Discussion and perspectives

In this study, we provide the first evidence that a senescence process induced in astrocytes upon contact with malaria parasite could be one of the mechanisms that promotes the neuroinflammatory response contributing to CM both in the mouse and in humans. Indeed, accelerated cellular aging and reduced lifespan have recently been shown in birds and patients with acute malaria but was not assessed in CM patients [283-286]. In contrast, to what observed in birds infected with *P. Ashfordii* inducing chronic malaria that causes senescence in the brain, spleen and other tissues, only astrocytes but not microglial cells undergo senescent [284]. We have identified a P53/P21-dependent pathway implied in astrocyte senescence induced by malaria parasite by differential transcriptomic analysis of total brain and gene quantification comparing *PbA*-infected CM^S and CM^R mice with their respective uninfected controls. These data were confirmed by confocal imaging and immunostainning showing expression of P21 on brain sections from CM^+ mice and on primary astrocyte cultures stimulated with *Pb*A-infected RBCs. These data were also extended to humans by showing higher frequency of $GFAP^+$ astrocytes co-expressing P21 on brain section of *P. falciparum* infected patients who died from CM. Expression of P21 was colocalized with astrogliosis principally in the cortex and hippocampus areas. High expression P16 and P21 expression has been also detected in the frontal cortex during neuroinflammation associated to amyotrophic lateral sclerosis brains, suggesting cell cycle dysregulation and astrocyte senescence activation in the early stages of the disease. The two mechanisms were linked to aging and DDR [301]. Furthermore, in the brain cortex, which undergoes major molecular and functional changes with aging, no increase in $p21^+$ cells compared to $P16^+$staining were described in persons across a broad spectrum of ages with no neurological disorder suggesting that expression of P21 is related to neuroinflammatory process [366]. In addition another recent study demonstrated that SARS-CoV-2 spike S1 subunit protein-induced endothelial senescence which is characterized by the expression of both P16 and P21 which weakens the function of brain vessels that may consequently initiate cerebral vascular disorders, including stroke and hemorrhage [367]. Of note, P16 and P21 pathways play distinct roles during senescence. P21 is involved in the initiation of the process, whereas P16 pathway is required for the long-term maintenance of the senescence state [368, 369]. During ECM, infected mice develop early neurological symptoms and die between 6 to 10 days post infection, which is probably why we didn't see a difference in p16 expression.

In addition, the senescent state of astrocytes was also accompanied by the activation of cell death sensitivity and apoptosis resistance as shown by the significant increase in the expression

of *Bcl-x* and but not *Mcl-1*, *Bcl-w* and *Bcl-2* and in the amount of SA-β-Gal$^+$ cells in CM$^+$ compared to control mice. The upregulation of BCL-2 or BCL-x proteins support the survival of senescent cell [370, 371]. In fact, BCL protein family activation is a central molecular mechanism by which senescent cells acquire resistance to apoptosis. The inhibition of BCL-2, BCL-w and BCL-x protein causes preferential apoptosis of senescent cells and the decrease of SA-β-Gal$^+$ cells [371]. Apoptosis-resistant phenotype of senescent cell might explain why astrocytes express less apoptotic marker caspase-3 during ECM [372]. Likewise, we also observed an increase in levels of P53 protein, which is known to be regulated by the proteasome and ATM [373]. Activation of ATM- dependent DDR by p53 elicits a cell cycle arrest leading to senescence in response to DNA damage [374]. The increase of phosphorylation of ATM and P53 in the brain of CM$^+$ mice suggest that DDR-ATM/P53 pathway may be involved in regulating senescence during ECM.

We also identified a link between the cellular senescence process and the involvement of a LC3-dependant non-conventional autophagy which is elicited during the transfer of parasites microvesicles in the astrocytes. In fact, the P21-mediated senescence process induced in astrocytes after *Pb*A contact was totally abolished when autophagy was inhibited either by silencing of RUBCN/rubicon and ATG5 using siRNA or by BAF A_1 treatment. Autophagy and senescence are two cellular stress responses, sharing a complex relationship in which autophagy can play opposite roles as pro- or anti-senescence inducer [232, 375]. Several studies reported that autophagy, which is a process acting for recycling of damages components, could be a negative-regulator of senescence to prevent disorders and to maintain homeostatic cellular state [376, 377] . Nevertheless, autophagy could also promote senescence during infection for long-term survival although promoting cell dysfunction and/or damages [378]. Autophagy contributes also to the establishment of senescence by facilitating the release of SASP cytokines as we observed in CM [233, 234, 378, 379] . In addition, an increase of P38MAPK interacting with NF-κB, which is essential for the induction of SASP, was observed in the brain during ECM (Figure 53). Involvement of P38MAPK in the production of SASP via NF-κB was confirmed in senescent human astrocytes treated with P38MAPK inhibitor, in which SASP secretion was significantly reduced [198].

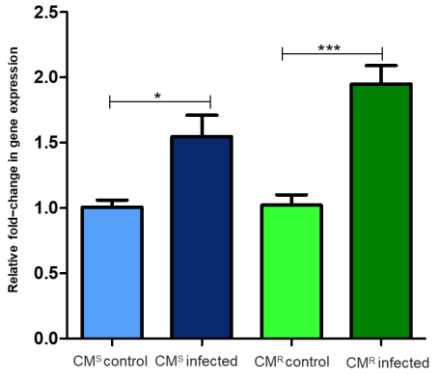

Figure 53 : NF-κB expression in the brain of control and infected mice.

Fold relative expression of NF-κB was quantified by RT-PCR in whole-brain of control and infected CM^S and CM^R mice. Relative mRNA levels in the infected groups were normalized to the respective control group. Data are presented as mean ± SEM. Values (n= 3-10 per group) were compared to the control group or between selected groups using a Mann–Whitney test. *p < 0.05; **p < 0.01; ***p < 0.001; ****p < 0.0001.

However, we showed that the knockdown of the Rubcn/Rubicon and Atg5 genes, decreases the expression of senescence markers and the expression of CXCL-10, while increasing in the expression of another cytokines and chemokines of SASP including IL-6 and CCL-2. Similar results was described during OIS, when autophagy-related genes are knocked down, senescence is delayed and IL6/8 protein levels are decreased, but their mRNA levels are increased [233]. Herein, we did not assess the protein levels of these factors. In this regard, it will be interesting to look the levels of SASP proteins using ELISA.

An interesting study show that autophagy can induce senescence by degradation of nuclear Lamina. In proliferating cells, LC3 can interact with nuclear lamina component Lamin B1 at heterochromatin regions LADs. But during OIS, LC3 mobilizes chromatin-associated Lamin B1 into the cytoplasm for degradation via autophagy, which reinforces senescence as shown in Figure 54 [380]. Inhibition of autophagy suppresses Lamin B1 degradation and attenuates OIS, partially by maintaining nuclear membrane integrity [236, 381]. After Lamin B1 silencing, an increase in the expression of ATM, leading to activation of p53/P21 pathway was observed [382]. It will be interesting to investigate whether autophagy affects Lamin B1 expression in stimulated astrocytes using RT-qPCR and by immunofluorescence. Furthermore, autophagy can also degrade the inhibitory p53 isoform, Δ133p53α, by activation of STUB1, which in turn activate p53-mediated senescence [235]. Interestingly, Δ133p53 by inhibition of p53, regulate p21 [383, 384] and IL-6 [384, 385]. But the regulatory interaction between these factors has yet

to be elucidated. It has been demonstrated that the treatment with Δ133p53 prevents astrocyte senescence and inhibits astrocyte-mediated neuroinflammation during radiation-induced senescence [386]. The expression of Δ133p53 can be assessed by western blot in stimulated astrocytes and after knockdown of autophagy. It is important to note that treating *Pb*A-infected mice with autophagy inhibitor Bafilomycin A1 protects mice from ECM [94]. Bafilomycin A1 can eliminate senescent cells and is use as senolytics [387].

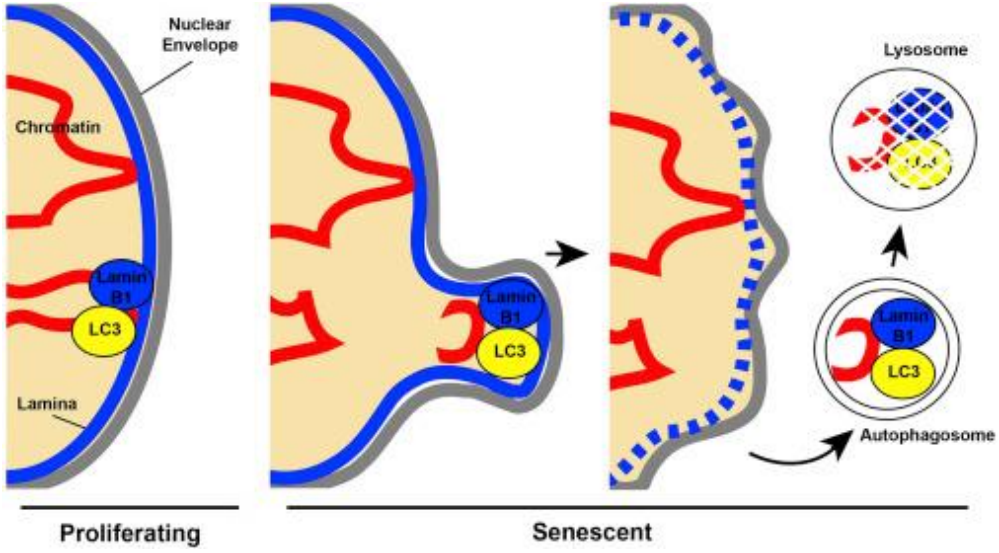

Figure 54: Autophagy-Dependent Degradation of the Nuclear Lamina. Reprinted from (Leidal et al., 2015)[380].

Several cytokines and chemokines component of SASP such as IL-6, CCL-2 and CXCL-10 are significantly associated to CM [3, 4, 57]. Our transcriptomic data identifying *Pml*, *P21*, *Calr* and *Cxcl-10,* predict a premature senescence associated to inflammation that occur in the brain of CM^{+} mice. The strong secretion of CXCL-10, CCL-2 and TNF-α by astrocytes observed in primary culture stimulated with *Pb*A is directly dependent of autophagy of *Pb*A-microvesicules [94]. It is noteworthy that the long-term maintenance of CXCL-10 production by astrocytes will be dependent on the senescence process which is suppressed when autophagy is inhibited. This strongly suggests a causal relationship between autophagy, astrocyte senescence and the neuroinflammatory response. Indeed, the link between astrocyte senescence and CM is confirmed in CM^{R} mice that do not express the hallmark of senescence in the brain after *Pb*A infection, and also in CM^{S} mice protected from CM when treated with Dasatinib/Quercetin. Altogether these observations are comforted by the statistical modeling showing that CXCL-10

produced by astrocytes in response to *Pb*A-infection is a key factor which participate in early mechanisms that create a neuroinflammatory environment contributing to CM.

In addition, we showed that D/Q killed senescent astrocytes more efficiently than Fisetin and Navitoclax in the context of ECM. Accordingly, we observed that D/Q treatment reduced inflammation, the main mechanism of ECM pathogenesis. We should point out that D/Q have been shown to cross BBB [388, 389], which is consistent with previously studies reporting a reduction of senescent astrocytes in the murine brain after treatment with D/Q [255]. The treatment of *Pb*A infected mice with Navitoclax and Fisetin were not effective in the removal of all senescent astrocytes; this can explain the weak percentage of infected mice protected from ECM after treatment. By RT-qPCR, we show that infected and treated mice, not protected from ECM, have not significant difference in the expression of p21 in the brain (Figure 55). More analysis of senescent cell markers in the brain of these mice can be interesting to comprehension why did it work less well. Despite that the Navitoclax has been previously shown to clear senescent astrocytes in a mouse model Alzheimer's disease [302], but it is not senolytic against human astrocytes [390]. It has been shown to cross the BBB in other studies [391-393].

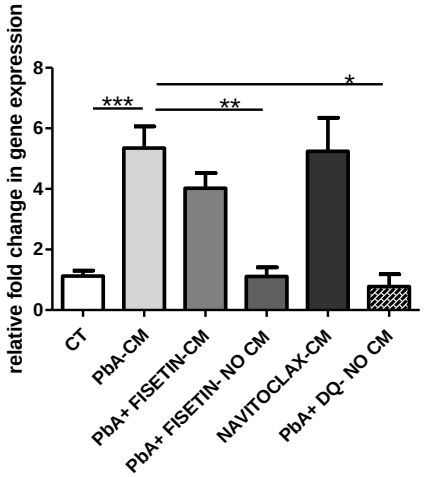

Figure 55 : Relative expression of p21

Fold relative expression of P21 was quantified by RT-PCR in whole-brain of mice infected and treated with Fisetin or Navitoclax, wchich developed CM compared to those protected from CM. Relative mRNA levels in the infected groups were normalized to the respective control group. Data are presented as mean ± SEM. Values (n= 3-11 per group) were compared to the control group or between selected groups using a Mann–Whitney test. *p < 0.05; **p < 0.01; ***p < 0.001; ****p < 0.0001.

The senescence process was also confirmed in human CM brain section in which sequestration of iRBCs was observed in the same regions as those where $GFAP^{+}P21^{+}$ senescent astrocytes were found. This is also highlighted by high *p21* and low *p16* expression in PBMCs of CM and CM-MOD while in MM increased *p16* gene and slight *p21* were detected. Increase of p21 but not p16 was observed in peripheral blood of patients with COPD [308]. Senescence has been already described in *P. falciparum* patients with MM that were characterized by elevated P16 expression and telomere shortening in peripheral blood [284-286]. In addition to a role for senescence of astrocyte in CM, our study strongly suggests also balance of P16/P21 associated to disease severity in human malaria as P21 driven-senescence occurred concomitantly in peripheral blood and in brain cells of CM patients. In addition, CM-MOD, most severe complications during malaria, produce the highest levels of CXCL-10 which is associated with expression of P21 and high parasite load, particularly in deceased patients. These observation reinforce the fact that high plasma level of CXCL-10 and expression of p21 could be propose as biomarker for lethal malaria because detectable in the peripheral blood as it is done for Alzheimer's disease [313].

To investigate the role of senescent cells *in vivo*, the INK-ATTAC and P16-3MR mouse models are currently the most widely used transgenic models. These models were designed to exclusively target $p16^{high}$ cells. In a recent published study, Wang et al., generated a p21-Cre transgenic mouse model allowing to investigate the role of $p21^{high}$ senescent cells *in vivo* in different pathological conditions such as aging and obesity. By crossing p21-Cre mice with different floxed mice, this model allows researchers to monitor, sort, image, eliminate or modulate $p21^{high}$ cells in vivo [394]. It would be interesting to use this mouse model, in order to learn more about the biology of senescent astrocytes during ECM. In particular, the p21-cre mouse model allows for the suppression of SASP only in $p21^{high}$ cells, making it a very interesting model for determining the contribution of SASP during ECM.

During ECM, the mechanisms underlying neurocognitive impairments are still unknown. Several studies have found a correlation between inflammation and cognitive dysfunction. Anxious behavior in *Pb*A-infected mice for instance, was related with the increase of pro-inflammatory cytokines such as IL-1β, IL-4, IL-10, TNF-α and IFN-γ [124]. Additionally, a decrease in working memory during ECM, was associated with inflammation [11]. Furthermore, short-term memory impairment was associated with increased expression of inflammatory cytokines (IL-6, TNF-a, IFN-γ, and CCL11) in the frontal cortex and hippocampus during ECM [127]. Our findings that senescent astrocytes were associated with a

pro- inflammatory response, particularly increased CXCL-10 production, (although other cytokines and chemokines may be expressed by senescent astrocytes during ECM), strongly suggest a link between astrocytes senescence and cognitive impairment. Senescence of astrocytes is strongly correlated with cognitive decline in aging and neurodegenerative diseases [395]. The elimination of senescent cells decreases anxiety and restores neurogenesis [255]. These studies support the hypothesis that senescent astrocytes play a role in the development of cognitive impairment during CM. Interestingly, we show specifically that senescence occurs in the cortex and hippocampus during ECM, two important areas of the brain implicated in the memory [121]. Statistical analysis will be performed to confirm our hypothesis, which will correlate the expression of CXCL-10, p21, GADD45 and p38 MAPK with anxiety levels and spatial memory alteration. To further confirmation, it will be interesting to evaluate the behavior of *Pb*A-infected mice after treatment with senolytic drugs.

The reasons for persistent cognitive deficits after *Plasmodium* infection and anti-malaria treatment is currently unknown, but our preliminary results raise the possibility that astrocyte senescence may play a role. Because the senescence process is irreversible, once established, it persists for long intervals [258]. We believe that even anti-malaria treatment, senescent astrocytes can persist over long periods and are probably implicated in cognitive impairment. The most intriguing aspect of this novel process that we deciphered during CM is that senescence is a therapeutic target relevant for a wide range of pathologies [179]. We anticipate that the use of senolytic drugs can be a promising strategy for preventing CM and related cognitive impairment.

Our results show that *Pb*A-infected mice have the same phenotype as aged mice. As evidenced by increased anxiety, impaired of spatial memory and an increase of glutamine/glutamate levels in the brain. We suggest that *Plasmodium* infection may cause functional rather than chronological aging, and can potentially shortening lifespan. It has been demonstrated that persistent chronic asymptomatic malaria infections result in reduced lifespan in infected birds [283]. Nonetheless, the effect of malaria, or other acute infections, on cellular aging has not been reported in humans.

As previously described, senescence process is not uniformly negative, but can have beneficial roles. We discovered that astrocyte senescence is a critical mechanism during CM. That probably, on the other hand, exerts protective effects against *Pb*A infection during aging. The role of aging in the context of infection is still in its infancy [396]. Elderly mice were more susceptible to *Trypanosoma cruzi* infection [397]. However, senescent BALB/c mice are

resistant to *Leishmania major* infection. This protection was associated with a release of IL-12 by macrophages from aged but not from young mice [398]. The effect of aging on the host's ability to resist *PbA* infection remains poorly understood. During aging, senescent astrocytes produce SASP such as IL-12 [399]. Il-12 induced by the chronic *Toxoplasma gondii* infection protected mice from ECM [400]. Furthermore, the expression of inducible nitric oxide synthase (iNOS), an enzyme responsible for the production Nitric Oxide (NO) increases in astrocytes during ageing [401, 402]. Increased NO levels reduce the intracerebral leukocyte accumulation by downregulating cell-adhesion molecules [44]. Endothelial dysfunction in malaria is associated with reduced levels of NO [44]. NO may be protective against *P. falciparum* infection by inhibiting cytoadherence of iRBCs to ECs [403]. Endothelial dysfunction can also be prevented by supplementing l-arginine, the substrate for the synthesis of NO. l-arginine supplementation resulted in the dilation of constricted arterioles and increased regional cerebral blood flow during ECM [404]. Altogether, we anticipate the metabolic and morphological changes in astrocytes during ageing can play a protective role from ECM.

In conclusion, we provide a novel mechanism by which the malaria parasite can promote the inflammatory response in the brain through a senescence pathway that contribute to CM development and cognitive deficits, which may represent a potential therapeutic target for CM prevention. In addition, we propose P21 and CXCL-10 as potential co-biomarkers to detect severity and lethality from CM in human.

Bibliography

1. *World Health Organization* 2021.
2. Baptista, F.G., et al., *Accumulation of Plasmodium berghei-infected red blood cells in the brain is crucial for the development of cerebral malaria in mice.* Infection and Immunity, 2010. **78**(9): p. 4033-4039.
3. Dalko, E., et al., *Heme dampens T-cell sequestration by modulating glial cell responses during rodent cerebral malaria.* Brain, Behavior and Immunity, 2016. **58**: p. 280-290.
4. Shrivastava, S.K., et al., *Uptake of parasite-derived vesicles by astrocytes and microglial phagocytosis of infected erythrocytes may drive neuroinflammation in cerebral malaria.* Glia, 2017. **65**(1): p. 75-92.
5. Kossod, S.d. and G.E. Grau, *Role of Cytokines and Adhesion Molecules in Malaria Immunopathology.* Stem Cells, 1993. **11**(1): p. 41-48.
6. Dominique, M., N. Josiane, and I.-B. Marianna, *Cerebral malaria and immunogenetics.* Parasite Immunology, 2000. **22**(11): p. 613-623.
7. Shaw, T.N., et al., *Perivascular Arrest of CD8+ T Cells Is a Signature of Experimental Cerebral Malaria.* PLoS Pathogens, 2015. **11**(11): p. e1005210.
8. Carter, J.A., et al., *Persistent neurocognitive impairments associated with severe falciparum malaria in Kenyan children.* J Neurol Neurosurg Psychiatry, 2005. **76**(4): p. 476-481.
9. Boivin, M.J., et al., *Cognitive impairment after cerebral malaria in children: a prospective study.* Pediatrics, 2007. **119**(2): p. e360-366.
10. Ssenkusu, J.M., et al., *Long-term Behavioral Problems in Children With Severe Malaria.* Pediatrics, 2016. **138**(5): p. e20161965.
11. Desruisseaux, M.S., et al., *Cognitive dysfunction in mice infected with Plasmodium berghei strain ANKA.* J Infect Dis, 2008. **197**(11): p. 1621-7.
12. Reis, P.A., et al., *Cognitive dysfunction is sustained after rescue therapy in experimental cerebral malaria, and is reduced by additive antioxidant therapy.* PLoS Pathog, 2010. **6**(6): p. e1000963.
13. Hernandez-Segura, A., J. Nehme, and M. Demaria, *Hallmarks of Cellular Senescence.* Trends in Cell Biology, 2018. **28**(6): p. 436-453.
14. Wang, J., et al., *Potential roles of telomeres and telomerase in neurodegenerative diseases.* International Journal of Biological Macromolecules, 2020. **163**: p. 1060-1078.
15. Cohen, J. and C. Torres, *Astrocyte senescence: Evidence and significance.* Aging Cell, 2019. **18**(3): p. e12937.
16. Gorg, B., A. Karababa, and D. Haussinger, *Hepatic Encephalopathy and Astrocyte Senescence.* J Clin Exp Hepatol, 2018. **8**(3): p. 294-300.
17. Han, X., et al., *Astrocyte Senescence and Alzheimer's Disease: A Review.* Front Aging Neurosci, 2020. **12**(148): p. 148.
18. Cutts, J.C., et al., *Pregnancy-specific malarial immunity and risk of malaria in pregnancy and adverse birth outcomes: a systematic review.* BMC Med, 2020. **18**(1): p. 14.
19. Counihan, N.A., et al., *Plasmodium rhoptry proteins: why order is important.* Trends Parasitol, 2013. **29**(5): p. 228-36.
20. Cowman, A.F. and B.S. Crabb, *Invasion of red blood cells by malaria parasites.* Cell, 2006. **124**(4): p. 755-66.
21. Sinka, M.E., *Global Distribution of the Dominant Vector Species of Malaria.* 2013.
22. Beck-Johnson, L.M., et al., *The effect of temperature on Anopheles mosquito population dynamics and the potential for malaria transmission.* PLoS One, 2013. **8**(11): p. e79276.
23. Mueller, I., et al., *Key gaps in the knowledge of Plasmodium vivax, a neglected human malaria parasite.* Lancet Infect Dis, 2009. **9**(9): p. 555-566.

24. Matuschewski, K., *Getting infectious: formation and maturation of Plasmodium sporozoites in the Anopheles vector.* Cell Microbiol, 2006. **8**(10): p. 1547-56.
25. Cowman, A.F., et al., *Malaria: Biology and Disease.* Cell, 2016. **167**(3): p. 610-624.
26. Bartoloni, A. and L. Zammarchi, *Clinical aspects of uncomplicated and severe malaria.* Mediterr J Hematol Infect Dis, 2012. **4**(1): p. e2012026.
27. Andrej Trampuz, et al., *Clinical review: Severe malaria.* Critical Care 2003. **7**: p. 315-323.
28. Wassmer, S.C., et al., *Investigating the Pathogenesis of Severe Malaria: A Multidisciplinary and Cross-Geographical Approach.* Am J Trop Med Hyg, 2015. **93**(3): p. 42-56.
29. Lamb, T.J., et al., *Insights into the immunopathogenesis of malaria using mouse models.* Expert Rev Mol Med, 2006. **8**(6): p. 1-22.
30. Keswani, T., et al., *Expression of CD300lf by microglia contributes to resistance to cerebral malaria by impeding the neuroinflammation.* Genes Immun, 2020. **21**(1): p. 45-62.
31. Epiphanio, S., et al., *VEGF promotes malaria-associated acute lung injury in mice.* PLoS Pathog, 2010. **6**(5): p. e1000916.
32. Niikura, M., et al., *Coinfection with nonlethal murine malaria parasites suppresses pathogenesis caused by Plasmodium berghei NK65.* J Immunol, 2008. **180**(10): p. 6877-84.
33. Hojo-Souza, N.S., et al., *Contributions of IFN-gamma and granulysin to the clearance of Plasmodium yoelii blood stage.* PLoS Pathog, 2020. **16**(9): p. e1008840.
34. Abel, S., et al., *Strong impact of CD4+ Foxp3+ regulatory T cells and limited effect of T cell-derived IL-10 on pathogen clearance during Plasmodium yoelii infection.* J Immunol, 2012. **188**(11): p. 5467-77.
35. Ramaprasad, A., et al., *Plasmodium vinckei genomes provide insights into the pan-genome and evolution of rodent malaria parasites.* BMC Biol, 2021. **19**(1): p. 69.
36. Idro, R., N.E.N. Jenkins, and C.R.J. C., *Pathogenesis, clinical features, and neurological outcome of cerebral malaria.* The Lancet Neurology, 2005. **4**(12): p. 827-840.
37. Bangirana, P., et al., *Severe malarial anemia is associated with long-term neurocognitive impairment.* Clin Infect Dis, 2014. **59**(3): p. 336-44.
38. de Souza, J.B., et al., *Cerebral malaria: why experimental murine models are required to understand the pathogenesis of disease.* Parasitology, 2010. **137**(5): p. 755-72.
39. Jean Langhorne, et al., *The relevance of non-human primate and rodent malaria models for humans.* Malaria Journal, 2011. **10**(23): p. 1475-2875.
40. Tunon-Ortiz, A. and T.J. Lamb, *Blood brain barrier disruption in cerebral malaria: Beyond endothelial cell activation.* PLoS Pathog, 2019. **15**(6): p. e1007786.
41. Daneman, R. and A. Prat, *The blood-brain barrier.* Cold Spring Harb Perspect Biol, 2015. **7**(1): p. a020412.
42. Panda, C. and R.K. Mahapatra, *An update on cerebral malaria for therapeutic intervention.* Mol Biol Rep, 2022. **49**(11): p. 10579-10591.
43. Sue Adams, H. Brown, and G. Turner, *Breaking down the blood–brain barrier: signaling a path to cerebral malaria?* Trends Parasitol, 2002. **18**(8): p. 360-366.
44. Nishanth, G. and D. Schluter, *Blood-Brain Barrier in Cerebral Malaria: Pathogenesis and Therapeutic Intervention.* Trends Parasitol, 2019. **35**(7): p. 516-528.
45. Ghazanfari, N., S.N. Mueller, and W.R. Heath, *Cerebral Malaria in Mouse and Man.* Front Immunol, 2018. **10**(9): p. 2016.

46. Souza, J.B.d. and E.M. Riley, *Cerebral malaria: the contribution of studies in animal models to our understanding of immunopathogenesis.* Microbes Infect, 2002. **4**(3): p. 291-300.
47. Kessler, A., et al., *Linking EPCR-Binding PfEMP1 to Brain Swelling in Pediatric Cerebral Malaria.* Cell Host Microbe, 2017. **22**(5): p. 601-614 e5.
48. Storm, J., et al., *Cerebral malaria is associated with differential cytoadherence to brain endothelial cells.* EMBO Mol Med, 2019. **11**(2): p. e9164.
49. Bruneel, F., *Human cerebral malaria: 2019 mini review.* Rev Neurol, 2019. **175**(7-8): p. 445-450.
50. Arnab Pain, et al., *Platelet-mediated clumping of Plasmodium falciparum-infected erythrocytes is a common adhesive phenotype and is associated with severe malaria.* Proc Natl Acad Sci U S A, 2001. **98**(4): p. 1805-1810.
51. Dorovini-Zis, K., et al., *The neuropathology of fatal cerebral malaria in malawian children.* Am J Pathol, 2011. **178**(5): p. 2146-58.
52. Strangward, P., et al., *A quantitative brain map of experimental cerebral malaria pathology.* PLoS Pathog, 2017. **13**(3): p. e1006267.
53. Nicolas Favre, et al., *Role of ICAM-1 (CD54) in the development of murine cerebral malaria.* Microbes Infect, 1999. **1**(12): p. 961-968.
54. Mejia, P., et al., *A single rapamycin dose protects against late-stage experimental cerebral malaria via modulation of host immunity, endothelial activation and parasite sequestration.* Malar J, 2017. **16**(1): p. 455.
55. Cariaco, Y., et al., *Ethanolic extract of the fungus Trichoderma stromaticum decreases inflammation and ameliorates experimental cerebral malaria in C57BL/6 mice.* Sci Rep, 2018. **8**(1): p. 1547.
56. Medana, I.M. and G.D. Turner, *Human cerebral malaria and the blood-brain barrier.* Int J Parasitol, 2006. **36**(5): p. 555-68.
57. Dunst, J., F. Kamena, and K. Matuschewski, *Cytokines and Chemokines in Cerebral Malaria Pathogenesis.* Front Cell Infect Microbiol, 2017. **7**: p. 324.
58. Michael Boele van Hensbroek, et al., *The Effect of a Monoclonal Antibody to Tumor Necrosis Factor on Survival from Childhood Cerebral Malaria.* J Infect Dis, 1996. **174**(5): p. 1091-1097.
59. Engwerda, C.R., et al., *Locally up-regulated lymphotoxin alpha, not systemic tumor necrosis factor alpha, is the principle mediator of murine cerebral malaria.* J Exp Med, 2002. **195**(10): p. 1371-7.
60. Chua, C.L., et al., *Monocytes and macrophages in malaria: protection or pathology?* Trends Parasitol, 2013. **29**(1): p. 26-34.
61. Sarah E. Hochman, et al., *Fatal Pediatric Cerebral Malaria Is Associated with Intravascular Monocytes and Platelets That Are Increased with HIV Coinfection.* mBio, 2015. **6**(5): p. e01390-15.
62. Kamolrat Silamut, et al., *A Quantitative Analysis of the Microvascular Sequestration of Malaria Parasites in the Human Brain.* Am J Pathol, 1999. **155**(2): p. 395-410.
63. G. G. MACPHERSON, et al., *A Quantitative Ultrastructural Analysis of Parasitized Erythrocyte Sequestration.* Am J Pathol, 1985. **119**(3): p. 385–401.
64. Hansen, D.S., et al., *NK cells stimulate recruitment of CXCR3+ T cells to the brain during Plasmodium berghei-mediated cerebral malaria.* J Immunol, 2007. **178**(9): p. 5779-88.
65. Wesley Solomon , et al., *Neuregulin-1 attenuates mortality associated with experimental cerebral malaria.* J Neuroinflammation, 2014. **11**: p. 9.
66. Belnoue, E., et al., *On the pathogenic role of brain-sequestered alphabeta CD8+ T cells in experimental cerebral malaria.* J Immunol, 2002. **169**(11): p. 6369-75.

67. Belnoue, E., et al., *Control of pathogenic CD8+ T cell migration to the brain by IFN-gamma during experimental cerebral malaria.* Parasite Immunol, 2008. **30**(10): p. 544-53.
68. Nitcheu, J., et al., *Perforin-dependent brain-infiltrating cytotoxic CD8+ T lymphocytes mediate experimental cerebral malaria pathogenesis.* J Immunol, 2003. **170**(4): p. 2221-8.
69. Miu, J., et al., *Chemokine gene expression during fatal murine cerebral malaria and protection due to CXCR3 deficiency.* J Immunol, 2008. **180**(2): p. 1217-30.
70. Bagot, S., et al., *Comparative study of brain CD8+ T cells induced by sporozoites and those induced by blood-stage Plasmodium berghei ANKA involved in the development of cerebral malaria.* Infect Immun, 2004. **72**(5): p. 2817-26.
71. Swanson, P.A., et al., *CD8+ T Cells Induce Fatal Brainstem Pathology during Cerebral Malaria via Luminal Antigen-Specific Engagement of Brain Vasculature.* PLoS Pathog, 2016. **12**(12): p. e1006022.
72. Vigario, A.M., et al., *Regulatory CD4+ CD25+ Foxp3+ T cells expand during experimental Plasmodium infection but do not prevent cerebral malaria.* Int J Parasitol, 2007. **37**(8-9): p. 963-73.
73. Togbe, D., et al., *Both functional LTbeta receptor and TNF receptor 2 are required for the development of experimental cerebral malaria.* PLoS One, 2008. **3**(7): p. e2608.
74. Haque, A., et al., *Granzyme B expression by CD8+ T cells is required for the development of experimental cerebral malaria.* J Immunol, 2011. **186**(11): p. 6148-56.
75. Ham, K.M.V.D., et al., *Protein Tyrosine Phosphatase Inhibition Prevents Experimental Cerebral Malaria by Precluding CXCR3 Expression on T Cells.* Sci Rep, 2017. **7**(1): p. 5478.
76. Khakh, B.S. and M.V. Sofroniew, *Diversity of astrocyte functions and phenotypes in neural circuits.* Nat Neurosci, 2015. **18**(7): p. 942-952.
77. Zhang, Z., et al., *The Appropriate Marker for Astrocytes: Comparing the Distribution and Expression of Three Astrocytic Markers in Different Mouse Cerebral Regions.* Biomed Res Int, 2019. **24**: p. 9605265.
78. Sofroniew, M.V. and H.V. Vinters, *Astrocytes: biology and pathology.* Acta Neuropathol, 2010. **119**(1): p. 7-35.
79. Batiuk, M.Y., et al., *Identification of region-specific astrocyte subtypes at single cell resolution.* Nat Commun, 2020. **11**(1): p. 1220.
80. Farina, C., F. Aloisi, and E. Meinl, *Astrocytes are active players in cerebral innate immunity.* Trends Immunol, 2007. **28**(3): p. 138-45.
81. Alireza Minagar, P.S., Robert Fujimura, Ray Ownby, Melvin Heyes and Carl Eisdorfer *The role of macrophage/microglia and astrocytes in the pathogenesis of three neurologic disorders: HIV-associated dementia, Alzheimer disease, and multiple sclerosis.*
82. Dossi, E., F. Vasile, and N. Rouach, *Human astrocytes in the diseased brain.* Brain Res Bull, 2018. **136**: p. 139-156.
83. Liddelow, S.A., et al., *Neurotoxic reactive astrocytes are induced by activated microglia.* Nature, 2017. **541**(7638): p. 481-487.
84. Andoh, N.E. and B.A. Gyan, *The Potential Roles of Glial Cells in the Neuropathogenesis of Cerebral Malaria.* Front Cell Infect Microbiol, 2021. **11**: p. 741370.
85. Medana, I.M., et al., *Central nervous system in cerebral malaria: 'Innocent bystander' or active participant in the induction of immunopathology?* Immunol Cell Biol, 2001. **79**(2): p. 101-20.

86. David, S. and A. Kroner, *Repertoire of microglial and macrophage responses after spinal cord injury.* Nature Reviews Neuroscience, 2011. **12**(7): p. 388-399.
87. Arcuri, C., et al., *The Pathophysiological Role of Microglia in Dynamic Surveillance, Phagocytosis and Structural Remodeling of the Developing CNS.* Front Mol Neurosci, 2017. **10**: p. 191.
88. Isabelle M. Medana, et al., *Axonal Injury in Cerebral Malaria.* Am J Pathol, 2002. **160**(2): p. 655-66.
89. Schluesener, H.J., P.G. Kremsner, and R. Meyermann, *Heme oxygenase-1 in lesions of human cerebral malaria.* Acta Neuropathol, 2001. **101**(1): p. 65-8.
90. Hermann J. Schluesener , P.G. Kremsner, and R. Meyermann, *Widespread expression of MRP8 and MRP14 in human cerebral malaria by microglial cells.* Acta Neuropathol, 1998. **96**(6): p. 575-80.
91. M.Medana, I., T. Chan-Ling, and N. H.Hunt, *Redistribution and Degeneration of Retinal Astrocytes in Experimental Murine Cerebral Malaria: Relationship to Disruption of the Blood-Retinal Barrier.* Glia, 1996. **16**(1): p. 51-64.
92. Isabelle M. Medana, Nicholas H. Hunt, and T. Chan-Ling, *Early Activation of Microglia in the Pathogenesis of Fatal Murine Cerebral Malaria.* Glia, 1997. **19**(2): p. 91-103.
93. Capuccini, B., et al., *Transcriptomic profiling of microglia reveals signatures of cell activation and immune response, during experimental cerebral malaria.* Sci Rep, 2016. **6**: p. 39258.
94. Leleu, I., et al., *A noncanonical autophagy is involved in the transfer of Plasmodium-microvesicles to astrocytes.* Autophagy, 2021. **18**(7): p. 1583-1598.
95. Nie, C.Q., et al., *IP-10-mediated T cell homing promotes cerebral inflammation over splenic immunity to malaria infection.* PLoS Pathog, 2009. **5**(4): p. e1000369.
96. Henry Armah, et al., *Cytokines and Adhesion Molecules Expression in the Brain in Human Cerebral Malaria.* Int J Environ Res Public Health, 2005. **2**(1): p. 123-31.
97. Herbert, F., et al., *Evidence of IL-17, IP-10, and IL-10 involvement in multiple-organ dysfunction and IL-17 pathway in acute renal failure associated to Plasmodium falciparum malaria.* Journal of Translational Medicine, 2015. **13**: p. 369.
98. Jo, D.H., et al., *Interaction between pericytes and endothelial cells leads to formation of tight junction in hyaloid vessels.* Mol Cells, 2013. **36**(5): p. 465-71.
99. Daneman, R., et al., *Pericytes are required for blood-brain barrier integrity during embryogenesis.* Nature, 2010. **468**(7323): p. 562-6.
100. Conroy, A.L., et al., *Angiopoietin-2 levels are associated with retinopathy and predict mortality in Malawian children with cerebral malaria: a retrospective case-control study.* Crit Care Med, 2012. **40**(3): p. 952-9.
101. Conroy, A.L., et al., *Endothelium-based biomarkers are associated with cerebral malaria in Malawian children: a retrospective case-control study.* PLoS One, 2010. **5**(12): p. e15291.
102. Lovegrove, F.E., et al., *Serum angiopoietin-1 and -2 levels discriminate cerebral malaria from uncomplicated malaria and predict clinical outcome in African children.* PLoS One, 2009. **4**(3): p. e4912.
103. Tsin W. Yeoa, et al., *Angiopoietin-2 is associated with decreased endothelial nitric oxide and poor clinical outcome in severe falciparum malaria.* Proc Natl Acad Sci U S A, 2008. **105**(44): p. 17097-102.
104. Rustenhoven, J., et al., *TGF-beta1 regulates human brain pericyte inflammatory processes involved in neurovasculature function.* J Neuroinflammation, 2016. **13**: p. 37.
105. Medana, I.M. and M.M. Esiri, *Axonal damage: a key predictor of outcome in human CNS diseases.* Brain, 2003. **126**(Pt 3): p. 515-30.

106. Medana, I.M., R. Idro, and C.R. Newton, *Axonal and astrocyte injury markers in the cerebrospinal fluid of Kenyan children with severe malaria.* J Neurol Sci, 2007. **258**(1-2): p. 93-8.
107. Medana, I.M., et al., *Cerebrospinal fluid levels of markers of brain parenchymal damage in Vietnamese adults with severe malaria.* Trans R Soc Trop Med Hyg, 2005. **99**(8): p. 610-7.
108. Mizee, M.R. and H.E. de Vries, *Blood-brain barrier regulation: Environmental cues controlling the onset of barrier properties.* Tissue Barriers, 2013. **1**(5): p. e26882.
109. Eeka, P. and P.B. Phanithi, *Cytotoxic T Lymphocyte Granzyme-b mediates neuronal cell death during Plasmodium berghei ANKA induced experimental cerebral malaria.* Neurosci Lett, 2018. **664**: p. 58-65.
110. Selma Bedri, et al., *Azadirachta indica ethanolic extract protects neurons from apoptosis and mitigates brain swelling in experimental cerebral malaria.* Malar J, 2013. **12**: p. 298.
111. Symon M Kariuki, et al., *Impairment of executive function in Kenyan children exposed to severe falciparum malaria with neurological involvement.* Malar J, 2014. **13**: p. 365.
112. Birbeck, G.L., et al., *Blantyre Malaria Project Epilepsy Study (BMPES) of neurological outcomes in retinopathy-positive paediatric cerebral malaria survivors: a prospective cohort study.* The Lancet Neurology, 2010. **9**(12): p. 1173-1181.
113. Julie A. Carter, et al., *Developmental impairments following severe falciparum malaria in children.* Trop Med Int Health, 2005. **10**(1): p. 3-10.
114. Oluwayemi, I.O., et al., *Neurological sequelae in survivors of cerebral malaria.* Pan Afr Med J, 2013. **15**: p. 88.
115. Brim, R., et al., *Cognitive Outcomes and Psychiatric Symptoms of Retinopathy-Positive Cerebral Malaria: Cohort Description and Baseline Results.* Am J Trop Med Hyg, 2017. **97**(1): p. 225-231.
116. Idro, R., et al., *Risk factors for persisting neurological and cognitive impairments following cerebral malaria.* Arch Dis Child, 2006. **91**(2): p. 142-8.
117. P. A. Holding, et al., *Cognitive sequelae of severe malaria with impaired consciousness.* Trans R Soc Trop Med Hyg, 1999. **93**(5): p. 529-34.
118. Boivin, M.J., et al., *Developmental outcomes in Malawian children with retinopathy-positive cerebral malaria.* Trop Med Int Health, 2011. **16**(3): p. 263-71.
119. Christensen, S.S. and G.D. Eslick, *Cerebral malaria as a risk factor for the development of epilepsy and other long-term neurological conditions: a meta-analysis.* Trans R Soc Trop Med Hyg, 2015. **109**(4): p. 233-8.
120. Lackner, P., et al., *Behavioural and histopathological alterations in mice with cerebral malaria.* Neuropathol Appl Neurobiol, 2006. **32**(2): p. 177-88.
121. Stoltenburg-Didinger, G., et al., *Selective damage of hippocampal neurons in murine cerebral malaria prevented by pentoxifylline.* J Neurol Sci, 1992. **114**(1): p. 20-4.
122. Isabelle M. Medana, Nicholas H. Hunt, and G. Chaudhri, *Tumor Necrosis Factor-a Expression in the Brain during Fatal Murine Cerebral Malaria.* Am J Pathol, 1997. **150**(4): p. 1473-86.
123. Medana, I.M., N.H. Hunt, and T. Chan-Ling, *Early activation of microglia in the pathogenesis of fatal murine cerebral malaria.* Glia, 1997. **19**(2): p. 91-103.
124. de Miranda, A.S., et al., *Anxiety-like behavior and proinflammatory cytokine levels in the brain of C57BL/6 mice infected with Plasmodium berghei (strain ANKA).* Neurosci Lett, 2011. **491**(3): p. 202-6.
125. Brant, F., et al., *Suppressor of cytokine signaling 2 modulates the immune response profile and development of experimental cerebral malaria.* Brain Behav Immun, 2016. **54**: p. 73-85.

126. Schiess, N., et al., *Pathophysiology and neurologic sequelae of cerebral malaria.* Malar J, 2020. **19**(1): p. 266.
127. Aline S Miranda , et al., *Further evidence for an anti-inflammatory role of artesunate in experimental cerebral malaria.* Malar J, 2013. **12**: p. 388.
128. Comim, C.M., et al., *Effects of experimental cerebral malaria in memory, brain-derived neurotrophic factor and acetylcholinesterase activity in the hippocampus of survivor mice.* Neurosci Lett, 2012. **523**(2): p. 104-7.
129. Reverchon, F., et al., *IL-33 receptor ST2 regulates the cognitive impairments associated with experimental cerebral malaria.* PLoS Pathog, 2017. **13**(4): p. e1006322.
130. Campisi, J. and F. d'Adda di Fagagna, *Cellular senescence: when bad things happen to good cells.* Nat Rev Mol Cell Biol, 2007. **8**(9): p. 729-40.
131. HAYFLICK L, M.P., *The serial cultivation of human diploid cell strains.* Exp Cell Res, 1961. **25**: p. 585-621.
132. Kang, C., et al., *The DNA damage response induces inflammation and senescence by inhibiting autophagy of GATA4.* Science, 2015. **349**(6255): p. aaa5612.
133. Zhang, M., et al., *Hepatic stellate cell senescence in liver fibrosis: Characteristics, mechanisms and perspectives.* Mech Ageing Dev, 2021. **199**: p. 111572.
134. Bent, E.H., L.A. Gilbert, and M.T. Hemann, *A senescence secretory switch mediated by PI3K/AKT/mTOR activation controls chemoprotective endothelial secretory responses.* Genes Dev, 2016. **30**(16): p. 1811-21.
135. Dasari, A., et al., *Oxidative stress induces premature senescence by stimulating caveolin-1 gene transcription through p38 mitogen-activated protein kinase/Sp1-mediated activation of two GC-rich promoter elements.* Cancer Res, 2006. **66**(22): p. 10805-14.
136. Neurohr, G.E., et al., *Excessive Cell Growth Causes Cytoplasm Dilution And Contributes to Senescence.* Cell, 2019. **176**(5): p. 1083-1097 e18.
137. *<pnas01498-0361.pdf>*.
138. Debacq-Chainiaux, F., et al., *Protocols to detect senescence-associated beta-galactosidase (SA-betagal) activity, a biomarker of senescent cells in culture and in vivo.* Nat Protoc, 2009. **4**(12): p. 1798-806.
139. Goberdhan P. Dimri, et al., *A biomarker that identifies senescent human cells in culture and in aging skin in vivo.* Proc Natl Acad Sci U S A., 1995. **92**(20): p. 9363-9367.
140. Wissler Gerdes, E.O., et al., *Cellular senescence in aging and age-related diseases: Implications for neurodegenerative diseases.* Int Rev Neurobiol, 2020. **155**: p. 203-234.
141. Zou, L., *Single- and double-stranded DNA: building a trigger of ATR-mediated DNA damage response.* Genes Dev, 2007. **21**(8): p. 879-85.
142. Shiloh, Y., *The ATM-mediated DNA-damage response: taking shape.* Trends Biochem Sci, 2006. **31**(7): p. 402-10.
143. Celeste, A., et al., *Genomic instability in mice lacking histone H2AX.* Science, 2002. **296**(5569): p. 922-7.
144. Ayrapetov, M.K., et al., *DNA double-strand breaks promote methylation of histone H3 on lysine 9 and transient formation of repressive chromatin.* Proc Natl Acad Sci U S A, 2014. **111**(25): p. 9169-74.
145. Takahashi, A., et al., *DNA damage signaling triggers degradation of histone methyltransferases through APC/C(Cdh1) in senescent cells.* Mol Cell, 2012. **45**(1): p. 123-31.
146. Bekker-Jensen, S., et al., *Spatial organization of the mammalian genome surveillance machinery in response to DNA strand breaks.* J Cell Biol, 2006. **173**(2): p. 195-206.
147. Lukas, C., et al., *Distinct spatiotemporal dynamics of mammalian checkpoint regulators induced by DNA damage.* Nat Cell Biol, 2003. **5**(3): p. 255-60.

148. Gaetan A Turenne, et al., *Activation of p53 transcriptional activity requires ATM's kinase domain and multiple N-terminal serine residues of p53.* Oncogene, 2001. **20**(37): p. 5100-10.
149. Munoz-Espin, D. and M. Serrano, *Cellular senescence: from physiology to pathology.* Nat Rev Mol Cell Biol, 2014. **15**(7): p. 482-96.
150. Sharpless, N.E. and C.J. Sherr, *Forging a signature of in vivo senescence.* Nat Rev Cancer, 2015. **15**(7): p. 397-408.
151. Beauséjour, C.M., et al., *Reversal of human cellular senescence: roles of the p53 and p16 pathways.* The EMBO Journal, 2003. **22**(16): p. P. 4212-4222.
152. Kumari, R. and P. Jat, *Mechanisms of Cellular Senescence: Cell Cycle Arrest and Senescence Associated Secretory Phenotype.* Front Cell Dev Biol, 2021. **9**: p. 645593.
153. Kruse, J.P. and W. Gu, *Modes of p53 regulation.* Cell, 2009. **137**(4): p. 609-22.
154. Levine, A.J., *p53, the Cellular Gatekeeper for Growth and Division.* Cell, 1997. **88**(3): p. 323-31.
155. Chuxia Deng, et al., *Mice Lacking p21CIP1/WAF1 Undergo Normal Development, but Are Defective in Gl Checkpoint Control.* Cell, 1995. **82**(4): p. 675-84.
156. Roberts, C.J.S.a.J.M., *Inhibitors of mammalian G 1 cyclin-dependent kinases.* Genes Dev, 1995. **9**(10): p. 1149-63.
157. Heiko Muller, et al., *E2Fs regulate the expression of genes involved in differentiation, development, proliferation, and apoptosis.* Genes Dev, 2001. **15**(3): p. 267-85.
158. Zuckerman, V., et al., *Tumour suppression by p53: the importance of apoptosis and cellular senescence.* J Pathol, 2009. **219**(1): p. 3-15.
159. Zhang, R.P., J.Z. Shao, and L.X. Xiang, *GADD45A protein plays an essential role in active DNA demethylation during terminal osteogenic differentiation of adipose-derived mesenchymal stem cells.* J Biol Chem, 2011. **286**(47): p. 41083-94.
160. Xin Wei Wang , et al., *GADD45 induction of a G2/M cell cycle checkpoint.* Proc Natl Acad Sci U S A, 1999. **96**(7): p. 3706-11.
161. Moskalev, A.A., et al., *Gadd45 proteins: relevance to aging, longevity and age-related pathologies.* Ageing Res Rev, 2012. **11**(1): p. 51-66.
162. Jacobs, J.J. and T. de Lange, *Significant role for p16INK4a in p53-independent telomere-directed senescence.* Curr Biol, 2004. **14**(24): p. 2302-8.
163. Kim, W.Y. and N.E. Sharpless, *The regulation of INK4/ARF in cancer and aging.* Cell, 2006. **127**(2): p. 265-75.
164. Roussel, M.F., *The INK4 family of cell cycle inhibitors in cancer.* Oncogene, 1999. **18**(38): p. 5311-7.
165. Nadezhda V. Petrova, et al., *Small molecule compounds that induce cellular senescence.* Aging Cell, 2015. **15**(6).
166. Gonzalez-Gualda, E., et al., *A guide to assessing cellular senescence in vitro and in vivo.* FEBS J, 2021. **288**(1): p. 56-80.
167. Vjekoslav Dulić, et al., *Uncoupling between Phenotypic Senescence and Cell Cycle Arrest in Aging p21-Deficient Fibroblasts.* Mol Cell Biol, 2000. **20**(18): p. 6741-54.
168. Christopher D. Wiley, et al., *Analysis of individual cells identifies cell-to-cell variability following induction of cellular senescence.* Aging Cell, 2017. **16**(5): p. 1043-1050.
169. Demirci, D., et al., *The Jekyll and Hyde of Cellular Senescence in Cancer.* Cells, 2021. **10**(2): p. 208.
170. Childs, B.G., et al., *Senescence and apoptosis: dueling or complementary cell fates?* EMBO Rep, 2014. **15**(11): p. 1139-53.
171. Yi Zhu, et al., *Identification of a novel senolytic agent navitoclax targeting the Bcl-2 family of anti-apoptotic factors.* Aging Cell, 2016. **15**(3): p. 428-35.

172. Yosef, R., et al., *Directed elimination of senescent cells by inhibition of BCL-W and BCL-XL.* Nat Commun, 2016. **7**: p. 11190.
173. Cory, S., D.C. Huang, and J.M. Adams, *The Bcl-2 family: roles in cell survival and oncogenesis.* Oncogene, 2003. **22**(53): p. 8590-607.
174. Jerry E. Chipuk, et al., *Direct Activation of Bax by p53 Mediates Mitochondrial Membrane Permeabilization and Apoptosis.* Science, 2004. **303**(5660): p. 1010-4.
175. Rochette, P.J. and D.E. Brash, *Progressive apoptosis resistance prior to senescence and control by the anti-apoptotic protein BCL-xL.* Mech Ageing Dev, 2008. **129**(4): p. 207-14.
176. Gartel, A.L. and A.L. Tyner, *The Role of the Cyclin-dependent Kinase Inhibitor p21 in Apoptosis.* Mol Cancer Ther, 2002. **1**(8): p. 639-49.
177. Fielder, E., T. von Zglinicki, and D. Jurk, *The DNA Damage Response in Neurons: Die by Apoptosis or Survive in a Senescence-Like State?* J Alzheimers Dis, 2017. **60**(s1): p. S107-S131.
178. Baar, M.P., et al., *Targeted Apoptosis of Senescent Cells Restores Tissue Homeostasis in Response to Chemotoxicity and Aging.* Cell, 2017. **169**(1): p. 132-147 e16.
179. Kirkland, J.L., et al., *The Clinical Potential of Senolytic Drugs.* J Am Geriatr Soc, 2017. **65**(10): p. 2297-2301.
180. de Oliveira Mann, C.C. and P.J. Kranzusch, *cGAS Conducts Micronuclei DNA Surveillance.* Trends Cell Biol, 2017. **27**(10): p. 697-698.
181. Chandra, T., et al., *Global reorganization of the nuclear landscape in senescent cells.* Cell Rep, 2015. **10**(4): p. 471-83.
182. Zhang, R., et al., *Formation of MacroH2A-containing senescence-associated heterochromatin foci and senescence driven by ASF1a and HIRA.* Dev Cell, 2005. **8**(1): p. 19-30.
183. Gerardo Ferbeyre, et al., *PML is induced by oncogenic ras and promotes premature senescence.* Genes Dev, 2000. **14**(16): p. 2015-27.
184. Mark Pearson, et al., *PML regulates p53 acetylation and premature senescence induced by oncogenic Ras.* Nature, 2000. **406**(6792): p. 207-10.
185. Narita, M., et al., *Rb-Mediated Heterochromatin Formation and Silencing of E2F Target Genes during Cellular Senescence.* Cell, 2003. **113**(6): p. 703-716.
186. Zhang, R., W. Chen, and P.D. Adams, *Molecular dissection of formation of senescence-associated heterochromatin foci.* Mol Cell Biol, 2007. **27**(6): p. 2343-58.
187. Adam Freunda, et al., *Lamin B1 loss is a senescence-associated biomarker.* Mol Biol Cell, 2012. **23**(11): p. 2066-75.
188. Freund, A., et al., *Inflammatory networks during cellular senescence: causes and consequences.* Trends Mol Med, 2010. **16**(5): p. 238-46.
189. Xu, M., et al., *JAK inhibition alleviates the cellular senescence-associated secretory phenotype and frailty in old age.* Proc Natl Acad Sci U S A, 2015. **112**(46): p. E6301-10.
190. Herranz, N., et al., *mTOR regulates MAPKAPK2 translation to control the senescence-associated secretory phenotype.* Nat Cell Biol, 2015. **17**(9): p. 1205-17.
191. Laberge, R.M., et al., *MTOR regulates the pro-tumorigenic senescence-associated secretory phenotype by promoting IL1A translation.* Nat Cell Biol, 2015. **17**(8): p. 1049-61.
192. di Martino, S., et al., *HSP90 inhibition alters the chemotherapy-driven rearrangement of the oncogenic secretome.* Oncogene, 2018. **37**(10): p. 1369-1385.
193. Chen, H., et al., *MacroH2A1 and ATM Play Opposing Roles in Paracrine Senescence and the Senescence-Associated Secretory Phenotype.* Mol Cell, 2015. **59**(5): p. 719-31.

194. Salminen, A., A. Kauppinen, and K. Kaarniranta, *Emerging role of NF-kappaB signaling in the induction of senescence-associated secretory phenotype (SASP).* Cell Signal, 2012. **24**(4): p. 835-45.
195. Kuilman, T., et al., *Oncogene-induced senescence relayed by an interleukin-dependent inflammatory network.* Cell, 2008. **133**(6): p. 1019-31.
196. Acosta, J.C., et al., *Chemokine signaling via the CXCR2 receptor reinforces senescence.* Cell, 2008. **133**(6): p. 1006-18.
197. Hui Yang, et al., *cGAS is essential for cellular senescence.* Proc Natl Acad Sci U S A, 2017. **114**(23): p. E4612-E4620.
198. Freund, A., C.K. Patil, and J. Campisi, *p38MAPK is a novel DNA damage response-independent regulator of the senescence-associated secretory phenotype.* EMBO J, 2011. **30**(8): p. 1536-48.
199. Xu, Y., et al., *Emerging roles of the p38 MAPK and PI3K/AKT/mTOR pathways in oncogene-induced senescence.* Trends Biochem Sci, 2014. **39**(6): p. 268-76.
200. Xue, W., et al., *Senescence and tumour clearance is triggered by p53 restoration in murine liver carcinomas.* Nature, 2007. **445**(7128): p. 656-60.
201. Sagiv, A. and V. Krizhanovsky, *Immunosurveillance of senescent cells: the bright side of the senescence program.* Biogerontology, 2013. **14**(6): p. 617-28.
202. Di Mitri, D., et al., *Tumour-infiltrating Gr-1+ myeloid cells antagonize senescence in cancer.* Nature, 2014. **515**(7525): p. 134-7.
203. Eggert, T., et al., *Distinct Functions of Senescence-Associated Immune Responses in Liver Tumor Surveillance and Tumor Progression.* Cancer Cell, 2016. **30**(4): p. 533-547.
204. Coppe, J.P., et al., *Secretion of vascular endothelial growth factor by primary human fibroblasts at senescence.* J Biol Chem, 2006. **281**(40): p. 29568-74.
205. Eyman, D., et al., *CCL5 secreted by senescent aged fibroblasts induces proliferation of prostate epithelial cells and expression of genes that modulate angiogenesis.* J Cell Physiol, 2009. **220**(2): p. 376-81.
206. Pazolli, E., et al., *Senescent stromal-derived osteopontin promotes preneoplastic cell growth.* Cancer Res, 2009. **69**(3): p. 1230-9.
207. Krizhanovsky, V., et al., *Senescence of activated stellate cells limits liver fibrosis.* Cell, 2008. **134**(4): p. 657-67.
208. Demaria, M., et al., *An essential role for senescent cells in optimal wound healing through secretion of PDGF-AA.* Dev Cell, 2014. **31**(6): p. 722-33.
209. Kuilman, T. and D.S. Peeper, *Senescence-messaging secretome: SMS-ing cellular stress.* Nat Rev Cancer, 2009. **9**(2): p. 81-94.
210. Acosta, J.C., et al., *A complex secretory program orchestrated by the inflammasome controls paracrine senescence.* Nat Cell Biol, 2013. **15**(8): p. 978-90.
211. Faget, D.V., Q. Ren, and S.A. Stewart, *Unmasking senescence: context-dependent effects of SASP in cancer.* Nat Rev Cancer, 2019. **19**(8): p. 439-453.
212. Kim, Y.H., et al., *Senescent tumor cells lead the collective invasion in thyroid cancer.* Nat Commun, 2017. **8**: p. 15208.
213. Patel, T.N., et al., *Shelterin proteins and cancer.* Asian Pac J Cancer Prev, 2015. **16**(8): p. 3085-90.
214. Michael Z. Levy , et al., *Telomere End-replication Problem and Cell Aging.* J Mol Biol, 1992. **225**(4): p. 951-60.
215. Fabrizio d'Adda di Fagagna, et al., *A DNA damage checkpoint response in telomere-initiated senescence.* Nature, 2003. **426**(6963): p. 194-8.
216. Qin M. Chen, et al., *Molecular analysis of H2O2 human fibroblasts : p53 and Rb control G1 arrest but not cell replication.* Biochem J, 1998. **332**(Pt 1): p. 43-50.

217. Sun, P., et al., *PRAK is essential for ras-induced senescence and tumor suppression.* Cell, 2007. **128**(2): p. 295-308.
218. Serrano, M., et al., *Oncogenic ras Provokes Premature Cell Senescence Associated with Accumulation of p53 and p16^{INK4a}.* Cell Press, March 07, 1997. **88**(5): p. P593-602.
219. Courtois-Cox, S., S.L. Jones, and K. Cichowski, *Many roads lead to oncogene-induced senescence.* Oncogene, 2008. **27**(20): p. 2801-9.
220. Hirotada Kojima, et al., *IL-6-STAT3 signaling and premature senescence.* JAKSTAT, 2013. **2**(4): p. e25763.
221. Sanada, F., et al., *IGF Binding Protein-5 Induces Cell Senescence.* Front Endocrinol (Lausanne), 2018. **9**: p. 53.
222. Hong, S. and M.M. Kim, *IGFBP-3 plays an important role in senescence as an aging marker.* Environ Toxicol Pharmacol, 2018. **59**: p. 138-145.
223. Severino, V., et al., *Insulin-like growth factor binding proteins 4 and 7 released by senescent cells promote premature senescence in mesenchymal stem cells.* Cell Death Dis, 2013. **4**(11): p. e911.
224. Senturk, S., et al., *Transforming growth factor-beta induces senescence in hepatocellular carcinoma cells and inhibits tumor growth.* Hepatology, 2010. **52**(3): p. 966-74.
225. Nelson, J.A., et al., *Expression of p16(INK4a) as a biomarker of T-cell aging in HIV-infected patients prior to and during antiretroviral therapy.* Aging Cell, 2012. **11**(5): p. 916-8.
226. Sona Hubackova, et al., *IL1- and TGFβ-Nox4 signaling, oxidative stress and DNA damage response are shared features of replicative, oncogene-induced, and drug-induced paracrine 'Bystander senescence'.* Aging (Albany NY), 2012. **4**(12): p. 932-51.
227. Patel, N.H., et al., *Autophagy and senescence in cancer therapy.* Adv Cancer Res, 2021. **150**: p. 1-74.
228. Glick, D., S. Barth, and K.F. Macleod, *Autophagy: cellular and molecular mechanisms.* J Pathol, 2010. **221**(1): p. 3-12.
229. Maycotte, P. and A. Thorburn, *Autophagy and cancer therapy.* Cancer Biol Ther, 2011. **11**(2): p. 127-37.
230. Brahimi-Horn, M.C., J. Chiche, and J. Pouyssegur, *Hypoxia and cancer.* J Mol Med (Berl), 2007. **85**(12): p. 1301-7.
231. Patricia Boya, F. Reggiori, and P. Codogno, *Emerging regulation and functions of autophagy.* Nat Cell Biol, 2013. **15**(7): p. 713-20.
232. Kwon, Y., et al., *Autophagy Is Pro-Senescence When Seen in Close-Up, but Anti-Senescence in Long-Shot.* Mol Cells, 2017. **40**(9): p. 607-612.
233. Young, A.R., et al., *Autophagy mediates the mitotic senescence transition.* Genes Dev, 2009. **23**(7): p. 798-803.
234. Narita, M., et al., *Spatial coupling of mTOR and autophagy augments secretory phenotypes.* Science, 2011. **332**(6032): p. 966-70.
235. Horikawa, I., et al., *Autophagic degradation of the inhibitory p53 isoform Delta133p53alpha as a regulatory mechanism for p53-mediated senescence.* Nat Commun, 2014. **5**: p. 4706.
236. Dou, Z., et al., *Autophagy mediates degradation of nuclear lamina.* Nature, 2015. **527**(7576): p. 105-109.
237. Huang, Y.H., et al., *Autophagy promotes radiation-induced senescence but inhibits bystander effects in human breast cancer cells.* Autophagy, 2014. **10**(7): p. 1212-28.
238. Kang, H.T., et al., *Autophagy impairment induces premature senescence in primary human fibroblasts.* PLoS One, 2011. **6**(8): p. e23367.

239. Storer, M., et al., *Senescence is a developmental mechanism that contributes to embryonic growth and patterning.* Cell, 2013. **155**(5): p. 1119-30.
240. Collado, M., M.A. Blasco, and M. Serrano, *Cellular senescence in cancer and aging.* Cell, 2007. **130**(2): p. 223-33.
241. Rodier, F. and J. Campisi, *Four faces of cellular senescence.* J Cell Biol, 2011. **192**(4): p. 547-56.
242. Lawrence A. Donehower, et al., *Mice deficient for p53 are developmentally normal but susceptible to spontaneous tumours.* Nature, 1992. **356**(6366): p. 215-21.
243. Norman E. Sharpless, et al., *Loss of p16Ink4a with retention of p19 Arf predisposes mice to tumorigenesis.* Nature, 2001. **413**(6851): p. 86-91.
244. Isabel GarcõÂa-Cao, et al., *`Super p53' mice exhibit enhanced DNA damage response, are tumor resistant and age normally.* EMBO J, 2002. **21**(22): p. 6225-35.
245. Kandoth, C., et al., *Mutational landscape and significance across 12 major cancer types.* Nature, 2013. **502**(7471): p. 333-339.
246. GOBERDHAN P. DIMRI, X.L., GEORGE BASILE, MEILEEN ACOSTA, GLYNIS SCOrrt, CALVIN ROSKELLEY, ESTELA E. MEDRANO, MAARTEN LINSKENSI, IVICA RUBELJII, OLIVIA PEREIRA-SMITHII, MONICA PEACOCKEt, AND JUDITH CAMPISI, *A biomarker that identifies senescent human cells in culture and in aging skin in vivo.*
247. Melk, A., et al., *Cell senescence in rat kidneys in vivo increases with growth and age despite lack of telomere shortening.* Kidney Int, 2003. **63**(6): p. 2134-43.
248. Brandon M. Hall, et al., *Aging of mice is associated with p16(Ink4a)- and β-galactosidasepositive macrophage accumulation that can be induced in young mice by senescent cells.* Aging (Albany NY), 2016. **8**(7): p. 1294-315.
249. Childs, B.G., et al., *Senescent cells: an emerging target for diseases of ageing.* Nat Rev Drug Discov, 2017. **16**: p. 718-735.
250. Baker, D.J., et al., *Clearance of p16Ink4a-positive senescent cells delays ageing-associated disorders.* Nature, 2011. **479**(7372): p. 232-6.
251. Baker, D.J., et al., *Naturally occurring p16(Ink4a)-positive cells shorten healthy lifespan.* Nature, 2016. **530**(7589): p. 184-9.
252. Burd, C.E., et al., *Monitoring tumorigenesis and senescence in vivo with a p16(INK4a)-luciferase model.* Cell, 2013. **152**(1-2): p. 340-51.
253. Baker, D.J. and R.C. Petersen, *Cellular senescence in brain aging and neurodegenerative diseases: evidence and perspectives.* The Journal of Clinical Investigation, 2018. **128**(4): p. 1208-1216.
254. Bennett G. Childs, et al., *Senescent intimal foam cells are deleterious at all stages of atherosclerosis.* Science, 2016. **354**(6311): p. 472-477.
255. Ogrodnik, M., et al., *Obesity-Induced Cellular Senescence Drives Anxiety and Impairs Neurogenesis.* Cell Metab, 2019. **29**(5): p. 1061-1077 e8.
256. Coppe, J.P., et al., *Senescence-associated secretory phenotypes reveal cell-nonautonomous functions of oncogenic RAS and the p53 tumor suppressor.* PLoS Biol, 2008. **6**(12): p. 2853-68.
257. Ana Krtolica, et al., *Senescent fibroblasts promote epithelial cell growth and tumorigenesis: A link between cancer and aging.* Proc Natl Acad Sci U S A, 2001. **98**(21): p. 12072-7.
258. Coppe, J.P., et al., *The senescence-associated secretory phenotype: the dark side of tumor suppression.* Annu Rev Pathol, 2010. **5**: p. 99-118.
259. de Magalhaes, J.P., *How ageing processes influence cancer.* Nat Rev Cancer, 2013. **13**(5): p. 357-65.

260. Demaria, M., et al., *Cellular Senescence Promotes Adverse Effects of Chemotherapy and Cancer Relapse.* Cancer Discov, 2017. **7**(2): p. 165-176.
261. Martinez, I., et al., *Induction of DNA double-strand breaks and cellular senescence by human respiratory syncytial virus.* Virulence, 2016. **7**(4): p. 427-42.
262. Noris, E., et al., *Cell cycle arrest by human cytomegalovirus 86-kDa IE2 protein resembles premature senescence.* J Virol, 2002. **76**(23): p. 12135-48.
263. Chuprin, A., et al., *Cell fusion induced by ERVWE1 or measles virus causes cellular senescence.* Genes Dev, 2013. **27**(21): p. 2356-66.
264. Yan, Y., et al., *NS1 of H7N9 Influenza A Virus Induces NO-Mediated Cellular Senescence in Neuro2a Cells.* Cell Physiol Biochem, 2017. **43**(4): p. 1369-1380.
265. Thangaraj, A., et al., *HIV TAT-mediated microglial senescence: Role of SIRT3-dependent mitochondrial oxidative stress.* Redox Biol, 2021. **40**: p. 101843.
266. Chen, N.C., et al., *Induction of a Senescence-Like Phenotype in Cultured Human Fetal Microglia During HIV-1 Infection.* J Gerontol A Biol Sci Med Sci, 2018. **73**(9): p. 1187-1196.
267. Carine Beaupere, et al., *The HIV proteins Tat and Nef promote human bone marrow mesenchymal stem cell senescence and alter osteoblastic differentiation.* Aging Cell, 2015. **14**(4): p. 534-46.
268. Susanne I.Wells, et al., *Papillomavirus E2 induces senescence in HPVpositive cells via pRB- and p21CIP-dependent pathways.* EMBO J, 2000. **19**(21): p. 5762-71.
269. Gorgoulis, V., et al., *Cellular Senescence: Defining a Path Forward.* Cell, 2019. **179**(4): p. 813-827.
270. Klok, F.A., et al., *Confirmation of the high cumulative incidence of thrombotic complications in critically ill ICU patients with COVID-19: An updated analysis.* Thromb Res, 2020. **191**: p. 148-150.
271. Wiley, C.D., et al., *SILAC Analysis Reveals Increased Secretion of Hemostasis-Related Factors by Senescent Cells.* Cell Rep, 2019. **28**(13): p. 3329-3337 e5.
272. Kohli, J., I. Veenstra, and M. Demaria, *The struggle of a good friend getting old: cellular senescence in viral responses and therapy.* EMBO Rep, 2021. **22**(4): p. e52243.
273. Khomich, O.A., et al., *Redox Biology of Respiratory Viral Infections.* Viruses, 2018. **10**(8): p. 392.
274. Aoshiba, K., T. Tsuji, and A. Nagai, *Bleomycin induces cellular senescence in alveolar epithelial cells.* Eur Respir J, 2003. **22**(3): p. 436-43.
275. Baz-Martinez, M., et al., *Cell senescence is an antiviral defense mechanism.* Sci Rep, 2016. **6**: p. 37007.
276. Kim, C.O., et al., *Analysis of cellular senescence induced by lipopolysaccharide in pulmonary alveolar epithelial cells.* Arch Gerontol Geriatr, 2012. **54**(2): p. e35-41.
277. Yu, H.M., et al., *Repeated lipopolysaccharide stimulation induces cellular senescence in BV2 cells.* Neuroimmunomodulation, 2012. **19**(2): p. 131-6.
278. Wei, W. and S. Ji, *Cellular senescence: Molecular mechanisms and pathogenicity.* J Cell Physiol, 2018. **233**(12): p. 9121-9135.
279. Cougnoux, A., et al., *Bacterial genotoxin colibactin promotes colon tumour growth by inducing a senescence-associated secretory phenotype.* Gut, 2014. **63**(12): p. 1932-42.
280. Cuevas-Ramos, G., et al., *Escherichia coli induces DNA damage in vivo and triggers genomic instability in mammalian cells.* Proc Natl Acad Sci U S A, 2010. **107**(25): p. 11537-42.
281. Isabella M. Tollera, et al., *Carcinogenic bacterial pathogen Helicobacter pylori triggers DNA double-strand breaks and a DNA damage response in its host cells.* Proc Natl Acad Sci U S A, 2011. **108**(36): p. 14944-9.

282. Guimaraes-Pinto, K., et al., *Trypanosoma cruzi Infection Induces Cellular Stress Response and Senescence-Like Phenotype in Murine Fibroblasts.* Front Immunol, 2018. **9**: p. 1569.
283. Asghar, M., et al., *Hidden costs of infection: Chronic malaria accelerates telomere degradation and senescence in wild birds.* Science, 2015. **347**(6220): p. 436-438.
284. Asghar, M., et al., *Parallel telomere shortening in multiple body tissues owing to malaria infection.* Proceedings of the Royal Society of London B: Biological Sciences, 2016. **283**(1836): p. 20161184.
285. Asghar, M., et al., *Cellular aging dynamics after acute malaria infection: A 12-month longitudinal study.* Aging Cell, 2018. **17**(1): p. e12702.
286. Miglar, A., et al., *Biomarkers of cellular aging during a controlled human malaria infection.* Scientific Reports, 2021. **11**(1): p. 18733.
287. Alexei Verkhratsky , et al., *Astrocytes in Alzheimer's disease* Neurotherapeutics, 2010. **7**(4): p. 399-412.
288. Alexei Verkhratsky, et al., *Astrocytes in Alzheimer's Disease.* Neurotherapeutics, 2010. **7**(4): p. 399-412.
289. Bitto, A., et al., *Stress-induced senescence in human and rodent astrocytes.* Exp Cell Res, 2010. **316**(17): p. 2961-8.
290. Gorg, B., et al., *Ammonia-induced senescence in cultured rat astrocytes and in human cerebral cortex in hepatic encephalopathy.* Glia, 2015. **63**(1): p. 37-50.
291. Bang, M., et al., *Tenovin-1 Induces Senescence and Decreases Wound-Healing Activity in Cultured Rat Primary Astrocytes.* Biomol Ther (Seoul), 2019. **27**(3): p. 283-289.
292. Bang, M., et al., *Etoposide Induces Mitochondrial Dysfunction and Cellular Senescence in Primary Cultured Rat Astrocytes.* Biomol Ther (Seoul), 2019. **27**(6): p. 530-539.
293. Limbad, C., et al., *Astrocyte senescence promotes glutamate toxicity in cortical neurons.* PLoS One, 2020. **15**(1): p. e0227887.
294. Cohen, J., et al., *Astrocyte Senescence and Metabolic Changes in Response to HIV Antiretroviral Therapy Drugs.* Front Aging Neurosci, 2017. **9**: p. 281.
295. Salminen, A., et al., *Astrocytes in the aging brain express characteristics of senescence-associated secretory phenotype.* Eur J Neurosci, 2011. **34**(1): p. 3-11.
296. Farahzad Jabbari Azad, et al., *Association between Cytokine Production and Disease Severity in Alzheimer's Disease.* Iran J Allergy Asthma Immunol, 2014. **13**(6): p. 433-9.
297. Benzing WC, et al., *Evidence for glial-mediated inflammation in aged APPSW transgenic mice.* Neurobiol Aging, 1999. **20**(6): p. 581-9.
298. Bhat, R., et al., *Astrocyte senescence as a component of Alzheimer's disease.* PLoS One, 2012. **7**(9): p. e45069.
299. Chinta, S.J., et al., *Cellular Senescence Is Induced by the Environmental Neurotoxin Paraquat and Contributes to Neuropathology Linked to Parkinson's Disease.* Cell Rep, 2018. **22**(4): p. 930-940.
300. Chinta, S.J., et al., *Environmental stress, ageing and glial cell senescence: a novel mechanistic link to Parkinson's disease?* J Intern Med, 2013. **273**(5): p. 429-36.
301. Vazquez-Villasenor, I., et al., *Expression of p16 and p21 in the frontal association cortex of ALS/MND brains suggests neuronal cell cycle dysregulation and astrocyte senescence in early stages of the disease.* Neuropathology and Applied Neurobiology, 2020. **46**(2): p. 171-185.
302. Bussian, T.J., et al., *Clearance of senescent glial cells prevents tau-dependent pathology and cognitive decline.* Nature, 2018. **562**(7728): p. 578-582.

303. Guan, L., K.C. Crasta, and A.B. Maier, *Assessment of cell cycle regulators in human peripheral blood cells as markers of cellular senescence.* Ageing Res Rev, 2022. **78**: p. 101634.
304. Zhangfa Song, et al., *Lifestyle impacts on the aging-associated expression of biomarkers of DNA damage and telomere dysfunction in human blood.* Aging Cell, 2010. **9**(4): p. 607-15.
305. Pustavoitau, A., et al., *Role of senescence marker p16 INK4a measured in peripheral blood T-lymphocytes in predicting length of hospital stay after coronary artery bypass surgery in older adults.* Exp Gerontol, 2016. **74**: p. 29-36.
306. Yan Liu, et al., *Expression of p16INK4a in peripheral blood T-cells is a biomarker of human aging.* Aging Cell, 2009. **8**(4): p. 439-48.
307. Hagman, M., et al., *Reduced telomere shortening in lifelong trained male football players compared to age-matched inactive controls.* Prog Cardiovasc Dis, 2020. **63**(6): p. 738-749.
308. Rutten, E.P., et al., *Various Mechanistic Pathways Representing the Aging Process Are Altered in COPD.* Chest, 2016. **149**(1): p. 53-61.
309. Rentscher, K.E., et al., *Chronic stress exposure and daily stress appraisals relate to biological aging marker p16(INK4a).* Psychoneuroendocrinology, 2019. **102**: p. 139-148.
310. Chebel, A., et al., *Rapamycin safeguards lymphocytes from DNA damage accumulation in vivo.* Eur J Cell Biol, 2016. **95**(9): p. 331-41.
311. Pathai, S., et al., *Accelerated biological ageing in HIV-infected individuals in South Africa: a case-control study.* AIDS, 2013. **27**(15): p. 2375-84.
312. Lichterfeld, M., et al., *Shelterin dysfunction and p16(INK4a)-mediated growth inhibition in HIV-1-specific CD8 T cells.* J Virol, 2012. **86**(10): p. 5533-40.
313. Tan, M., et al., *Combination of p53(ser15) and p21/p21(thr145) in peripheral blood lymphocytes as potential Alzheimer's disease biomarkers.* Neurosci Lett, 2012. **516**(2): p. 226-31.
314. Damjanac, M., et al., *PKR, a cognitive decline biomarker, can regulate translation via two consecutive molecular targets p53 and Redd1 in lymphocytes of AD patients.* J Cell Mol Med, 2009. **13**(8B): p. 1823-1832.
315. Jolanta Dorszewska, et al., *Polymorphisms of the CHRNA4 Gene Encoding the a4 Subunit of Nicotinic Acetylcholine Receptor as Related to the Oxidative DNA Damage and the Level of Apoptotic Proteins in Lymphocytes of the Patients with Alzheimer's Disease.* DNA Cell Biol, 2005. **24**(12): p. 786-94.
316. Hochstrasser, T., et al., *Two Blood Monocytic Biomarkers (CCL15 and p21) Combined with the Mini-Mental State Examination Discriminate Alzheimer's Disease Patients from Healthy Subjects.* Dement Geriatr Cogn Dis Extra, 2011. **1**(1): p. 297-309.
317. Martin-Ruiz, C., et al., *Senescence and Inflammatory Markers for Predicting Clinical Progression in Parkinson's Disease: The ICICLE-PD Study.* J Parkinsons Dis, 2020. **10**(1): p. 193-206.
318. Kouli, A., et al., *T lymphocyte senescence is attenuated in Parkinson's disease.* J Neuroinflammation, 2021. **18**(1): p. 228.
319. Teyssier, J.R., et al., *Up-regulation of leucocytes genes implicated in telomere dysfunction and cellular senescence correlates with depression and anxiety severity scores.* PLoS One, 2012. **7**(11): p. e49677.
320. Al Dubayee, M., et al., *Metformin alters peripheral blood mononuclear cells (PBMC) senescence biomarkers gene expression in type 2 diabetic patients.* J Diabetes Complications, 2021. **35**(1): p. 107758.

321. Soundararajan, A., et al., *Novel insights of elevated systemic levels of bisphenol-A (BPA) linked to poor glycemic control, accelerated cellular senescence and insulin resistance in patients with type 2 diabetes.* Mol Cell Biochem, 2019. **458**(1-2): p. 171-183.
322. Sathishkumar, C., et al., *Linking a role of lncRNAs (long non-coding RNAs) with insulin resistance, accelerated senescence, and inflammation in patients with type 2 diabetes.* Hum Genomics, 2018. **12**(1): p. 41.
323. Maas, B.M., et al., *Concentrations of Pro-Inflammatory Cytokines Are Not Associated with Senescence Marker p16INK4a or Predictive of Intracellular Emtricitabine/Tenofovir Metabolite and Endogenous Nucleotide Exposures in Adults with HIV Infection.* PLoS One, 2016. **11**(12): p. e0168709.
324. Bazyka, D., et al., *Biological Markers of External and Internal Exposure in Shelter Construction Workers: A 13-Year Experience.* Radiat Prot Dosimetry, 2018. **182**(1): p. 146-153.
325. Chang-Lung Lee, Jordan M. Blum, and D.G. Kirsch, *Role of p53 in regulating tissue response to radiation by mechanisms independent of apoptosis.* Transl Cancer Res, 2013. **2**(5): p. 412-421.
326. Behboudi, H., et al., *DNA damage and telomere length shortening in the peripheral blood leukocytes of 20years SM-exposed veterans.* Int Immunopharmacol, 2018. **61**: p. 37-44.
327. Carolyn M. Roos, et al., *Chronic senolytic treatment alleviates established vasomotor dysfunction in aged or atherosclerotic mice.* Aging Cell, 2016. **15**(5): p. 973-7.
328. Yi Zhu, et al., *The Achilles' heel of senescent cells: from transcriptome to senolytic drugs.* Aging Cell, 2015. **14**(4): p. 644-58.
329. Xu, M., et al., *Senolytics improve physical function and increase lifespan in old age.* Nat Med, 2018. **24**(8): p. 1246-1256.
330. Farr, J.N., et al., *Targeting cellular senescence prevents age-related bone loss in mice.* Nat Med, 2017. **23**(9): p. 1072-1079.
331. Hickson, L.J., et al., *Senolytics decrease senescent cells in humans: Preliminary report from a clinical trial of Dasatinib plus Quercetin in individuals with diabetic kidney disease.* EBioMedicine, 2019. **47**: p. 446-456.
332. Zhang, L., et al., *Targeting cellular senescence with senotherapeutics: senolytics and senomorphics.* FEBS J, 2022. **290**(5): p. 1362-1383.
333. Khan, N., et al., *Fisetin: a dietary antioxidant for health promotion.* Antioxid Redox Signal, 2013. **19**(2): p. 151-62.
334. Kumiko Ishige, David Schubert, and Y. Sagara, *Flavonoids protect neuronal cells from oxidative stress by three distinct mechanisms.* Free Radic Biol Med, 2001. **30**(4): p. 433-46.
335. Prasath, G.S., S.I. Pillai, and S.P. Subramanian, *Fisetin improves glucose homeostasis through the inhibition of gluconeogenic enzymes in hepatic tissues of streptozotocin induced diabetic rats.* Eur J Pharmacol, 2014. **740**: p. 248-54.
336. Prasath, G.S. and S.P. Subramanian, *Antihyperlipidemic effect of fisetin, a bioflavonoid of strawberries, studied in streptozotocin-induced diabetic rats.* J Biochem Mol Toxicol, 2014. **28**(10): p. 442-9.
337. Zheng, L.T., et al., *Suppressive effects of flavonoid fisetin on lipopolysaccharide-induced microglial activation and neurotoxicity.* Int Immunopharmacol, 2008. **8**(3): p. 484-94.
338. Chen, Y.C., et al., *Wogonin and fisetin induction of apoptosis through activation of caspase 3 cascade and alternative expression of p21 protein in hepatocellular carcinoma cells SK-HEP-1.* Arch Toxicol, 2002. **76**(5-6): p. 351-9.

339. Zbarsky, V., et al., *Neuroprotective properties of the natural phenolic antioxidants curcumin and naringenin but not quercetin and fisetin in a 6-OHDA model of Parkinson's disease.* Free Radic Res, 2005. **39**(10): p. 1119-25.
340. Yang, P.M., et al., *Dietary flavonoid fisetin targets caspase-3-deficient human breast cancer MCF-7 cells by induction of caspase-7-associated apoptosis and inhibition of autophagy.* Int J Oncol, 2012. **40**(2): p. 469-78.
341. Youns, M. and W. Abdel Halim Hegazy, *The Natural Flavonoid Fisetin Inhibits Cellular Proliferation of Hepatic, Colorectal, and Pancreatic Cancer Cells through Modulation of Multiple Signaling Pathways.* PLoS One, 2017. **12**(1): p. e0169335.
342. Syed, D.N., et al., *Exploring the molecular targets of dietary flavonoid fisetin in cancer.* Semin Cancer Biol, 2016. **40-41**: p. 130-140.
343. Yi Zhu , et al., *New agents that target senescent cells: the flavone, fisetin, and the BCL-XL inhibitors, A1331852 and A1155463.* Aging (Albany NY), 2017. **9**(3): p. 955-963.
344. Yousefzadeh, M.J., et al., *Fisetin is a senotherapeutic that extends health and lifespan.* EBioMedicine, 2018. **36**: p. 18-28.
345. Adhami, V.M., et al., *Dietary flavonoid fisetin: a novel dual inhibitor of PI3K/Akt and mTOR for prostate cancer management.* Biochem Pharmacol, 2012. **84**(10): p. 1277-81.
346. Maher, P., *Fisetin Acts on Multiple Pathways to Reduce the Impact of Age and Disease on CNS Function.* Front Biosci (Schol Ed), 2015. **7**: p. 58-82.
347. Chang, J., et al., *Clearance of senescent cells by ABT263 rejuvenates aged hematopoietic stem cells in mice.* Nat Med, 2016. **22**(1): p. 78-83.
348. Bennett G Childs, et al., *Senescent intimal foam cells are deleterious at all stages of atherosclerosis.* Science, 2016. **354**(6311): p. 472-477.
349. Schoenwaelder, S.M., et al., *Bcl-xL-inhibitory BH3 mimetics can induce a transient thrombocytopathy that undermines the hemostatic function of platelets.* Blood, 2011. **118**(6): p. 1663-74.
350. Fuhrmann-Stroissnigg, H., et al., *Identification of HSP90 inhibitors as a novel class of senolytics.* Nat Commun, 2017. **8**(1): p. 422.
351. Ovadya, Y. and V. Krizhanovsky, *Strategies targeting cellular senescence.* J Clin Invest, 2018. **128**(4): p. 1247-1254.
352. *World Health Organization.* 2010.
353. Isabelle M. Medana, N.H.H., and Geeta Chaudhri, *Tumor Necrosis Factor-a Expression in the Brain during Fatal Murine Cerebral Malaria.*
354. Dalko, E., et al., *Multifaceted Role of Heme during Severe Plasmodium falciparum Infections in India.* Infect Immun, 2015. **83**(10): p. 3793-9.
355. Dalko, E., et al., *Erythropoietin Levels Increase during Cerebral Malaria and Correlate with Heme, Interleukin-10 and Tumor Necrosis Factor-Alpha in India.* PLoS One, 2016. **11**(7): p. e0158420.
356. Shan-Rong, S., E.K. Marc, and L.K. Krishan, *Antigen retrieval in formalin-fixed, paraffin-embedded tissues: an enhancement method for immunohistochemical staining based on microwave oven heating of tissue sections. .* Journal of Histochemistry & Cytochemistry, 1991. **39**(6): p. 741-748.
357. Tominaga, T., et al., *Senescence-associated-beta-galactosidase staining following traumatic brain injury in the mouse cerebrum.* PLoS One, 2019. **14**(3): p. e0213673.
358. Lozano-Gerona, J. and A.L. Garcia-Otin, *ImageJ-based semiautomatic method to analyze senescence in cell culture.* Anal Biochem, 2018. **543**: p. 30-32.
359. Walf, A.A. and C.A. Frye, *The use of the elevated plus maze as an assay of anxiety-related behavior in rodents.* Nat Protoc, 2007. **2**(2): p. 322-8.

360. Bergeron, S., et al., *Beneficial effects of atorvastatin on sex-specific cognitive impairment induced by a cerebral microhaemorrhage in mice.* Br J Pharmacol, 2021. **178**(7): p. 1705-1721.
361. Penet, M.F., et al., *Imaging experimental cerebral malaria in vivo: significant role of ischemic brain edema.* J Neurosci, 2005. **25**(32): p. 7352-8.
362. Wilson, M., et al., *A constrained least-squares approach to the automated quantitation of in vivo (1)H magnetic resonance spectroscopy data.* Magn Reson Med, 2011. **65**(1): p. 1-12.
363. Reynolds, G., et al., *An algorithm for the automated quantitation of metabolites in in vitro NMR signals.* Magn Reson Med, 2006. **56**(6): p. 1211-9.
364. Zhang, P., et al., *Senolytic therapy alleviates Abeta-associated oligodendrocyte progenitor cell senescence and cognitive deficits in an Alzheimer's disease model.* Nat Neurosci, 2019. **22**: p. 719-728.
365. Calas, A.G., et al., *Chronic exposure to glufosinate-ammonium induces spatial memory impairments, hippocampal MRI modifications and glutamine synthetase activation in mice.* Neurotoxicology, 2008. **29**(4): p. 740-7.
366. Idda, M.L., et al., *Survey of senescent cell markers with age in human tissues.* Aging (Albany NY), 2020. **12**(5): p. 4052-4066.
367. Choi, J.-Y., et al., *SARS-CoV-2 spike S1 subunit protein-mediated increase of beta-secretase 1 (BACE1) impairs human brain vessel cells.* Biochemical and Biophysical Research Communications, 2022. **626**: p. 66-71.
368. Mijit, M., et al., *Role of p53 in the Regulation of Cellular Senescence.* Biomolecules, 2020. **10**(3): p. 420.
369. Rayess, H., M.B. Wang, and E.S. Srivatsan, *Cellular senescence and tumor suppressor gene p16.* Int J Cancer, 2012. **130**(8): p. 1715-25.
370. Childs, B.G., et al., *Senescence and apoptosis: dueling or complementary cell fates?* EMBO reports, 2014. **15**(11): p. 1139-1153.
371. Yosef, R., et al., *Directed elimination of senescent cells by inhibition of BCL-W and BCL-XL.* Nature communications, 2016. **7**(1): p. 1-11.
372. Lackner, P., et al., *Apoptosis in experimental cerebral malaria: spatial profile of cleaved caspase-3 and ultrastructural alterations in different disease stages.* Neuropathol Appl Neurobiol, 2007. **33**(5): p. 560-71.
373. Haupt, Y., et al., *Mdm2 promotes the rapid degradation of p53.* Nature, 1997. **387**(6630): p. 296-299.
374. Rufini, A., et al., *Senescence and aging: the critical roles of p53.* Oncogene, 2013. **32**(43): p. 5129-43.
375. Kang, C. and S.J. Elledge, *How autophagy both activates and inhibits cellular senescence.* Autophagy, 2016. **12**(5): p. 898-9.
376. Komatsu, M., et al., *Loss of autophagy in the central nervous system causes neurodegeneration in mice.* Nature, 2006. **441**(7095): p. 880-4.
377. Hara, T., et al., *Suppression of basal autophagy in neural cells causes neurodegenerative disease in mice.* Nature, 2006. **441**(7095): p. 885-9.
378. Young, A.R. and M. Narita, *Connecting autophagy to senescence in pathophysiology.* Curr Opin Cell Biol, 2010. **22**(2): p. 234-40.
379. Young, A.R., M. Narita, and M. Narita, *Spatio-temporal association between mTOR and autophagy during cellular senescence.* Autophagy, 2011. **7**(11): p. 1387-8.
380. Leidal, A.M. and J. Debnath, *Autophagy Devours the Nuclear Lamina to Thwart Oncogenic Stress.* Dev Cell, 2015. **35**(5): p. 529-530.
381. Dou, Z., et al., *Mammalian autophagy degrades nuclear constituents in response to tumorigenic stress.* Autophagy, 2016. **12**(8): p. 1416-7.

382. Shimi, T., et al., *The role of nuclear lamin B1 in cell proliferation and senescence.* Genes Dev, 2011. **25**(24): p. 2579-93.
383. Fujita, K., et al., *p53 isoforms Delta133p53 and p53beta are endogenous regulators of replicative cellular senescence.* Nat Cell Biol, 2009. **11**(9): p. 1135-42.
384. von Muhlinen, N., et al., *p53 isoforms regulate premature aging in human cells.* Oncogene, 2018. **37**(18): p. 2379-2393.
385. Turnquist, C., et al., *p53 isoforms regulate astrocyte-mediated neuroprotection and neurodegeneration.* Cell Death Differ, 2016. **23**(9): p. 1515-28.
386. Turnquist, C., et al., *Radiation-induced astrocyte senescence is rescued by Delta133p53.* Neuro Oncol, 2019. **21**(4): p. 474-485.
387. Dorr, J.R., et al., *Synthetic lethal metabolic targeting of cellular senescence in cancer therapy.* Nature, 2013. **501**(7467): p. 421-5.
388. Porkka, K., et al., *Dasatinib crosses the blood-brain barrier and is an efficient therapy for central nervous system Philadelphia chromosome-positive leukemia.* Blood, 2008. **112**(4): p. 1005-12.
389. Ishisaka, A., et al., *Accumulation of orally administered quercetin in brain tissue and its antioxidative effects in rats.* Free Radic Biol Med, 2011. **51**(7): p. 1329-36.
390. Robbins, P.D., et al., *Senolytic Drugs: Reducing Senescent Cell Viability to Extend Health Span.* Annu Rev Pharmacol Toxicol, 2021. **61**: p. 779-803.
391. Fletcher-Sananikone, E., et al., *Elimination of Radiation-Induced Senescence in the Brain Tumor Microenvironment Attenuates Glioblastoma Recurrence.* Cancer Res, 2021. **81**(23): p. 5935-5947.
392. Karpel-Massler, G., et al., *Induction of synthetic lethality in IDH1-mutated gliomas through inhibition of Bcl-xL.* Nat Commun, 2017. **8**(1): p. 1067.
393. Yabluchanskiy, A., et al., *Pharmacological or genetic depletion of senescent astrocytes prevents whole brain irradiation-induced impairment of neurovascular coupling responses protecting cognitive function in mice.* Geroscience, 2020. **42**(2): p. 409-428.
394. Wang, B., et al., *An inducible p21-Cre mouse model to monitor and manipulate p21-highly-expressing senescent cells in vivo.* Nat Aging, 2021. **1**(10): p. 962-973.
395. Chinta, S.J., et al., *Cellular senescence and the aging brain.* Exp Gerontol, 2015. **68**: p. 3-7.
396. Humphreys, D., M. ElGhazaly, and T. Frisan, *Senescence and Host-Pathogen Interactions.* Cells, 2020. **9**(7): p. 1747.
397. Felizardo, A.A., et al., *Impact of Trypanosoma cruzi infection on nitric oxide synthase and arginase expression and activity in young and elderly mice.* Free Radic Biol Med, 2018. **129**: p. 227-236.
398. Ehrchen, J., et al., *Senescent BALB/c mice are able to develop resistance to Leishmania major infection.* Infect Immun, 2004. **72**(9): p. 5106-14.
399. Nagat Abbas , et al., *Up-regulation of the inflammatory cytokines IFN-g and IL-12 and down-regulation of IL-4 in cerebral cortex regions of APP SWE transgenic mice.* J Neuroimmunol, 2002. **126**(1-2): p. 50-7.
400. Erik W. Settles, et al., *Toxoplasma gondii Upregulates Interleukin-12 To Prevent Plasmodium berghei-Induced Experimental Cerebral Malaria.* Infect Immun, 2014. **82**(3): p. 1343-53.
401. Pertusa, M., et al., *Astrocytes aged in vitro show a decreased neuroprotective capacity.* J Neurochem, 2007. **101**(3): p. 794-805.
402. Matias, I., et al., *Loss of lamin-B1 and defective nuclear morphology are hallmarks of astrocyte senescence in vitro and in the aging human hippocampus.* Aging Cell, 2022. **21**(1): p. e13521.

403. Supattra Serirom, et al., *Anti-Adhesive Effect of Nitric Oxide on Plasmodium falciparum Cytoadherence under Flow.* Am J Pathol, 2003. **162**(5): p. 1651-60.
404. Ong, P.K., et al., *Reversal of cerebrovascular constriction in experimental cerebral malaria by L-arginine.* Sci Rep, 2018. **8**(1): p. 15957.